

DOKUZ EYLÜL UNIVERSITY
GRADUATE SCHOOL OF NATURAL AND APPLIED SCIENCES

**HIGH FREQUENCY VIBRATION ANALYSIS OF
LAMINATED COMPOSITE STRUCTURES VIA
STATISTICAL ENERGY ANALYSIS**

by
Murat KARA

January, 2015
İZMİR

HIGH FREQUENCY VIBRATION ANALYSIS OF LAMINATED COMPOSITE STRUCTURES VIA STATISTICAL ENERGY ANALYSIS

**A Thesis Submitted to the
Graduate School of Natural and Applied Sciences of Dokuz Eylül University
In Partial Fulfillment of the Requirements for the Degree of Master of Science
in Mechanical Engineering, Machine Theory and Dynamics Program**

**by
Murat KARA**

January, 2015

İZMİR

M.Sc. THESIS EXAMINATION RESULT FORM

We have read the thesis entitled “**HIGH FREQUENCY VIBRATION ANALYSIS OF LAMINATED COMPOSITE STRUCTURES VIA STATISTICAL ENERGY ANALYSIS**” completed by **MURAT KARA** under supervision of **Assoc. Prof. Dr. ABDULLAH SEÇGİN** and we certify that in our opinion it is fully adequate, in scope and in quality, as a thesis for the degree of Master of Science.



Assoc. Prof. Dr. Abdullah SEÇGİN

Supervisor



Prof. Dr. A. Saide SARIGÜL
(Jury Member)



Yrd. Doç. Dr. Mehmet SARIKANAT
(Jury Member)



Prof. Dr. Ayşe OKUR
Director
Graduate School of Natural and Applied Sciences

ACKNOWLEDGMENTS

This thesis with the title “*High frequency vibration analysis of laminated composite structures via statistical energy analysis*” is one of the outcomes of 112M836 numbered project supported by The Scientific and Technological Research Council of Turkey, TUBİTAK.

I would like to express my sincere appreciation to my thesis advisor Assoc. Prof. Dr. Abdullah SEÇGİN for all his time, effort and patience. His guidance and critical suggestions helped me to finish this project.

I would also like to thank Prof. Dr. A. Saide SARIGÜL and my friends Altay OZANKAN, Muzaffer KASABA and Murat HASIL.

Finally, my special thanks go to my wife Sinem KARA, my parents, my sister and my brother for their support in my entire master education.

Murat KARA

HIGH FREQUENCY VIBRATION ANALYSIS OF LAMINATED COMPOSITE STRUCTURES VIA STATISTICAL ENERGY ANALYSIS

ABSTRACT

Statistical energy analysis is a widely used high frequency vibro-acoustic analysis tool. It is based on power flow balance between subsystems. In the project, statistical energy analysis of several different systems; composite plate-acoustic volume structure and point-connected I, L and T type structures made of laminated composite plates are investigated for high frequency analysis.

Accuracy of method mainly depends on precise determination of statistical energy analysis parameters such as average modal spacing, coupling loss factor, damping loss factor. In the study, average modal spacings have been determined numerically by using uncoupled natural frequencies whereas loss factors have been obtained by using numerical (finite element method by ANSYS) and experimental power injection method. All these parameters have been compared with analytical ones. As the last but not the least, composite plates with random thickness/mass variability have been considered to carry out the effect of uncertainty by using finite element based Monte Carlo simulation. Mean responses of these results have been compared via statistical energy analysis to investigate the methodologies used in high frequency analysis of vibro-acoustic system with structural uncertainty.

Keywords: Statistical energy analysis, finite element analysis, power injection method, Monte Carlo simulation, uncertainty, laminated composite plates, acoustic volume.

İSTATİSTİKSEL ENERJİ ANALİZİ İLE LAMİNE KOMPOZİT YAPILARIN YÜKSEK FREKANS TİTREŞİM ANALİZİ

ÖZ

İstatistiksel enerji analizi, sık kullanılan bir yüksek frekans vibro-akustik analiz aracıdır. Alt sistemler arasındaki güç akış dengesine dayanır. Bu projede, farklı sistemlerin; katmanlı kompozit plakalardan yapılan kompozit plaka-akustik hacim yapısı ve noktasal bağlı I, L ve T tip yapıların istatistiksel enerji analizi yüksek frekanslı titreşim analizi için araştırılmıştır.

Yöntemin doğruluğu esasen ortalama modal uzaklık, bağlantı kayıp faktörü ve sönüm kayıp faktörü gibi istatistiksel enerji analizi parametrelerinin hassas olarak belirlenmesine dayanır. Çalışmada, ortalama modal uzaklık sayısal olarak alt sistemlerin ayırık doğal frekansları kullanarak belirlenirken, kayıp faktörleri sayısal (ANSYS ile sonlu elemanlar metodu) ve deneysel güç enjeksiyon yöntemi kullanılarak belirlenmiştir. Son olarak, rastgele kalınlık/kütle değişkenli kompozit plakalar belirsizlik uygulamak için sonlu elemanlar tabanlı Monte Carlo simülasyonunun kullanılmasıyla göz önüne alınmıştır. Bu sonuçların ortalama cevapları yapısal belirsizlikli vibro-akustik sistemlerin yüksek frekans analizlerinde kullanılan metodolojilerin incelenmesi için istatistiksel enerji analizi ile karşılaştırılmıştır.

Anahtar kelimeler: İstatistiksel enerji analizi, sonlu elemanlar analizi, güç enjeksiyon yöntemi, Monte Carlo simülasyonu, belirsizlik, katmanlı kompozit plakalar, akustik hacim

CONTENTS

	Page
THESIS EXAMINATION RESULT FORM.....	ii
ACKNOWLEDGEMENTS	iii
ABSTRACT	iv
ÖZ	v
LIST OF FIGURES	viii
LIST OF TABLES.....	x
CHAPTER ONE - INTRODUCTION	1
1.1 General Information	1
1.2 About Statistical Energy Analysis (SEA).....	4
1.3 Thesis Organization.....	6
CHAPTER TWO - MATHEMATICAL DESCRIPTIONS.....	7
2.1 Statistical Energy Analysis (SEA)	7
2.2 Parameters of Statistical Energy Analysis.....	9
2.2.1 Coupling Loss Factor (CLF) and Damping Loss Factor (DLF)	9
2.2.2 Power Input	12
2.2.3 Modal Density and Average Modal Spacing	13
2.2.4 Infinite System Impedance	15
2.2.4.1 Dimension Reducing Principle (DRP).....	15
2.3 High Frequency Threshold	17
2.4 Power Injection Method (PIM).....	18
2.5 Uncertainty Analysis via Monte Carlo Simulation.....	20
CHAPTER THREE - COMPOSITE PLATE-ACOUSTIC VOLUME INTERACTION.....	21
3.1 Classical Statistical Energy Analysis	22

3.2 Numerical Modeling via Finite Element Method	25
3.3 Numerical Computation of Statistical Energy Analysis (SEA) Parameters.....	29
3.3.1 Computation of AMSs.....	29
3.3.2 Computations of CLFs.....	30
3.4 Response Analysis of CP-AV System Having Structural Uncertainty.....	31
3.4.1 Determination of High Frequency Threshold	32
3.4.2 Acoustic Excitation	33
3.4.3 Structural Excitation	36
CHAPTER FOUR - COMPOSITE STRUCTURES	40
4.1 Classical Statistical Energy Analysis	42
4.1.1 Force/Moment Power Transmission.....	42
4.1.2 Determination of Internal Damping (Damping Loss Factor, DLF)	45
4.1.3 Determination of Coupling Loss Factors (CLF)	46
4.2 Numerical Computation of Loss Factors.....	47
4.3 Experimental Determination of Loss Factors	48
4.4 Uncertainty Analysis via FEM-Monte Carlo Simulation.....	52
CHAPTER FIVE - CONCLUSION	57
REFERENCES	59
APPENDICES.....	64

LIST OF FIGURES

	Page
Figure 1.1 Uncertain acoustic response of pickup trucks.....	3
Figure 2.1 Power balance of structure having two subsystems.....	8
Figure 2.2 Modal spacing representation of a frequency response function.....	13
Figure 2.3 Structures and reducing dimensions.....	16
Figure 3.1 Line and area connections of acoustic volume-composite plate structure.....	22
Figure 3.2 Power flow between acoustic volume and composite plate.....	24
Figure 3.3 CLF between acoustic volume and composite plate.....	24
Figure 3.4 Numerical model of subsystems a) Acoustic volume, b) Composite plate, c) Acoustic volume-composite plate coupling.....	25
Figure 3.5 Average modal spacings for different number of elements for a) Acoustic volume, b) Composite plate.....	30
Figure 3.6 Loss factors of subsystems (black dash: initial damping, black solid: analytical CLF, blue solid: PIM results).....	31
Figure 3.7 Numerical and analytical modal overlap factor of subsystems a) Acoustic volume, b) Plate.....	33
Figure 3.8 Sound pressure response of acoustic volume under acoustic excitation a) 1-1000 Hz, b) 1000-3000 Hz, c) 3000-5000 Hz (blue: numerical SEA, red: classical SEA, grey: uncertain results black dot: mean of uncertain results).....	34
Figure 3.9 Velocity response of composite plate under acoustic excitation a) 1-1000 Hz, b) 1000-3000, Hz c) 3000-5000 Hz (blue: numerical SEA, red: classical SEA, grey: uncertain results black dot: mean of uncertain results).....	35
Figure 3.10 Sound pressure response of acoustic volume under plate excitation a) 1-1000 Hz, b) 1000-3000 Hz, c) 3000-5000 Hz (blue: numerical SEA, red: classical SEA, grey: uncertain results black dot: mean of uncertain results).....	36

Figure 3.11 Velocity response of composite plate under plate excitation a) 1-1000 Hz, b) 1000-3000 Hz, c) 3000-5000 Hz (blue: numerical SEA, red: classical SEA, grey: uncertain results black dot: mean of uncertain results).....	37
Figure 4.1 Composite structures a) I-type, b) L-type, c) T-type.....	41
Figure 4.2 SEA model of structures a) I/L type, b) T type.....	44
Figure 4.3 DLF of a single plate obtained by experimental PIM.....	45
Figure 4.4 MOF of composite plate.....	45
Figure 4.5 CLFs between subsystems a) I type, b) L type, c) T type.....	46
Figure 4.6 Loss factors of I-connected composite structure (dash-dot line: analytical, solid line: numerical PIM, dot line: experimental PIM, gray solid line: DLF of a single plate).....	50
Figure 4.7 Loss factors of L-connected composite structure (dash-dot line: analytical, solid line: numerical PIM, dot line: experimental PIM, gray solid line: DLF of a single plate).....	50
Figure 4.8 Loss factors of T-connected composite structure (dash-dot line: analytical, solid line: numerical PIM, dot line: experimental PIM, gray solid line: DLF of a single plate).....	51
Figure 4.9 Experimental setup.....	52
Figure 4.10 Velocity of subsystem 1, a) 10-1000 Hz, b) 1000-3000 Hz, c) 3000-5000 Hz (grey: uncertain results, black dot: mean of uncertain results, blue: classical SEA, red: numerical SEA, green: experimental SEA).....	53
Figure 4.11 Velocity of subsystem 2, a) 10-1000 Hz, b) 1000-3000 Hz, c) 3000-5000 Hz (grey: uncertain results, black dot: mean of uncertain results, blue: classical SEA, red: numerical SEA, green: experimental SEA).....	54
Figure 4.12 Velocity of subsystem 3, a) 10-1000 Hz, b) 1000-3000 Hz, c) 3000-5000 Hz (grey: uncertain results, black dot: mean of uncertain results, blue: classical SEA, red: numerical SEA, green: experimental SEA).....	55

LIST OF TABLES

	Page
Table 2.1 Sound power of different acoustic sources.....	12
Table 2.2 Average modal spacings (AMSs) for common subsystems.....	14
Table 2.3 Driving point impedance of structures.....	16
Table 2.4 Bending line and area impedances of flexible structures obtained from point connections via dimension reducing principle.....	17
Table 3.1 Mechanical properties of subsystems.....	23
Table 3.2 Natural frequencies of the acoustic volume.....	27
Table 3.3 Natural frequencies of the composite plate.....	28
Table 4.1 Properties of the composite plate.....	42
Table 4.2 Power transmission between subsystems.....	43

CHAPTER ONE

INTRODUCTION

1.1 General Information

Nowadays, composite materials are widely used in aerospace and automobile industry since they provide high strength/weight ratio that leads less fuel consumption. Therefore, investigation of vibro-acoustic behavior of structures made of composite materials becomes one of the most important studies. Generally, in vibro-acoustics, analyses are examined in three frequency regions; low, mid and high frequency ranges. Conventional analyses are usually performed for low frequencies at which resonant modes dominate the response. However, using lightweight structures in automobile, vessel and aerospace engineering reduces fuel expenses; however it leads to shifting the vibro-acoustic problems to mid and high frequency analysis. High frequency region shows smooth response predictions due to modal overlapping, whereas mid frequency region exhibits much more complex response characteristics. Although, there is no exact quantification that separates these regions from each other, an approximate high frequency threshold can be computed for simple structures by using modal overlap factor (count) (MOF).

In low frequency region, deterministic techniques such as finite element method (FEM), boundary element method (BEM) are generally used. However, in analysis of high frequency vibrations with deterministic techniques, excessive number of elements is required, which make them inefficient because of high solution time and memory usage. Therefore for mid and high frequency region, special approaches should be considered.

In high frequency region, statistic and energy based methods are generally used. Statistical energy analysis (SEA) (Fahy, 1994; Lyon & DeJong, 1998) is the most popular and widely used approach in many areas in engineering. SEA divides a complex structure to its subsystems that each of which composed of common modal behavior. But these subsystems need to include sufficient number of modes for

reliability. A power balance between subsystems is then set up to predict the mean energy level of each subsystem. By this way, small dimension of system matrix is set, thus the solution time becomes insignificant. Success of SEA mainly depends on the accurate evaluation of SEA parameters such as coupling loss factor (CLF), damping loss factor (DLF), average modal spacing ($\overline{\delta f}$) and power input. For simple structures, CLFs can be analytically determined by using finite/semi-infinite system impedances (Lyon & DeJong, 1998) or dual modal formulation (Maxit & Guyader, 2009a, 2009b). For more complex structures, they can be determined by numerical/experimental power injection method (PIM) (Bies & Hamid, 1980; Langhe & Sas, 1996). Beside that decay rate method (Bloss & Rao, 2005; Lyon & DeJong, 1998) and quality factor (Lyon & DeJong, 1998; Rao, 1995) are other experimental methods for obtaining DLFs. In numerical PIM, DLFs of subsystems has to be initially known for modeling the structure.

Beside that, accurate modeling of coupling type (point, line and area), coupling geometry (angle between subsystems, number of subsystem at junction), element type (beam, plate, bar, shell, membrane, acoustics etc.,) and modal classification (longitudinal, bending, torsional, shear etc.,) of subsystems are very important for SEA system. These require experience in SEA modeling.

For mid frequency region, neither deterministic techniques nor statistical and energy based methods are applicable alone. In this region, hybrid methods combining deterministic and statistical methods (Cotoni et al., 2007; DeRosa & Franco, 2010; Ji et al., 2006; Langley & Bremner, 1999; Langley & Cordioli, 2009; Seçgin, 2013; Shorter & Langley, 2005; Vanmaele et al., 2007; Vlahopoulos & Zhao, 2001) are commonly used. However, developments on this issue are still under consideration by the experts.

Products that are manufactured from the same production line and that have the same manufacturing processes can exhibit different vibro-acoustic response characteristics. This variability in vibro-acoustics is called as “uncertainty”. The uncertainty arises from small differences in geometry, material property,

characteristic of excitation, initial and boundary conditions of structures. Uncertainty in vibro-acoustic systems makes response unreliable not only for low frequencies but for higher frequencies. Figure 1.1 (Fahy, 1994) shows acoustic response variation of several pickup trucks which are the same model produced in the same line, this uncertainty increases as the frequency increases.

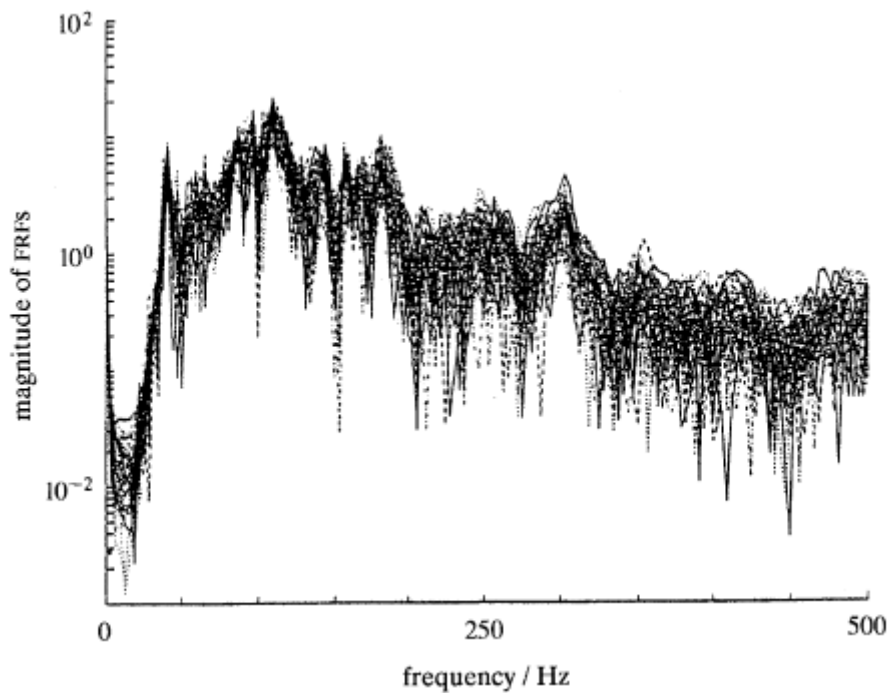


Figure 1.1 Uncertain acoustic response of pickup trucks (Fahy, 1994)

For low frequencies, the effect of uncertainty is evaluated by some statistical classifications based on experiments or deterministic methods such as finite element method, boundary element method via Monte-Carlo simulation (Evans & Swartz, 2000; Fahy, 1994; Hobenbichler & Rackwitz, 1988; Lewis & Böhm, 1984). However, for higher frequencies at which the response is sensitive to structural variations, statistical approaches such as statistical energy analysis (SEA), and power flow methods are often used. These approaches due to their average response prediction capability implicitly consider uncertainty in the systems subjected to high frequency excitations.

1.2 About Statistical Energy Analysis (SEA)

Statistical energy analysis (SEA) was developed by R. H. Lyon (Lyon & DeJong, 1998) in 1960s. This method arose from the need for the prediction of vibration response in aerospace engineering products. In those days, technology was allowing engineers to predict limited number of modes. For that reason, engineers were not able to perform analysis in higher frequencies. Then, it was suggested that determination of local vibration response can be ignored for larger systems at which high number of modes are existing. Consequently, an energy-based statistical approach known as statistical energy analysis was developed.

Statistical energy analysis (SEA) determines the response of subsystems by means of statistical parameters such as mean and variance value. Dynamic values of subsystems such as pressure, displacement, velocity, acceleration can be calculated from time-, spatial- and frequency- averaged energies.

In this method, complex structure is divided into subsystems and their parameters are determined statistically. The primary parameter for this method is the mean energies of each subsystem. Other parameters such as displacement, velocity, pressure etc. can be derived from these mean energies. Up to now, this method is successfully used in various applications such as building, automobile, ships and trains; however, it is radically evolved.

Since statistical energy analysis predicts mean response behavior of a structure, the method can be used in early design. Beside that since complex structure is divided into few subsystems, process takes less time than that of deterministic methods such as finite element method and boundary element method.

Determination of SEA parameters is very important step for an accurate analysis. Therefore, SEA assumptions and limitations should be clearly understood. First and the most important SEA assumption is that the power flow between coupled subsystems is proportional to the energy of subsystems by a coupling loss quantity.

Another important assumption of SEA is that subsystems are weakly coupled which means that coupling loss factors (CLF) should be much smaller than internal or damping loss factors (DLF). In the process of exciting subsystems, all power sources have to be uncorrelated that leads to give a chance to sum energies linearly. Further information about other limitations and assumptions of SEA can be found in (Lyon & DeJong, 1998).

As mentioned previously, SEA parameters including DLF, CLF, average modal spacing and power input need to be determined for accurate analysis. Here, the most critical parameter is coupling loss factor. Although several approaches are available in SEA, wave and modal approaches are generally used to determine the coupling loss factor. Wave approach uses wave transmission between substructures at a common boundary to compute power transmission coefficient. Modal approach uses separate modal energies to relate power transmission between subsystems at a common boundary.

In the wave approach which is also known as travelling wave approach (Fahy, 1990; Lyon & DeJong, 1998), vibration field is described in terms of superposition of travelling waves where power transfer coefficients are evaluated by transmission and reflection at boundaries. Nowadays, researchers are more likely studying on wave approach.

Lyon showed that power flow occurs between two coupled oscillators proportional to energies of oscillators (Lyon & DeJong, 1998) which is known as fundamental of modal approach. In modal approach, each mode of a subsystem couples with the other subsystem and a coupling loss factor is generated by using this procedure for larger systems.

1.3 Thesis Organization

In the thesis, high frequency analysis of composite structures interacted by themselves and an acoustic volume is mainly investigated. There are few studies on high frequency analysis of composite structures. It is believed that this thesis will fill the gap about high frequency vibro-acoustic response of composite structures. Specifically, numerical determination of SEA parameters of composite structures and analyzing acoustic volume-composite plate interaction will be other contributions of the present thesis. The thesis is organized as five chapters with supportive appendices:

- General descriptions about SEA and SEA modeling including coupling loss factor, damping loss factor, power input, modal density, impedance and modal overlap factor are given in Chapter 2. Note that, determination of coupling loss factor is given for point, line and area coupling. Power injection method which is originally an experimental procedure for evaluating coupling loss factor and damping loss factor is also given in this chapter. Then, brief explanation of Monte-Carlo simulation for uncertainty analysis is also given in this chapter.
- Chapter 3 is devoted for high frequency analysis of an acoustic volume-composite plate (AV-CP) interaction having structural uncertainty is considered via SEA and FEM.
- Chapter 4 is concerned with high frequency analysis of various types of structures (I, L and T type) composed of laminated composite plates.
- In Chapter 5, main conclusions of the study are briefed.
- In Appendix 1, computer programs used in thesis are presented.
- Finally, determination of rigidities and mechanical properties of composite structures are given in Appendix 2.

Each section in this study is presented uniquely and it has its own references for integrity.

CHAPTER TWO

MATHEMATICAL DESCRIPTIONS

2.1 Statistical Energy Analysis (SEA)

SEA equations are written by setting power balance between subsystems. A subsystem dissipates energy as (Lyon & DeJong, 1998):

$$\langle \overline{P_{i,diss}} \rangle = \omega \eta_{ii} \langle \overline{E_i} \rangle, \quad (2.1)$$

where ω is angular velocity of vibration, η_{ii} is damping loss factor (DLF), E_i is vibration energy of i^{th} subsystem, $\langle \rangle$ represents time average and over bar represent frequency average. Power transmission from i^{th} subsystem to j^{th} subsystem is expressed as (Lyon & DeJong, 1998):

$$\langle \overline{P_{ij}} \rangle = \omega \eta_{ij} \langle \overline{E_i} \rangle, \quad (2.2)$$

where η_{ij} , coupling loss factor (CLF) between i^{th} subsystem to j^{th} subsystem. Net power transmission between two subsystems can be expressed by using Equation (2.2) as:

$$\langle \overline{P_{ij}} \rangle = \omega \left(\eta_{ij} \langle \overline{E_i} \rangle - \eta_{ji} \langle \overline{E_j} \rangle \right). \quad (2.3)$$

Relation between coupling loss factors of two-connected subsystems can be determined in terms of modal density of subsystems as (Lyon & DeJong, 1998):

$$n_i(\omega) \eta_{ij} = n_j(\omega) \eta_{ji}, \quad (2.4)$$

where $n_i(\omega) = \Delta N / \Delta \omega$ is modal density of i^{th} subsystem, ΔN is number of mode in a frequency band $\Delta \omega$. Equation (2.4) can be rewritten in terms of average modal spacing (AMS):

$$\frac{\eta_{ij}}{2\pi \overline{\delta f}_i} = \frac{\eta_{ji}}{2\pi \overline{\delta f}_j}. \quad (2.5)$$

Here, $\overline{\delta f}_i$ shows AMS of i^{th} subsystem. More information about modal density and AMS are given in Section 2.2.3.

Here, power flow of between two subsystems of a structure is given in Figure 2.1 for clarifying SEA power balance.

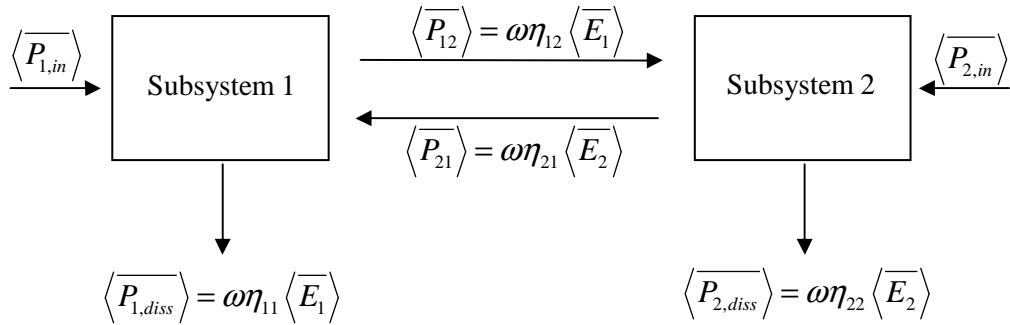


Figure 2.1 Power balance of structure having two subsystems

Each subsystem dissipates power by proportional to damping loss factor, frequency and energy of subsystem and transmits power by proportional to coupling loss factor, frequency and energy of subsystem that injects power to other subsystem. Power balance for each subsystem can be written for the first subsystem;

$$\frac{\langle \overline{P}_{1,in} \rangle}{\omega} = (\eta_{11} + \eta_{12}) \langle \overline{E}_1 \rangle - \eta_{21} \langle \overline{E}_2 \rangle, \quad (2.6)$$

and for the second subsystem;

$$\frac{\langle \overline{P_{2,in}} \rangle}{\omega} = (\eta_{22} + \eta_{21}) \langle \overline{E_2} \rangle - \eta_{12} \langle \overline{E_1} \rangle. \quad (2.7)$$

Equations (2.6) and (2.7) can also be expressed in a matrix form as:

$$\begin{bmatrix} \eta_{11} + \eta_{12} & -\eta_{21} \\ -\eta_{12} & \eta_{22} + \eta_{21} \end{bmatrix} \begin{Bmatrix} \langle \overline{E_1} \rangle \\ \langle \overline{E_2} \rangle \end{Bmatrix} = \frac{1}{\omega} \begin{Bmatrix} \langle \overline{P_1} \rangle \\ \langle \overline{P_2} \rangle \end{Bmatrix}, \quad (2.8)$$

or,

$$[\eta] \{E\} = \{P\}, \quad (2.9)$$

where vector $\{P\}$ is input power, vector $\{E\}$ is total energy of each subsystem and matrix $[\eta]$ is known as loss matrix. Energy of each subsystem can be calculated from Equation (2.9). For vibrating subsystems, velocity can be calculated by $\langle \overline{v_i} \rangle = \sqrt{\langle \overline{E_i} \rangle / m_i}$ where m_i is mass of subsystem i and for acoustic subsystems, pressure can be obtained by $\langle \overline{p_i} \rangle = \sqrt{\langle \overline{E_i} \rangle \rho_i c_i^2 / V_i}$ in terms of volume of acoustic space (V_i), density of air (ρ_i) and speed of sound (c_i). For a reliable analysis, loss matrix has to be accurately determined.

2.2 Parameters of Statistical Energy Analysis

In this section, parameters of SEA are introduced and their mathematical descriptions are presented.

2.2.1 Coupling Loss Factor (CLF) and Damping Loss Factor (DLF)

CLF and DLF are the most important parameters of SEA. They indicate the ratio of power transmission between subsystems and power converted to heat,

respectively. These parameters can be determined by experimental methods. However, for simple structures, CLFs can be computed by using some analytical approaches (Fahy, 1994; Lyon & DeJong, 1998). In this study, CLFs are determined by using wave approach in terms of transmission coefficients. Transmission coefficient can be obtained by using infinite/semi-infinite impedances of subsystems according to the type of connection. Subsystems can be connected to each other by point, line and area connections. Point connections can be supplied by bolts, pins or spot welding. In line connection, subsystems share a common line whereas in area connection, they have a common surface. Analytical derivations of CLFs can be given for point, line and area connections, respectively (Lyon & DeJong, 1998):

$$\eta_{ij}^{point} = \frac{\overline{\delta f_i}}{\pi f} \cdot \beta_{corr} \cdot \frac{\tau_{ij,\infty}(0)}{2 - \tau_{ij,\infty}(0)}, \quad (2.10)$$

$$\eta_{ij}^{line}(\theta) = \frac{\overline{\delta f_i}}{\pi f} \cdot \beta_{corr} \cdot \frac{k_i L_c \cos(\theta)}{2} \cdot \frac{\tau_{ij,\infty}(\theta)}{2 - \tau_{ij,\infty}(\theta)}, \quad (2.11)$$

$$\eta_{ij}^{area}(\phi) = \frac{\overline{\delta f_i}}{\pi f} \cdot \beta_{corr} \cdot \frac{k_i A_c \cos(\phi)}{2\pi} \cdot \frac{\tau_{ij,\infty}(\phi)}{2 - \tau_{ij,\infty}(\phi)}. \quad (2.12)$$

where,

$$\beta_{corr} = \frac{1}{\left(1 + \left(\frac{1}{2\pi(\beta_{i,net} + \beta_{j,net})}\right)^8\right)^{1/4}}. \quad (2.13)$$

and $\beta_{i,net}$ is net modal factor.

Here, k_i , L_c , A_c , τ_{ij} and $\beta_{i,net}$ are wave number, connection length, connection area, transmission coefficient and net modal factor, respectively. Modal factor can be

calculated by $f\eta_{i,net} / \overline{\delta f_i}$ in terms of net loss factor. Iteration is used for correct determination of coupling loss factor. Firstly, DLF is used in modal factor for calculating CLF. Then, net loss factor is used for satisfactory results. As it is seen in Equations (2.11) and (2.12), CLFs of line and area connections are function of incidence angles θ and ϕ . CLFs corresponding to each incidence angle should be computed and then averaged. In the process of averaging, it is assumed that energy is distributed equivalently to all incidence angles:

$$\langle \eta_{ij}^{line} \rangle_{\theta} = \frac{2}{\pi} \int_0^{\pi/2} \eta_{ij}^{line}(\theta) d\theta, \quad (2.14)$$

$$\langle \eta_{ij}^{area} \rangle_{\phi} = \frac{2}{\pi} \int_0^{\pi/2} \eta_{ij}^{area}(\phi) \sin(\phi) d\phi. \quad (2.15)$$

CLFs for line and area connections can be combined as:

$$\overline{\eta_{ij}} = \frac{\overline{\delta f_i}}{\pi f} \cdot I_{ij}^{line(area)}(k_i, k_j) \cdot \frac{\tau_{ij}(0)}{2 - \tau_{ij}(0)}, \quad (2.16)$$

where $I_{ij}^{line(area)}(k_i, k_j)$ is obtained by an integral over angle of incidence for each subsystem type. For high frequencies, transmission coefficient for normal incidence ($\theta, \phi = 0$) is determined by,

$$\tau_{ij}(0) = \frac{4 \cdot R_{i\infty} \cdot R_{j\infty}}{\left| \sum_{k=1}^s Z_{k\infty} \right|^2}. \quad (2.17)$$

Here, $Z_{k\infty}$ represents infinite system driving point impedances of subsystems at junction, $R_{i\infty}$ and $R_{j\infty}$ represent their real parts of impedances and s shows number

of subsystems at junction. For line and area couplings, transmission coefficient is calculated by using line and area impedances of subsystems at junctions.

2.2.2 Power Input

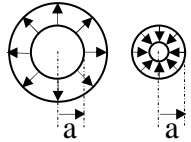
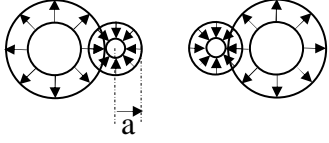
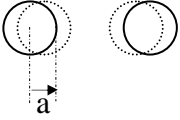
Structures can be excited by applying force, moment, sound pressure, fluid flow etc... For force and moment excitation, power injected to a structure can be written in terms of constant spectral force/moment amplitudes and driving point mobilities (Lyon & DeJong, 1998):

$$P_{in}^{tot} = P_{in}^F + P_{in}^M = (F(\omega))^2 \operatorname{Re}\{Y_0^F\} + (M(\omega))^2 \operatorname{Re}\{Y_0^M\}. \quad (2.18)$$

Here, Y_0 is driving point mobility of excited subsystem and equal to inverse of driving point impedance (Z_0), $F(\omega)$ and $M(\omega)$ are frequency dependent force and moment, respectively. If exciting force consists of discrete data, Equation (2.18) is multiplied by $\frac{1}{2}$.

For acoustic excitation, sound source type has to be determined to calculate power input. In Table 2.1, sound power of some simple sources is given (Beranek, 1992).

Table 2.1 Sound power of different acoustic sources (Beranek, 1992)

Source Type	Source Behavior	Sound Power
Monopole		$W_M = \frac{\rho c k^2 \hat{Q}_s^2}{8\pi(1+k^2 a^2)}; \hat{Q}_s = 4\pi a^2 \hat{v}_r$
Dipole		$W_D = \frac{\rho c k^4 d^2 \hat{Q}_s^2}{12\pi}; \hat{Q}_s = 4\pi a^2 \hat{v}_r$
Oscillating sphere		$W_{os} = \frac{2\pi \rho c k^4 a^6 \hat{v}_x^2}{3(4+k^4 a^4)}$

In Table 2.1, k is wave number, a is radius of sound source, \hat{v} is peak velocity on the direction of radiation, d is distance between sources.

2.2.3 Modal Density and Average Modal Spacing

To perform more realistic SEA analysis, assumptions and limitations of SEA should be considered. One of these assumptions is that each subsystem should include sufficient number of modes. Modal density is a parameter that shows mode number in a frequency band. As it is seen in Section 2.1, modal density is also used for calculating CLF from i^{th} subsystem to j^{th} subsystem when CLF from j^{th} subsystem to i^{th} subsystem is known. Modal density can be expressed as (Lyon & DeJong, 1998):

$$n(\omega) = \frac{1}{2\pi\delta f}. \quad (2.19)$$

where average modal spacing ($\overline{\delta f}$) shows average distance of two modes in terms of Hertz of a subsystem as shown in Figure 2.2. In Table 2.2, AMSs of some subsystems are shown for several waveguides.

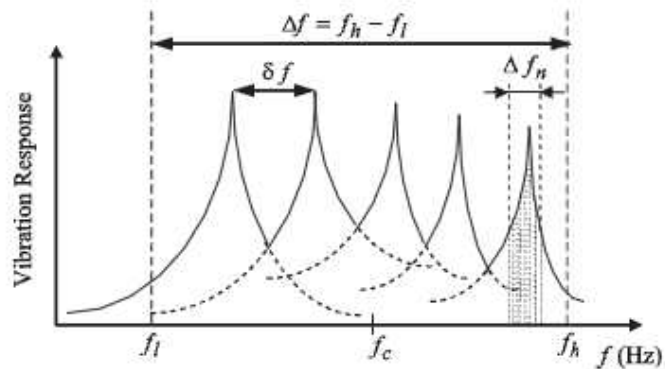


Figure 2.2 Modal spacing representation of a frequency response function

Table 2.2 Average modal spacings (AMSs) for common subsystems

Structure	Waveguide	Average Modal Spacing	Wave speed
Beam	Longitudinal	$\frac{c_L}{2L}$	$c_L = \sqrt{E_y/\rho}$
	Torsional	$\frac{c_T}{2L}$	$c_T = \sqrt{GJ/\rho I_p}$
	Flexural	$\frac{c_B}{L}$	$c_B = \sqrt{2\pi f \kappa c_L}$
Plate	Compression	$\frac{c_L'^2}{2\pi f A}$	$c_L' = \sqrt{E_y/\rho(1-\mu^2)}$
	Shear	$\frac{c_S^2}{2\pi f A}$	$c_S = \sqrt{G/\rho}$ $G = E_y/(2(1+\mu))$
	Flexural	$\frac{2\kappa c_L'}{A}$	$c_L' = \sqrt{E_y/\rho(1-\mu^2)}$
Acoustic Volume	---	$\frac{c_{air}^3}{4\pi V f^2}$	$c_{air} = 20.05\sqrt{{}^oC + 273.15}$

In the table, E_y is young modulus of subsystem, G is shear modulus, μ is poisson ratio, ρ is density, κ is radius of gyration, L is length of beam, A is area of plate, V is volume of acoustic space and $J = 4I_x I_y / (I_x + I_y)$ is torsional moment of rigidity, $I_p = I_x + I_y$ in terms of area moment of inertia I_x and I_y . For orthotropic structures, wave speeds can be approximately calculated as the geometric mean of wave speeds in two different directions x, y , i.e., $c_L = \sqrt{c_{Lx} \cdot c_{Ly}}$.

As shown in the Table 2.2, AMSs of torsional and longitudinal modes are not a function of frequency for beam where frequency dependency can be observed for flexural modes for beams. Beside that AMSs for shear and compression modes have frequency dependency for plates where flexural modes do not.

2.2.4 Infinite System Impedance

Impedance is a frequency response function that is defined as the ratio of force to velocity. In Table 2.3, driving point impedances of infinite systems are tabulated for some waveguides. In the table, r denotes radius of excitation and h represents thickness of plate. Beside force impedances, moment impedances are needed for torsional and flexural waveguides.

In the calculation of transmission coefficients, these impedances should be calibrated based on the boundary conditions. For example, point impedances for plate must be reduced by factor 2 for each free boundary and for beams by factor 4 under force excitation. Beside that acoustic impedance is reduced by factor 2 for each rigid boundary. For each pinned boundary, moment impedances are reduced by factor 2.

2.2.4.1 Dimension Reducing Principle (DRP)

As mentioned in Section 2.2.1, line and area impedances of subsystems are needed for line and area coupling. Line and area impedances can be evaluated by using “dimension reducing principle (DRP)” based on point impedance of structures. This principle is simply written as:

$$Z_{mD}^{(n)} = \frac{1}{L_{(m-1)D}} \cdot Z_{(m-1)D}^{(n-1)}, \quad (1 \leq (m, n) \leq 3 \text{ and } m \geq n). \quad (2.20)$$

Here, n stands for an integer denoting connection type in Table 2.4, and m denotes spatial dimension of the structure. Therefore, $Z_{mD}^{(n)}$ is the impedance of n th type of connection for mD th dimension structure. $L_{(m-1)D}$ is the physical parameter selected to be reduced, and is shown with dash dot arrows in Figure 2.3.

Table 2.3 Driving point impedance of structures (Lyon & DeJong, 1998)

Subsystem, Waveguide	Force Impedance	Moment Impedance
Thin beam, flexural	$2\rho A c_B (1+j)$	$\frac{2\rho A c_B}{k_B^2} (1-j)$
Thin plate, flexural	$8\rho h \kappa c'_L$	$\frac{16\rho h \kappa c_L / k_B^2}{1 + j(4/\pi) \ln\left(\frac{1}{k_B r}\right)}$
Bar, longitudinal	$2\rho A c_L$	---
Plate, inplane	$8\pi\rho h f r^2 \left(1 - \frac{j}{kr}\right)$	---
Bar, torsional	---	$2\rho I_p c_L$
Acoustic space	$\frac{\pi\rho f^2}{c} \left(1 + \frac{j}{kr}\right)$	---

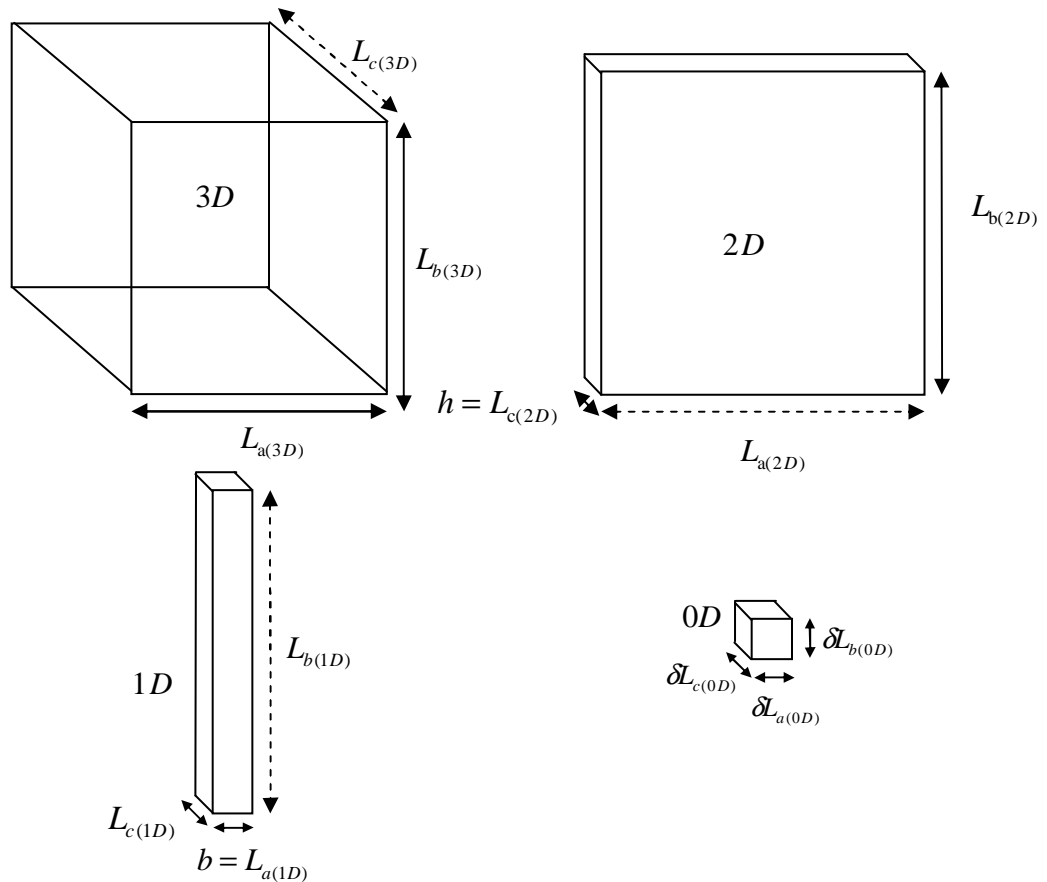


Figure 2.3 Structures and reducing dimensions

Bending line and area impedances of structures are derived by using point impedances and DRP in this section and presented in Table 2.4. In Table 2.4, m_L represents lumped mass of beam or plate.

Table 2.4 Bending line and area impedances of flexible structures obtained from point connections via dimension reducing principle

Type of Connection	Structure			
	Point ($m=0$)	Beam ($m=1$)	Plate ($m=2$)	Solid ($m=3$)
Point ($n=0$)	$j\omega m_L$	$2\rho A c_B(1+j)$	$8\rho h \kappa c_L$	$j\omega \rho V$
Line ($n=1$)	---	$j\omega \rho A$	$2\rho h c_B(1+j)$	$8\rho \kappa c_L$
Area ($n=2$)	---	---	$j\omega \rho h$	$2\rho c_B(1+j)$
Volume ($n=3$)	---	---	---	$j\omega \rho$

As an example, line impedance of 2D subsystem (plate, $Z_{2D}^{(1)}$), can be found by using point impedance of 1D subsystem (beam, $Z_{1D}^{(0)}$); the length of the plate $L_{a(2D)}$ reduces to the width of the beam b ($L_{a(2D)} \rightarrow b = L_{a(1D)}$). Therefore, line impedance of the plate subsystem is calculated by:

$$Z_{2D}^{(1)} = \frac{1}{L_{1D}} \cdot Z_{1D}^{(0)} = \frac{1}{b} \cdot 2\rho A c_B(1+j) = \frac{1}{b} \cdot 2\rho b h c_B(1+j) = 2\rho h c_B(1+j). \quad (2.21)$$

Note that, the same procedure can be applied for acoustic subsystems.

2.3 High Frequency Threshold

Modal overlap factor (MOF) is a statistical parameter that quantifies modal density in modal bandwidth (Δf_n) that is shown in Figure 2.2, and defined as $\Delta f_n / \overline{\delta f}$. For complex structures, it can be determined experimentally. MOF can also be expressed (Lyon & DeJong, 1998):

$$MOF = \frac{\pi f \eta}{2 \delta f}. \quad (2.22)$$

Here, η is damping loss factor of a subsystem. Rabbiolo et al. (2004) states that approximate MOFs can be used as an indicator for high frequency thresholds. For this purpose, the thresholds in terms of MOFs are 1, 2.5 and 3 for beams, plates and acoustic elements, respectively. However, MOF is not the only factor for deciding the threshold for high frequency transition. Observations on frequency spectra exhibiting smooth behavior should provide MOFs.

2.4 Power Injection Method (PIM)

In Section 2.2.1, analytical determination of CLF is described by using finite/semi-infinite system impedances. It is also stated that loss factors can be determined experimentally. Power injection method (PIM) (Bies & Hamid, 1980) is one of the most commonly used methods to determine the loss factors. PIM is based on the determination of random power injected to the subsystems and the measurement of the total vibrational energies of those subsystems. In this technique, first, the power is injected to the first subsystem and then total mean energies of each subsystem are measured. Normalized form of the balance equation between S number of subsystems can be written in terms of total loss quantities (factors) $\tilde{\eta}_{ij}$:

$$\begin{bmatrix} \tilde{\eta}_{11} & \tilde{\eta}_{12} & \cdots & \tilde{\eta}_{1s} \\ \tilde{\eta}_{21} & \tilde{\eta}_{22} & \cdots & \vdots \\ \vdots & \vdots & \ddots & \vdots \\ \tilde{\eta}_{s1} & \cdots & \cdots & \tilde{\eta}_{ss} \end{bmatrix} \begin{Bmatrix} E_{11}^n \\ E_{21}^n \\ \vdots \\ E_{s1}^n \end{Bmatrix} = \begin{Bmatrix} 1 \\ 0 \\ \vdots \\ 0 \end{Bmatrix} \quad (2.23)$$

where E_{ij}^n is the normalized vibrational energy, and is defined as:

$$E_{ij}^n = \frac{\omega \langle \overline{E_{ij}} \rangle}{\langle \overline{P_j} \rangle}. \quad (2.24)$$

Here, E_{ij} is the total energy of the i^{th} subsystem when the j^{th} subsystem is excited by P_j which is the injected power into the j^{th} subsystem. Then, second subsystem is excited, and the same procedure is followed. This is repeated for each subsystem, and finally following equality is obtained:

$$\begin{bmatrix} \tilde{\eta}_{11} & \tilde{\eta}_{12} & \cdots & \tilde{\eta}_{1S} \\ \tilde{\eta}_{21} & \tilde{\eta}_{22} & \cdots & \vdots \\ \vdots & \vdots & \ddots & \vdots \\ \tilde{\eta}_{S1} & \cdots & \cdots & \tilde{\eta}_{SS} \end{bmatrix} \begin{bmatrix} E_{11}^n & E_{12}^n & \cdots & E_{1S}^n \\ E_{21}^n & E_{22}^n & \cdots & \vdots \\ \vdots & \vdots & \ddots & \vdots \\ E_{S1}^n & \cdots & \cdots & E_{SS}^n \end{bmatrix} = \begin{bmatrix} 1 & 0 & \cdots & 0 \\ 0 & 1 & \cdots & \vdots \\ \vdots & \vdots & \ddots & \vdots \\ 0 & \cdots & \cdots & 1 \end{bmatrix} \quad (2.25)$$

Equation (2.25) implies that total loss quantity matrix is the inverse of the normalized energies. DLFs and CLFs are then calculated from the total loss quantities as follows:

$$\begin{cases} \eta_{ij} = -\tilde{\eta}_{ji}, & i \neq j \\ \eta_{ii} = \sum_{s=1}^S \tilde{\eta}_{si} \end{cases} \quad (2.26)$$

Normalized vibrational energy power can be approximately defined from the measured mobilities of the vibrating structures as:

$$E_{ij}^n = \frac{m\omega \langle \overline{Y_{ij}} \rangle^2}{\text{Re}\{Y_{0j}\}} \quad (2.27)$$

Here, m is mass of vibrating structure, $\langle \overline{Y_{ij}} \rangle$ is time- and frequency averaged mobility of point i under excitation of point j and $\text{Re}\{Y_{0j}\}$ is the real part of driving

point mobility. For acoustic elements, normalized energy can be calculated by using Equation (2.24) for various sound source types.

As it is seen from Equation (2.26), PIM can also estimate DLF of subsystems. If there is only one subsystem, PIM can estimate only DLF.

It should be noted that this procedure can also be numerically applied to determine CLFs by using any proper deterministic techniques. This application is then called as numerical power injection method.

2.5 Uncertainty Analysis via Monte Carlo Simulation

As mentioned before, products that are manufactured from the same production line and that have the same manufacturing processes can exhibit different vibro-acoustic response characteristics which are called as “uncertainty”.

For low frequencies, the effect of uncertainty is evaluated by some statistical classifications based on experiments or deterministic numerical methods (finite element method, boundary element method) via Monte-Carlo simulation (Evans & Swartz, 2000; Fahy, 1994; Hobenbichler & Rackwitz, 1988; Lewis & Böhm, 1984). Monte Carlo simulation is a statistical technique to predict outputs of systems that have uncertain inputs such as modeling stock market, natural events and numerical dynamic analyses. Uncertain inputs are chosen as a random distribution function and outputs are calculated for each input. But solution time increases between 100 and 1000 times for complex structures such as automobiles, planes and ships that has degree of freedom more than over a million. Beside that, degrees of freedom need to be increased with geometrical ratios that lead ineffective deterministic analyses for mid and high frequency analyses. Therefore, especially for higher frequencies, statistical and energy based approaches are much more convenient since they predict mean values both in space and frequency domains.

CHAPTER THREE

COMPOSITE PLATE-ACOUSTIC VOLUME INTERACTION

In this chapter, high frequency vibro-acoustic analysis of an enclosed system; composite plate-acoustic volume (CP-AV) having structural uncertainty is considered. There are several studies for sound transmission in plate-acoustic volume-structures; Craggs (1971) and Craik & Smith (2000) have stated that volume is an important parameter for dynamic response. Statistical energy analysis (SEA) is used to predict sound transmission by several authors (Brekke, 1981; Crocker & Price, 1969; Price & Crocker, 1970; Renji et al., 2001; Steel & Craik, 1994). Price & Crocker (1970) and Sgard et al. (2010) have examined the parameters effecting the sound transmission for such systems. Totaro et al. (2009) has determined coupling loss factor (CLF) of structure-cavity coupling by using dual modal formulation. However, as far as the author's knowledge, there is not any vibro-acoustic analysis concerning uncertain composite plate-acoustic volume interaction.

In the chapter, a CP-AV system is considered to demonstrate a reliable methodology for high frequency analysis having structural uncertainty. In this regard,

- Firstly, an SEA model for the coupled system is constructed.
- After that, SEA parameters of subsystems such as average modal spacing (AMS), CLF, damping loss factor (DLF) are analytically determined.
- Classical SEA equations are solved and mean sound pressure and velocity responses of frequency are obtained. These classical SEA results are indicated as “analytical SEA”.
- Then, finite element method (FEM) based numerical analyses are performed for the coupled structure.
- Natural frequencies are obtained to verify numerical model of subsystems and AMS of subsystems are determined.
- Afterwards, numerical power injection method (PIM) is performed to determine CLFs and DLFs.

- Computed DLFs are verified for initial DLFs for the considered system.
- Modal overlap factor (MOF) is also calculated by using computed AMSs and DLFs to approximately determine high frequency threshold.
- The data of statistical parameters computed by FEM are fed to SEA equations and solved and mean sound pressure and velocity responses of frequency are obtained. These results are indicated as “numerical SEA”.
- A set of plate thickness variation with normal (Gaussian) distribution is used to model structural uncertainty for the composite plate. Monte Carlo simulation is then performed based on frequency responses obtained by FEM. These results are indicated as “MC-FEM”.
- Finally, analytical SEA, numerical SEA and MC-FEM results are compared to discuss the methodologies performed for such kind of systems.

3.1 Classical Statistical Energy Analysis

Wave-based classical SEA approach uses infinite system impedance to compute transmission coefficients and then CLFs. One of six surfaces of the acoustic volume is assembled by a plate, while others are kept rigid. For SEA model, acoustic volume is labeled as subsystem 1 and the plate is labeled as subsystem 2 as shown in Figure 3.1. Coupling of these two subsystems are provided by line and area connections as also shown in Figure 3.1. Mechanical properties of subsystems are given in Table 3.1.

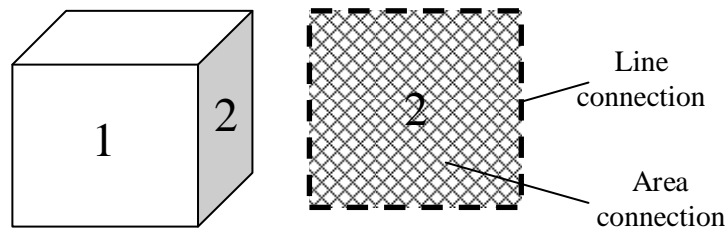


Figure 3.1 Line and area connections of acoustic volume-composite plate structure

Table 3.1 Mechanical properties of subsystems

	Acoustic volume (air)	Composite plate
Dimensions	1m x 1m x 1m	1m x 1m x 0.0025m
Young modulus along direction of x	-	21.3 [GPa]
Young modulus along direction of y	-	21.1 [GPa]
Shear modulus along direction of x	-	3003 [MPa]
Poisson ratio along direction of x (ν_{xy})	-	0.161
Density	1,225 [kg/m ³]	1771.21 [kg/m ³]
Internal Damping	0.0001	0.02

In Figure 3.2, SEA power flow diagram is given. Line and area impedances of acoustic volume are expressed to determine CLF as (Lyon & DeJong, 1998):

$$Z_{3D,a}^{line} = \rho_0 c_0 k_0 / k_p^2, \quad (3.1a)$$

$$Z_{3D,a}^{area} = \rho_0 c_0. \quad (3.1b)$$

Here, subscript 0 represents property of acoustic volume and k_p is wave number of plate which bounds the acoustic volume. CLF for line and area coupling between subsystems are determined by using the process mentioned in Section 2.2.1. Integral over angle of incidence wave that is shown in Equation (2.16) is given for acoustic volume-plate connections for line and area coupling respectively as (Lyon & DeJong, 1998):

$$I_{21}^{line} = \frac{2}{\pi} \frac{k_0 k^2 L_c}{\left(\frac{\pi}{2}\right) k_0^2 + k^2}, \quad (3.2a)$$

$$I_{21}^{area} = \frac{\frac{A_c k_0^6}{8\pi k^4}}{\sqrt{\left(1 - \frac{k_0^2}{k^2}\right)^2 \left(1 + \frac{k_0^4}{\pi k^4}\right)^2 + \frac{2}{\pi k \sqrt{A_c}}}}. \quad (3.2b)$$

Note that these results can be used for coupling losses from plate to acoustic volume i.e., CLF21 as indicated in Figure 3.3. Coupling losses from acoustic volume to plate (CLF12) can be determined by using reciprocity relation using Equation (2.5).

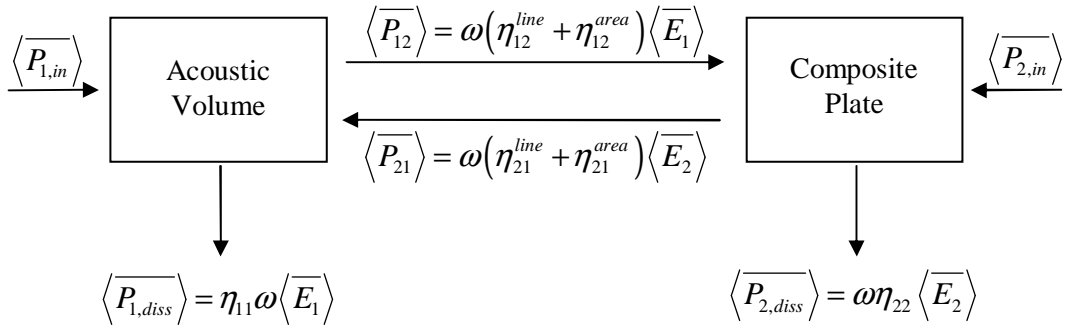


Figure 3.2 Power flow between acoustic volume and composite plate

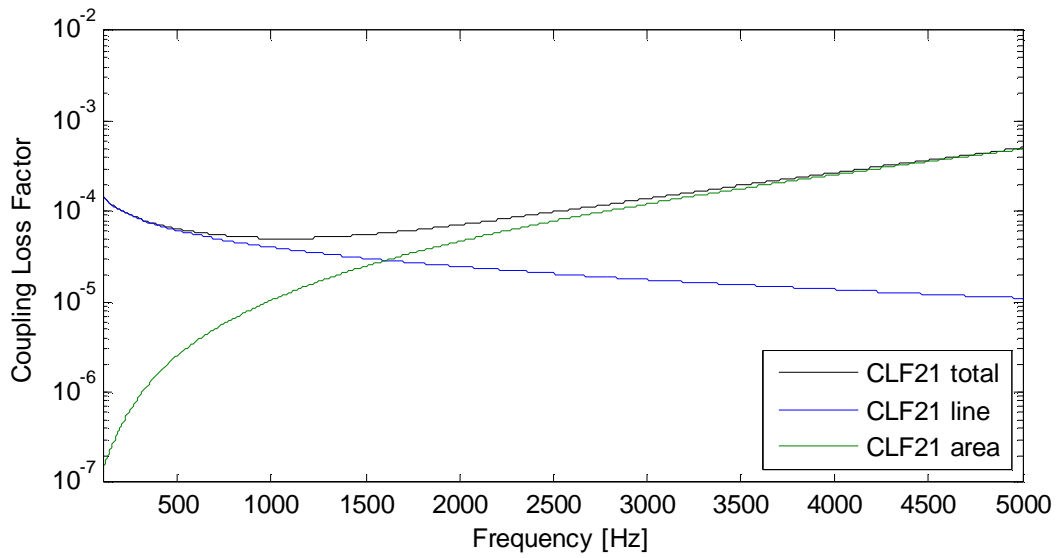


Figure 3.3 CLF between acoustic volume and composite plate

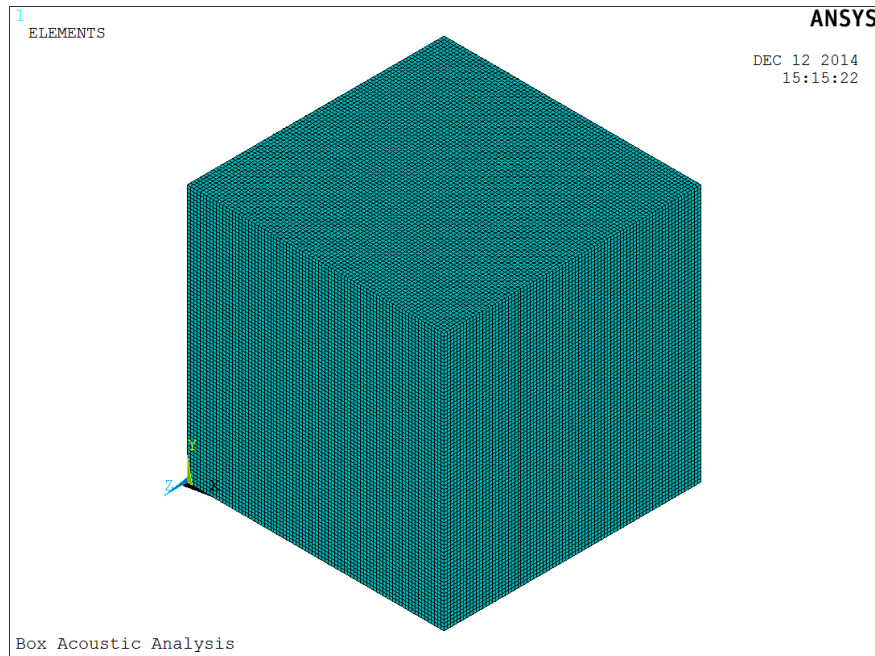
AMSs and MOFs of subsystems can be calculated for each subsystem as mentioned in Section 2.2.3 and Section 2.3, respectively. To provide integrity, these SEA parameters will be presented with numerical results in Section 3.3.

3.2 Numerical Modeling via Finite Element Method

In numerical computation of SEA parameters, finite element method software, ANSYS is utilized. In ANSYS modeling, element type shell 181 and fluid 30 are the element types those are used for plate and acoustic volume. To demonstrate the accuracy of the numerical model, natural frequencies of subsystems are determined and then compared with analytical results. Analytically, natural frequencies can be calculated for an acoustic volume with rigid walls (Nefske & Sung, 1992) as:

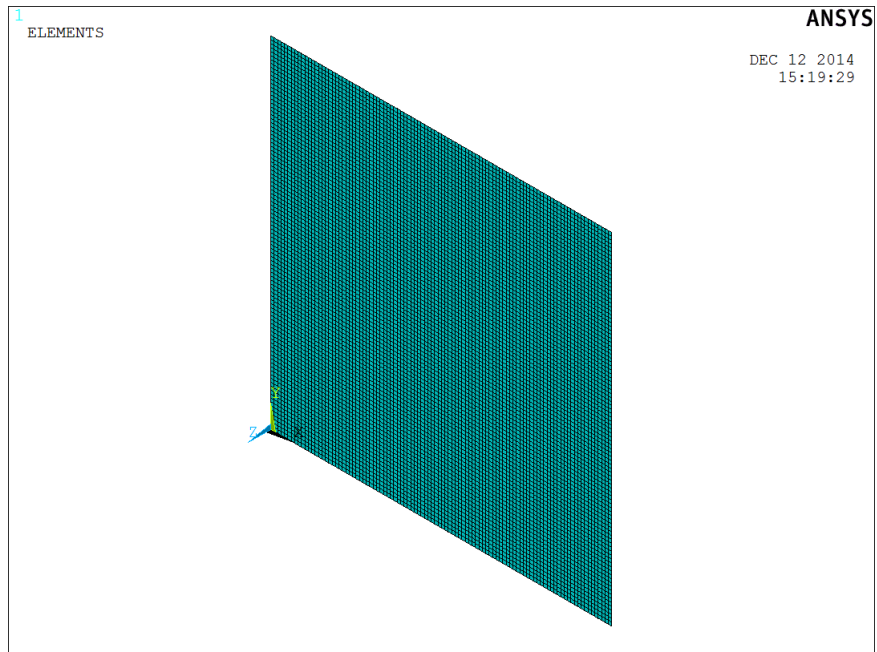
$$f_{m,n,p} = \frac{c}{2} \sqrt{\frac{m^2}{L_x^2} + \frac{n^2}{L_y^2} + \frac{p^2}{L_z^2}} . \quad (3.3)$$

where L_x , L_y and L_z are dimensions of acoustic volume on x, y and z coordinates, respectively. A MatLAB code constructing ANSYS log file including numerical model is given in Section A.1. The FEM model of the system is presented in Figure 3.4. Natural frequencies of acoustic volume are determined numerically with respect to different mesh sizes and compared with analytical results in Table 3.2.

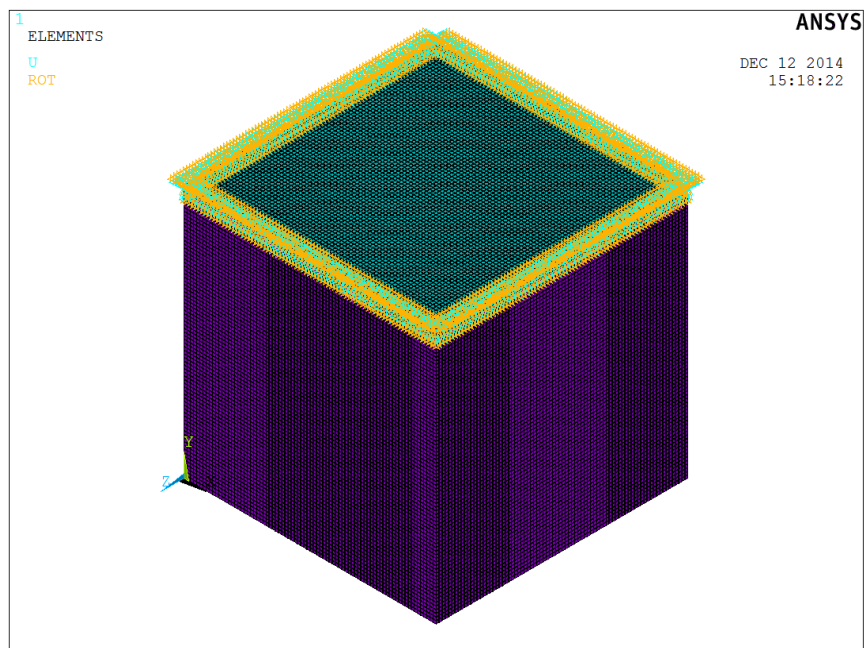


a)

Figure 3.4 Numerical model of subsystems a) Acoustic volume, b) Composite plate, c) Acoustic volume-composite plate coupling



b)



c)

Figure 3.4 Numerical model of subsystems a) Acoustic volume, b) Composite plate, c) Acoustic volume-composite plate coupling (continue)

Table 3.2 Natural frequencies of the acoustic volume

Mode Number	Numerical					Analytical
	N=20x20x20	N=30x30x30	N=40x40x40	N=50x50x50	N=60x60x60	
1	171.6764	171.5784	171.5441	171.5282	171.5196	171.5
2	171.6764	171.5784	171.5441	171.5282	171.5196	171.5
3	171.6764	171.5784	171.5441	171.5282	171.5196	171.5
4	242.7871	242.6485	242.6	242.5775	242.5653	242.5376
5	242.7871	242.6485	242.6	242.5775	242.5653	242.5376
6	242.7871	242.6485	242.6	242.5775	242.5653	242.5376
7	297.3522	297.1825	297.1231	297.0956	297.0806	297.0467
8	344.4122	343.6272	343.3527	343.2257	343.1567	343
9	344.4122	343.6272	343.3527	343.2257	343.1567	343
10	344.4122	343.6272	343.3527	343.2257	343.1567	343
11	384.828	384.0818	383.8209	383.7002	383.6346	383.4857
12	384.828	384.0818	383.8209	383.7002	383.6346	383.4857
13	384.828	384.0818	383.8209	383.7002	383.6346	383.4857
14	384.828	384.0818	383.8209	383.7002	383.6346	383.4857
15	384.828	384.0818	383.8209	383.7002	383.6346	383.4857
16	384.828	384.0818	383.8209	383.7002	383.6346	383.4857
17	421.385	420.6637	420.4115	420.2948	420.2315	420.0875
18	421.385	420.6637	420.4115	420.2948	420.2315	420.0875
19	421.385	420.6637	420.4115	420.2948	420.2315	420.0875
20	487.0724	485.9623	485.5741	485.3945	485.2969	485.0753

Natural frequencies of fully simply supported symmetrical composite plates having only orientation angle of 0-90, are expressed as (Whitney, 1987):

$$f_{m,n} = \frac{1}{2} \frac{\pi}{L_x^2} \frac{\sqrt{m^4 D_\gamma + 2m^2 n^2 \lambda^2 D_\phi + n^4 \lambda^4}}{\sqrt{\frac{\rho_0 h}{D_{22}}}} \quad (3.4)$$

Here non-dimensional parameters λ , D_γ and D_ϕ are determined as L_x/L_y , $D_\gamma = (D_{11} / D_{22})$ and $D_\phi = (D_{12} + 2D_{66}) / D_{22}$, respectively (L_x, L_y plate dimensions). Here, D_{11} , D_{12} , D_{22} and D_{66} are bending rigidities in the principal material directions and can be determined by evaluating the material matrix and z-coordinate of each laminate. Further information about determination of rigidities is given in Section A.2. Natural frequencies of the composite plate are determined with respect to different mesh sizes, and compared with analytical results in Table 3.3.

Table 3.3 Natural frequencies of the composite plates

Mode Number	Numerical					Analytical
	N=20x20	N=30x30	N=40x40	N=50x50	N=60x60	
1	5.9316	5.9291	5.928	5.9273	5.9269	5.926059
2	15.885	15.8546	15.8406	15.833	15.8284	15.82726
3	15.9056	15.8752	15.8611	15.8535	15.8489	15.82726
4	23.7933	23.7531	23.7345	23.7244	23.7183	23.70424
5	33.4843	33.3203	33.2449	33.204	33.1795	33.14356
6	33.5371	33.3729	33.2973	33.2564	33.2318	33.14356
7	39.9362	39.7868	39.718	39.6807	39.6583	39.62186
8	39.9723	39.8226	39.7537	39.7163	39.6938	39.62186
9	53.7864	53.5822	53.4879	53.4367	53.4059	53.33453
10	58.7022	58.1665	57.9213	57.7888	57.7091	57.55543
11	58.8001	58.2634	58.0178	57.885	57.8052	57.55543
12	64.3687	63.8735	63.6467	63.5241	63.4504	63.30904
13	64.4528	63.9566	63.7294	63.6066	63.5327	63.30904
14	76.2496	75.767	75.5453	75.4253	75.3531	75.20682
15	76.3016	75.8183	75.5962	75.476	75.4036	75.20682
16	91.8934	90.5524	89.9424	89.6138	89.4167	88.99348
17	92.0502	90.7068	90.0958	89.7666	89.5691	88.99348
18	96.2494	95.6008	95.2528	94.9412	94.7543	94.35709
19	97.1018	95.831	95.3021	95.0819	94.8946	94.35709
20	97.2466	95.9734	95.3941	95.1402	95.0427	94.81694

Table 3.2 and Table 3.3 show that numerical natural frequencies well converge with analytical ones as the number of elements increases.

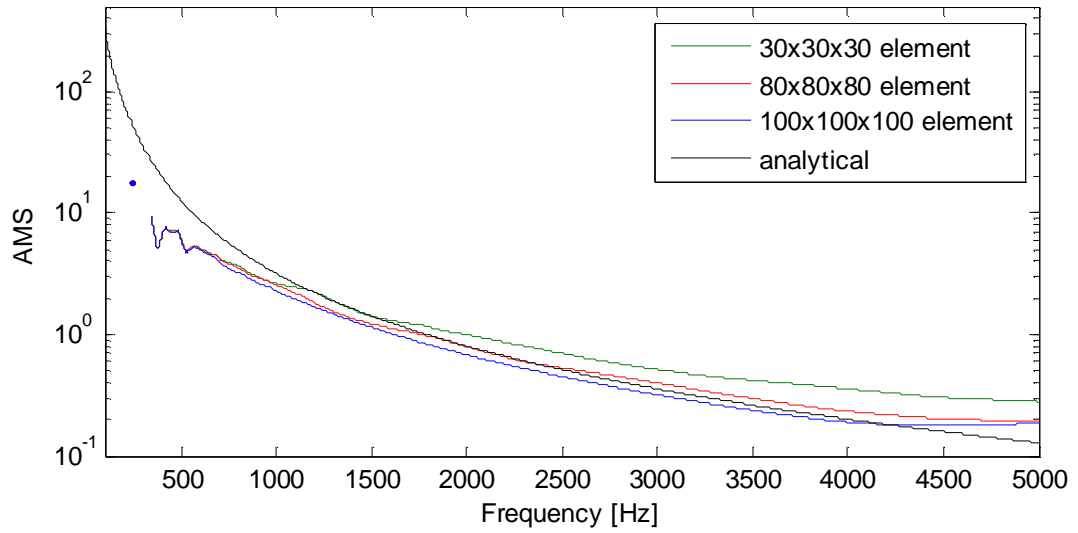
3.3 Numerical Computation of Statistical Energy Analysis (SEA) Parameters

3.3.1 Computation of AMSs

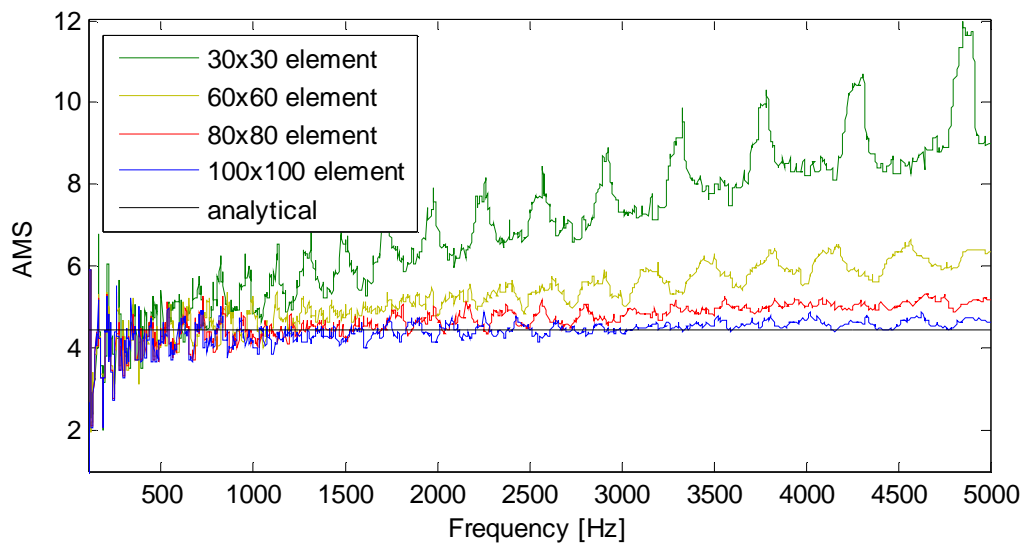
After demonstrating the accuracy of numerical model, AMSs of subsystems can be numerically determined by using natural frequencies of subsystems (Seçgin, 2013):

$$\overline{\delta f} \Big|_{\Delta f_c} = \frac{1}{P_{\Delta} - 1} \sum_{p=1}^{P_{\Delta}} (f_n)_p - (f_n)_{p-1}. \quad (3.5)$$

Here, P_{Δ} denotes number of modes in a frequency band, f_n is natural frequency and Δf_c is frequency band. In Figure 3.5, computed AMSs of Subsystem 1 and Subsystem 2 for 1/3 octave band are plotted with respect to different number of finite elements. Analytical determinations are also given in the figure. Note that analytical results in low frequencies are not reliable since there are not enough modes in this region. However, higher frequencies can be regarded as reference data. In this regard, as expected, increasing number of elements increases accuracy for numerical results for both subsystems. As shown in Figure 3.5(a), at some low frequencies, AMSs cannot be numerically calculated for the acoustic volume since there are not any modes encountered in those considered bands.



a)



b)

Figure 3.5 Average modal spacings for different number of elements for a) Acoustic volume, b) Composite plate

3.3.2 Computations of CLFs

After determination of AMSs, numerical power injection, (PIM) is applied to obtain CLFs of subsystems. Regarding memory usage and CPU time, 80 elements in each dimension of subsystems are selected in all analyses. Following the procedure given in Section 2.4, loss factors are determined numerically and are given in Figure

3.6. In the analyses, the volume is excited by 1 Pa of sound pressure, and the plate is excited by 1 N of force. Corresponding input powers to these pressure and force are determined using the evaluations in Section 2.2.2. To provide random field, spatial-averaging is performed for 200 nodes for acoustic space and 50 nodes for composite plate.

Considering Figure 3.6, obtained DLFs diverge from initially set damping values at small levels. These differences can be regarded as error of the PIM. However, they can be regarded as acceptable when considering CLFs tendencies.

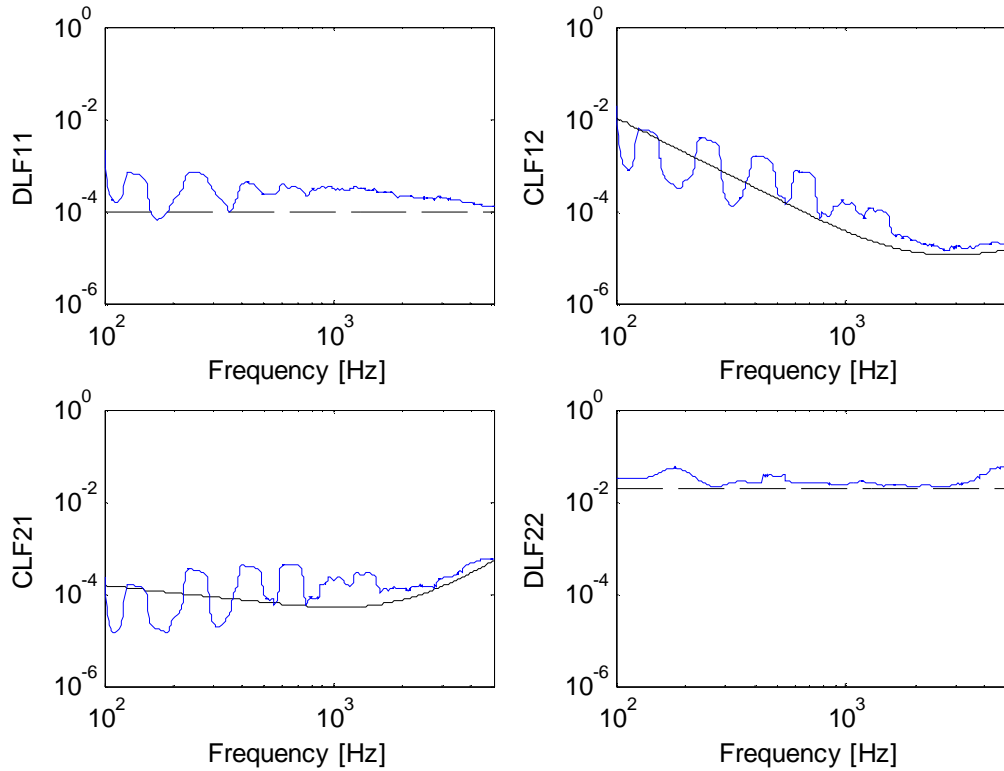


Figure 3.6 Loss factors of subsystems (black dash: initial damping, black solid: analytical CLF, blue solid: PIM results)

3.4 Response Analysis of CP-AV System Having Structural Uncertainty

In order to demonstrate the effect of structural uncertainty on vibro-acoustic response, FEM-Monte Carlo simulation is performed. The uncertainty is simulated via the variation of plate thickness with regard to normal (Gaussian) distribution. For

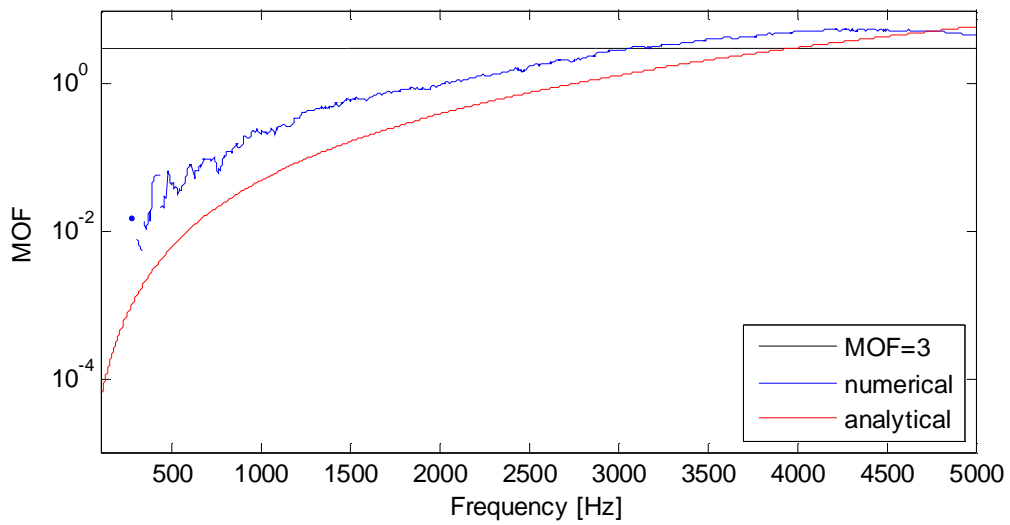
this purpose, statistical distribution of the plate thickness is selected as $h(m, \sigma) = h(0.0022, 0.025 \times 0.0022)$ mm. Then classical and numerical statistical energy analyses are employed for comparison. Analyses are performed for two different cases:

1. Acoustic excitation; it is applied to the mid-point of acoustic volume with 1 Pa.
2. Structural excitation; it is applied to the mid-point of composite plate with 1 N.

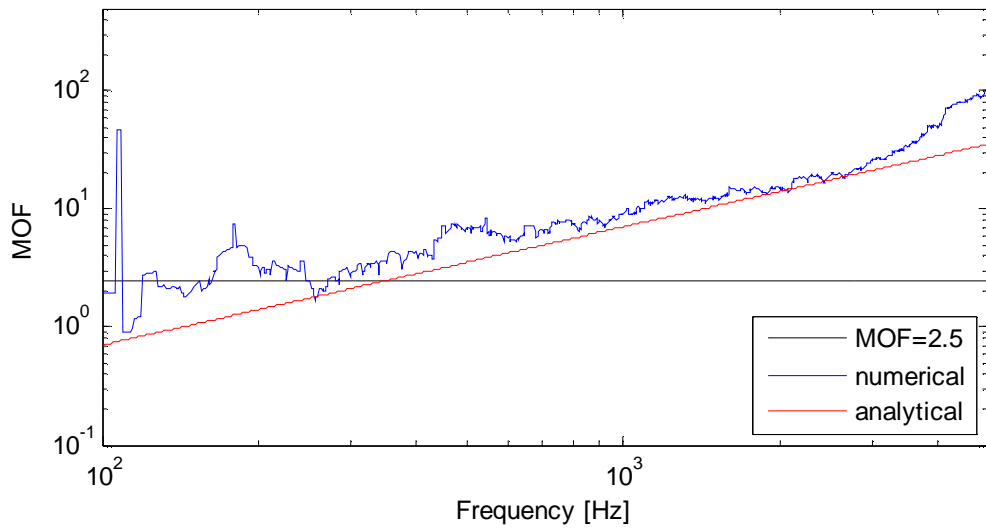
3.4.1 Determination of High Frequency Threshold

Before starting for uncertainty analysis, it is of importance to define approximate high frequency threshold. For this purpose, determining approximate MOF of each subsystem regarding the Rabbiolo *et.al.* (2004) criterion is useful; They state that approximate MOF is 2.5 for plates and 3 for acoustic volumes for thresholds. MOFs are computed via Equation (2.22) by using analytical and numerical data, and the results are given in Figure 3.7.

As shown in Figure 3.7, numerical and analytical MOFs are sufficiently consistent; the threshold for the acoustic volume is about 3800 Hz for analytical results and 3070 Hz for numerical results and it is about 270-350 Hz for the plate. These negligible inaccuracies arise from deviations in determination of AMSs and DLFs. For structural high frequency analysis, threshold value of the plate has to be considered. Therefore one can consider 270 Hz as a starting frequency of high frequency region for this system.



a)

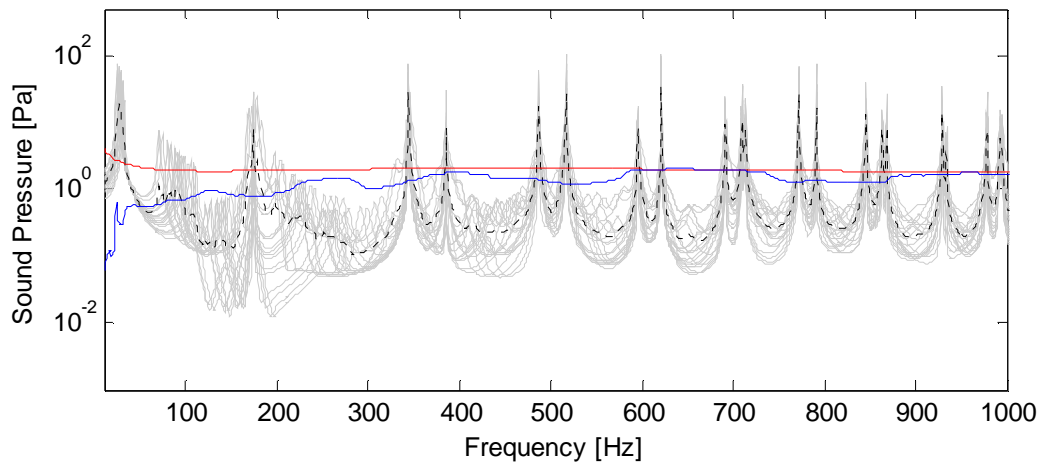


b)

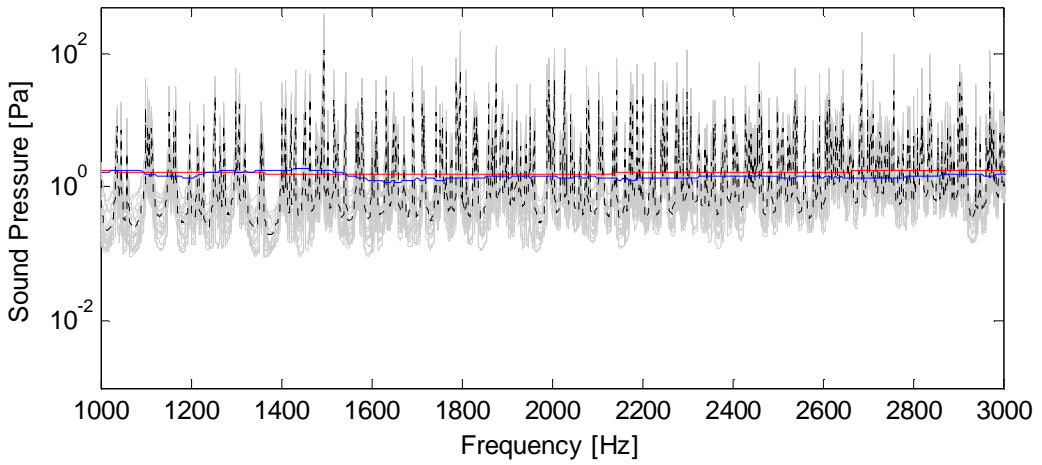
Figure 3.7 Numerical and analytical modal overlap factor of subsystems a) Acoustic volume, b) Plate

3.4.2 Acoustic Excitation

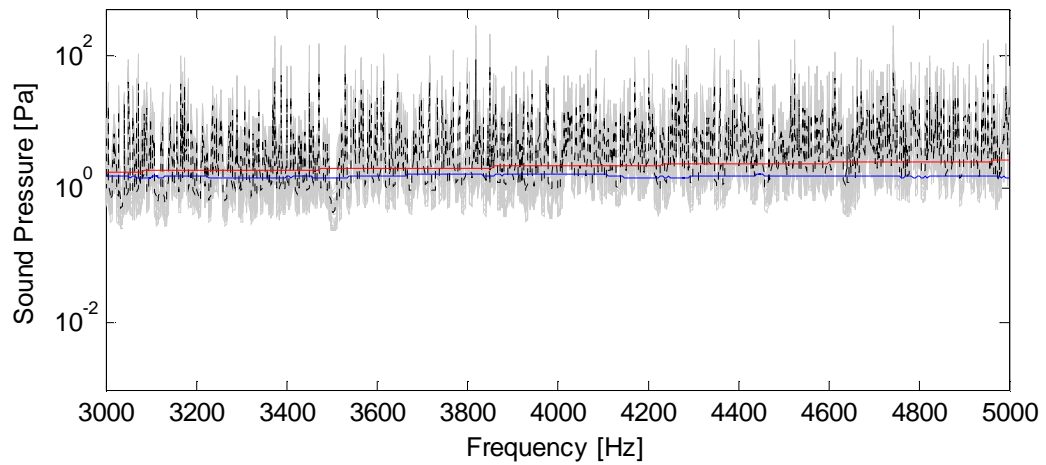
FEM-Monte Carlo analyses are performed for randomized plate thickness. Acoustic volume is excited from the mid-point by 1 Pa via a monopole spherical source with a diameter of 1/100 m. The mean sound pressure of the volume and mean velocity of the plate are compared via analytical and numerical SEA method and, are presented in Figures 3.8-3.9. The results showed that both analytical and numerical SEA are capable of predicting high frequency mean levels, however, lower frequencies have to be enhanced.



a)

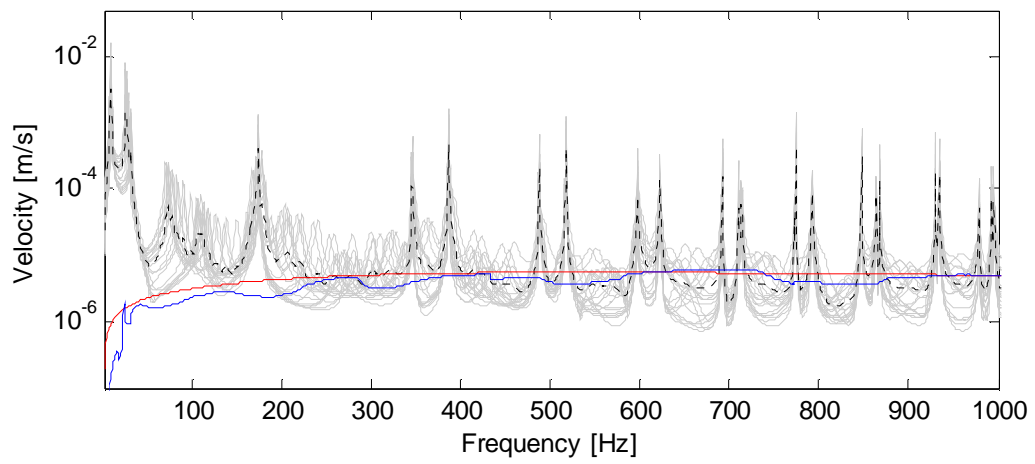


b)

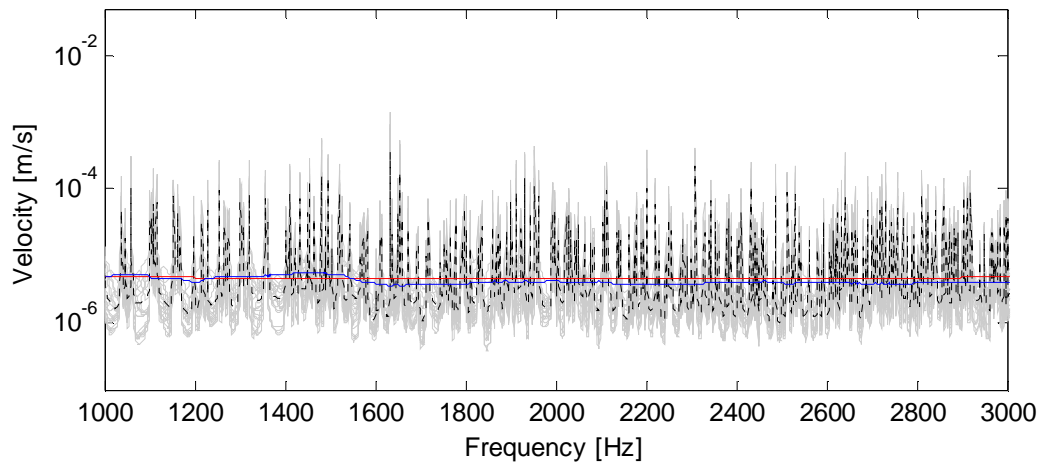


c)

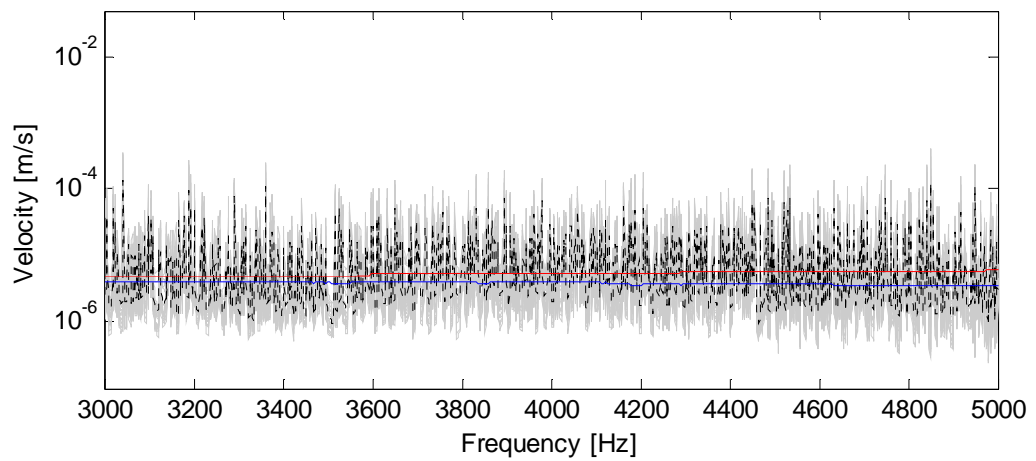
Figure 3.8 Sound pressure response of acoustic volume under acoustic excitation a) 1-1000 Hz, b) 1000-3000 Hz, c) 3000-5000 Hz (blue: numerical SEA, red: classical SEA, grey: uncertain results black dot: mean of uncertain results)



a)



b)

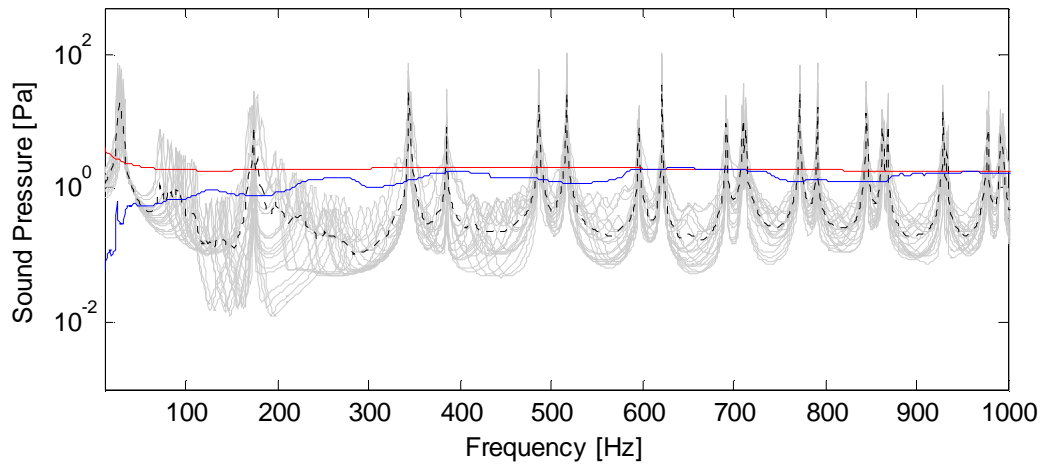


c)

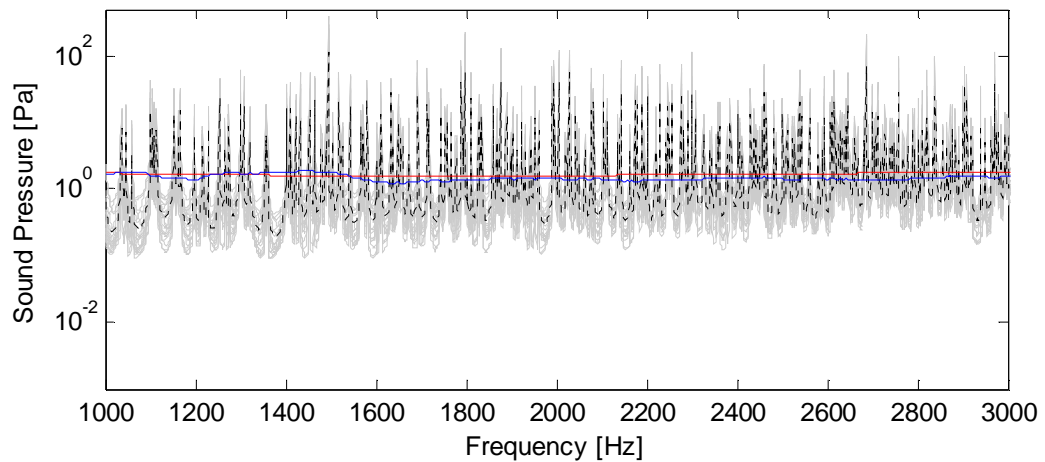
Figure 3.9 Velocity response of composite plate under acoustic excitation a) 1-1000 Hz, b) 1000-3000, Hz c) 3000-5000 Hz (blue: numerical SEA, red: classical SEA, grey: uncertain results black dot: mean of uncertain results)

3.4.3 Structural Excitation

For this case, the plate is excited from its mid-point by 1 N. Mean responses of sound pressure of the acoustic volume and vibration velocity of the plate are obtained and compared by SEA as previously done for the acoustical excitation case (Figure 3.10 and 3.11).

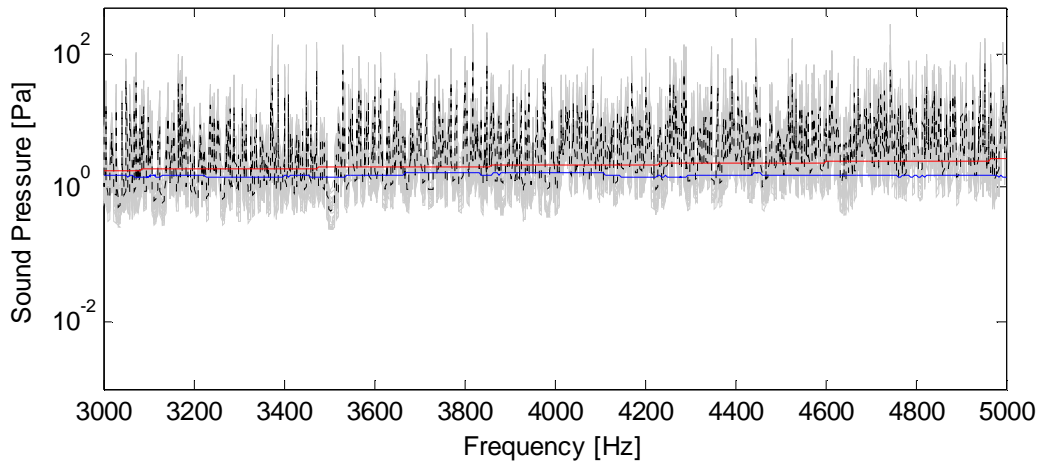


a)



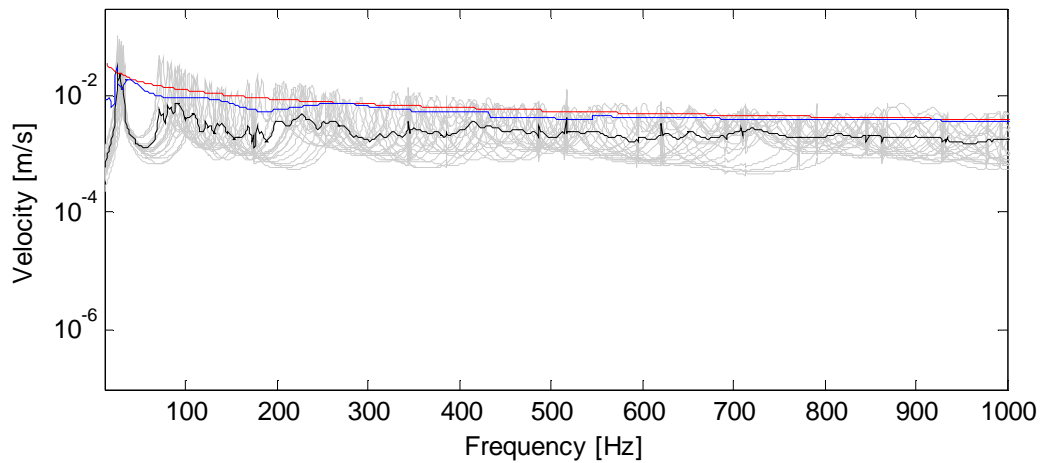
b)

Figure 3.10 Sound pressure response of acoustic volume under plate excitation a) 1-1000 Hz, b) 1000-3000 Hz, c) 3000-5000 Hz (blue: numerical SEA, red: classical SEA, grey: uncertain results black dot: mean of uncertain results)



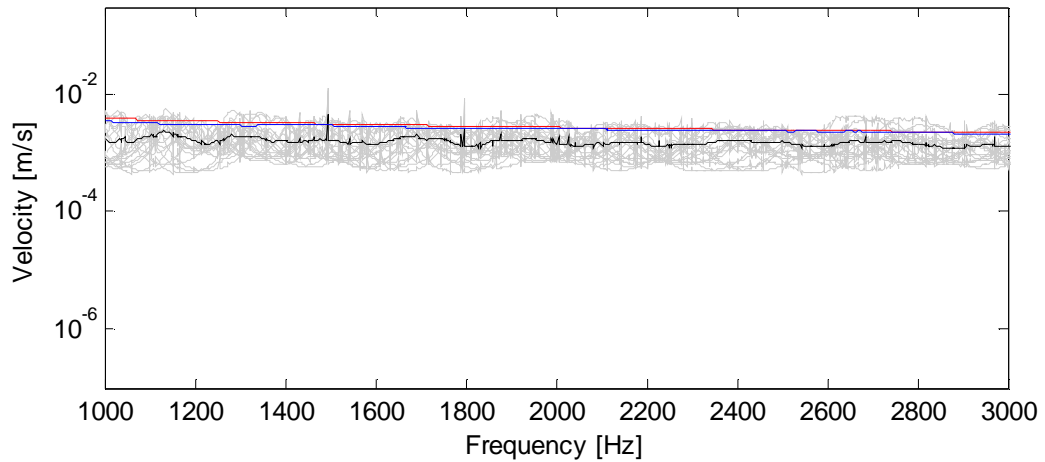
c)

Figure 3.10 Sound pressure response of acoustic volume under plate excitation a) 1-1000 Hz, b) 1000-3000 Hz, c) 3000-5000 Hz (blue: numerical SEA, red: classical SEA, grey: uncertain results black dot: mean of uncertain results) (continue)

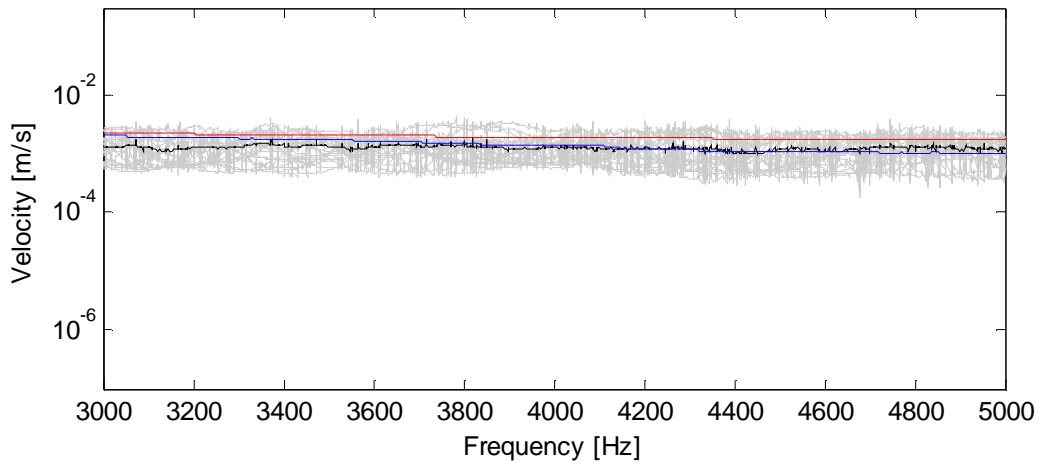


a)

Figure 3.11 Velocity response of composite plate under plate excitation a) 1-1000 Hz, b) 1000-3000 Hz, c) 3000-5000 Hz (blue: numerical SEA, red: classical SEA, grey: uncertain results black dot: mean of uncertain results)



b)



c)

Figure 3.11 Velocity response of composite plate under plate excitation a) 1-1000 Hz, b) 1000-3000 Hz, c) 3000-5000 Hz (blue: numerical SEA, red: classical SEA, grey: uncertain results black dot: mean of uncertain results) (continue)

Figure 3.8 and 3.10 represent spatial-averaged sound pressure amplitudes of 200 points in the acoustic volume and Figure 3.9 and 3.11 show spatial-averaged vibration velocity amplitudes of 50 points in the plate, in three parts; a) 1-1000 Hz, b) 1000-3000 Hz, c) 3000-5000 Hz. In these figures, as FEM-Monte Carlo simulation results, spatial averaged mean results and their mean values of 20 samples are given. Wider difference in maximum and minimum dynamic response in a frequency band means that the response is more sensitive to the plate variation and keep in mind that 270 Hz is the high frequency threshold. In this regard, considering Figure 3.8-3.11, following outcomes can be drawn;

- Main drawback of Monte Carlo simulation is that it needs high computation time and memory usage. All analyses are performed in ANSYS APDL 12.1 program with Intel Xeon E5-2643 2x3.3 GHz, 96 GB Ram, 64 Bit Win 7 workstation. The analysis took about 29490 sec = 491.5 min = 8.2 hours for just 1 sample. Performing more sensitive uncertainty analyses will take much more time that it will make analyses insufficient. These results show us that FEM-Monte Carlo simulation is not a sufficient way to consider uncertainty analysis.
- Analytical and numerical SEA results converge in high frequencies.
- The reason of inaccuracy of numerical SEA in low frequencies is the fact that since there is not enough modes in the computation of average modal spacing.
- Considering the difference of analytical SEA and numerical SEA, since the latter one uses more realistic data fed by FEM, it is much more reliable.

CHAPTER FOUR

COMPOSITE STRUCTURES

In this chapter, high frequency vibration analysis of point connected T-type composite structures having structural uncertainty is considered. As mentioned before, the success of vibration prediction of statistical energy analysis (SEA) mainly depends on the accurate prediction of loss factors. For simple structures, coupling loss factors (CLF) can be analytically determined using finite/semi-infinite system impedances/mobilities (Fahy, 1994; Lyon & DeJong, 1998); however, for relatively complex systems it requires auxiliary techniques based on numerical and/or experimental procedures. For this purpose, power injection method (PIM) (Bies & Hamid, 1980; Langhe & Sas, 1996) is a good alternative for determining loss factors of SEA without separating structure to its subsystems, i.e. as *in-situ*. Manik (1988) has developed PIM to determine loss factors for strong coupling. There are also different methods to determine coupling loss factors such as input power modulation technique (Fahy & Ruivo, 1997), dual formulation (Maxit & Guyader, 2009), spectral element method (Ahmida & Arruda, 2003) and matrix fitting method (Hodges, Nash & Woodhouse, 1987). Beside this, utilization of modal data is also used for CLF predictions; Seçgin (2013) has developed a modal-based approach for the determination of SEA parameters including CLFs for directly connected composite plates having different orientation angles. Totaro *et. al.* (2009) has used a finite element method (FEM) based modal approach for uncoupled subsystems to evaluate CLFs. Steel & Craik (1994) has also applied finite element model to determine CLF in a different manner. Fredö (1997) has combined FEM and an SEA-like approach to determine power transmission between two plates in terms of energy flow coefficients.

In this chapter, vibration response analyses of I, L and T type composite structures, as shown in Figure 4.1, having uncertain mass are considered. Composite structures are constructed by using laminated composite plates. The plates are connected to each other from three points by using corner irons. For T-type structure, there is no direct connection between the plates 1 and 2. In this study, three,

identical, eight-layered symmetrical composite plates orientated as $\{0-90-0-90-90-0-90-0\}$ are manufactured. The mechanical properties of these identical plates are measured in laboratory and given in Table 4.1. Procedure of the determination of mechanical properties is given in Appendix 2.

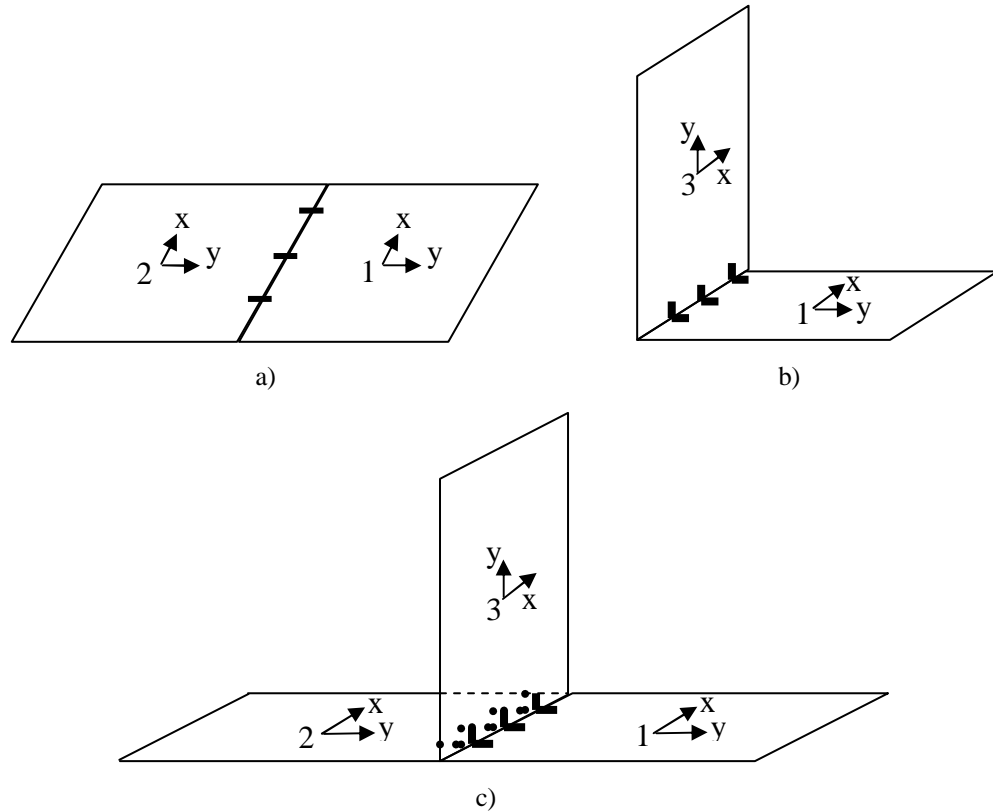


Figure 4.1 Composite structures a) I-type, b) L-type, c) T-type

In SEA, accurate determination of CLFs between subsystems is vital to predict realistic responses. For that reason, CLFs between subsystems for all types are determined via both numerical and experimental PIM and then, these results are compared with analytical CLFs. After determination of loss factors, classical (analytical) and numerical SEA are applied to have mean vibration responses. In numerical Monte-Carlo analysis for which uncertainty analysis is simulated, finite element method (FEM) is performed for each sample of normal distribution of mass variation. All these results are then compared to show the effect of uncertainty and the accuracy of SEA method with respect to the frequency range, i.e., low, mid and high frequency regions.

Table 4.1 Properties of the composite plate

Property	Value
Length along direction of x	0.5 [m]
Length along direction of y	0.6 [m]
Thickness	2.50E-03 [m]
Young modulus along direction of x	21.3 [GPa]
Young modulus along direction of y	21.1 [GPa]
Shear modulus along direction of x	3003 [MPa]
Poisson ratio along direction of x (ν_{xy})	0.161

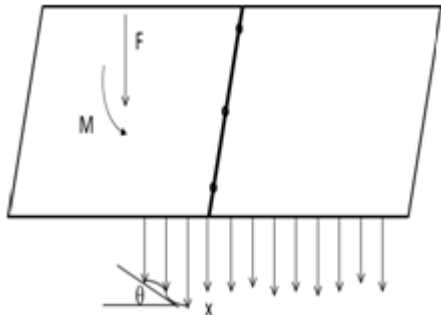
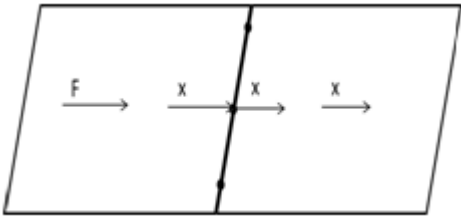
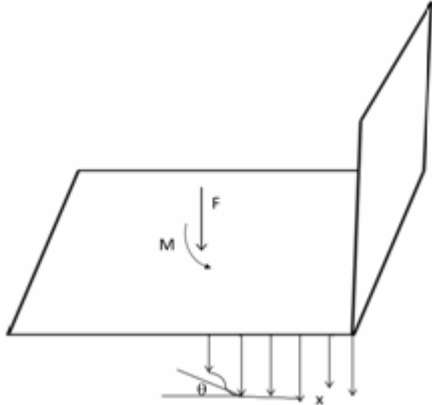
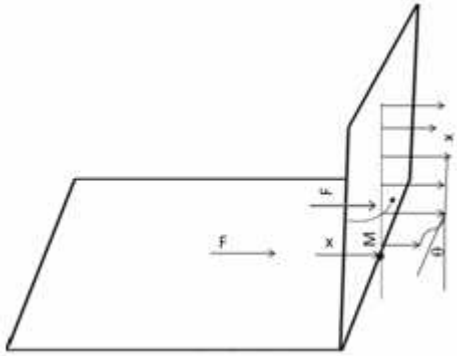
4.1 Classical Statistical Energy Analysis

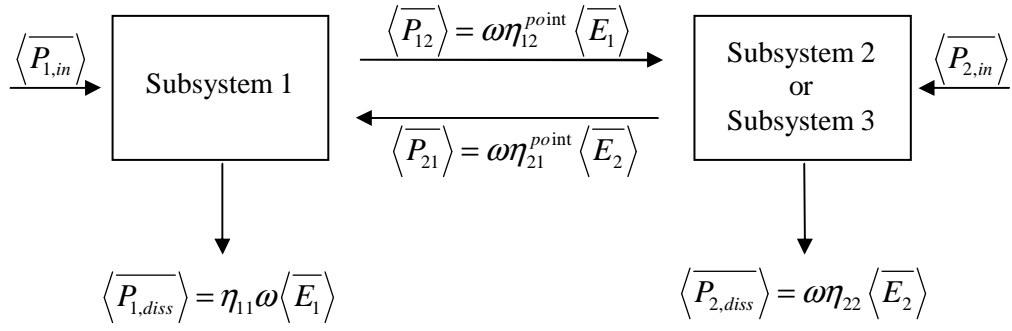
4.1.1 Force/Moment Power Transmission

As it is known, power transmission occurs by two different ways; 1) Force transmission and 2) Moment transmission. These transmissions differ according to construction of structure. In Table 4.2, force and moment transmissions for longitudinal and bending vibrations are outlined. For instance, for I type connections, both bending force and moment transmission occurs, whereas only force transmission occurs in longitudinal vibrations.

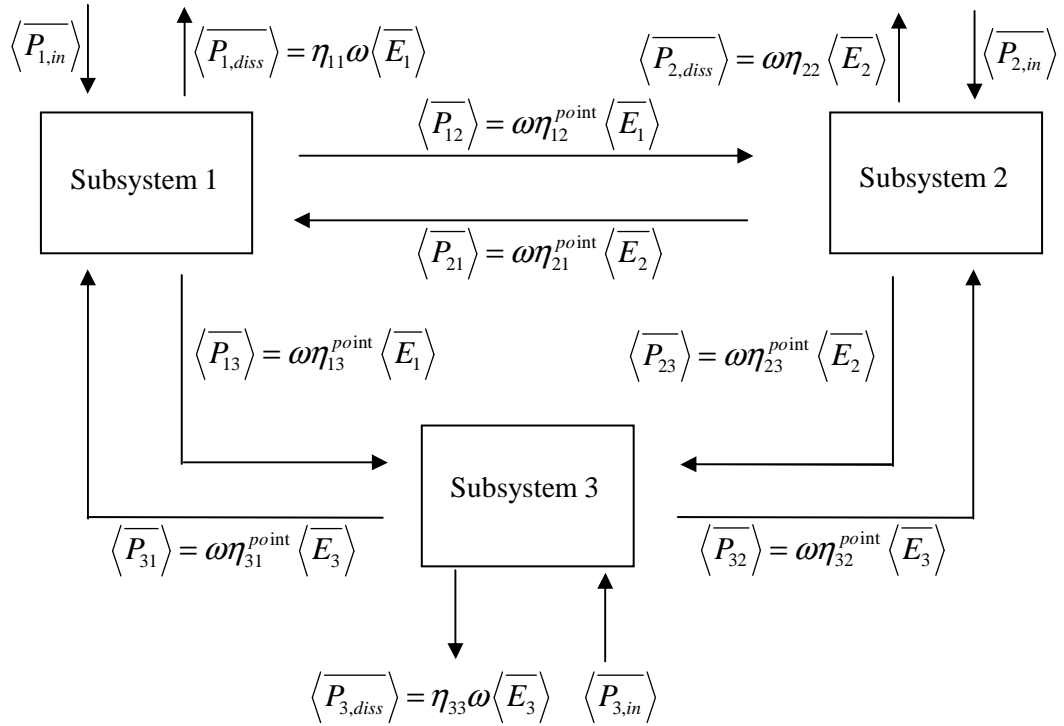
By using information that is given above, structures can be modeled for I, L and T type structure via SEA as shown in Figure 4.2. CLFs are determined by summing moment and force transmission coefficients for I type structure. Since there is no bending force transmission through the plates, only bending moment transmission coefficients are determined for L type structure. For T type structure, both moment and force transmission coefficients are considered to determine CLFs. Note that, there is no direct coupling between Plate 1 and Plate 2, however, indirect coupling exist for T type connection.

Table 4.2 Properties of the composite plate

Connection Type	Power Transmission	
	Source: 1st Plate	Receiver: 2nd Plate
	<p>Bending force power</p>	<p>Bending force power</p>
	<p>Longitudinal force power</p>	<p>Longitudinal force power</p>
	<p>Bending force power</p>	<p>Longitudinal force power</p>
	<p>Longitudinal force power</p>	<p>Bending force power</p>



a)



b)

Figure 4.2 SEA model of structures a) I/L type, b) T type

Besides, the coupling between any two plates is affected due to the coupling to the other plate. To consider this, an iterative procedure is applied between each couple. Firstly, CLFs are determined by using internal damping of subsystems and then calculated CLFs of subsystem are summed by damping loss factor (DLF) of subsystem and new CLF set are determined. This procedure can be extended until satisfactory results are evaluated. It should be also noted that, CLFs are multiplied by 3, since plates are connected from three points.

Before the determination of CLFs between plates for iterative procedure in T type structure, internal damping (damping loss factor, DLF) of plates has to be known. In this regard, firstly, an experimental PIM is applied to a single plate as proper to the procedure given in Section 2.4.

4.1.2 Determination of Internal Damping (Damping Loss Factor, DLF)

In experimental PIM, the plate is excited by a random noise signal from three different points, and point mobilities are measured from five different points. DLF of considered plate is obtained for 1/3 octave band averaging for each discrete frequency and presented in Figure 4.3. MOF is also calculated to predict approximate high frequency threshold by using Equation (2.22) and found as about 2100 Hz (Figure 4.4).

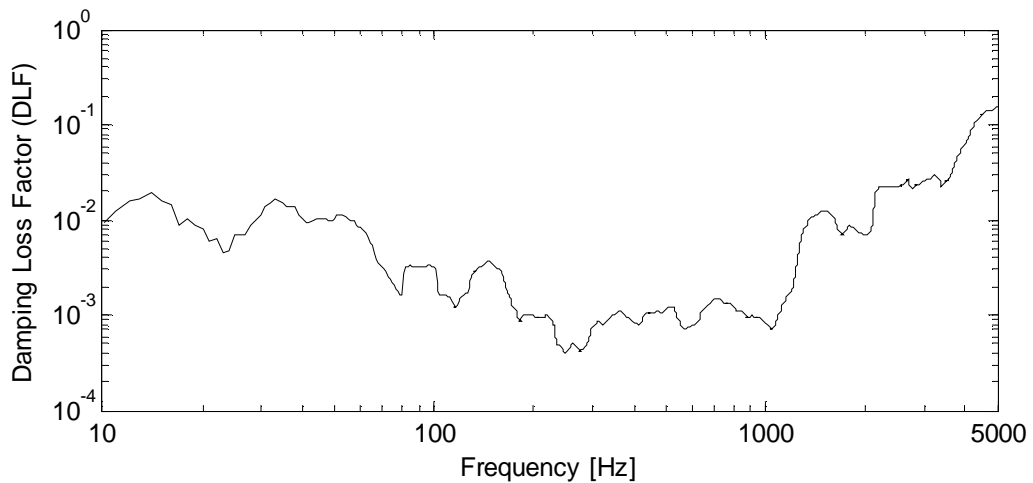


Figure 4.3 DLF of a single plate obtained by experimental PIM

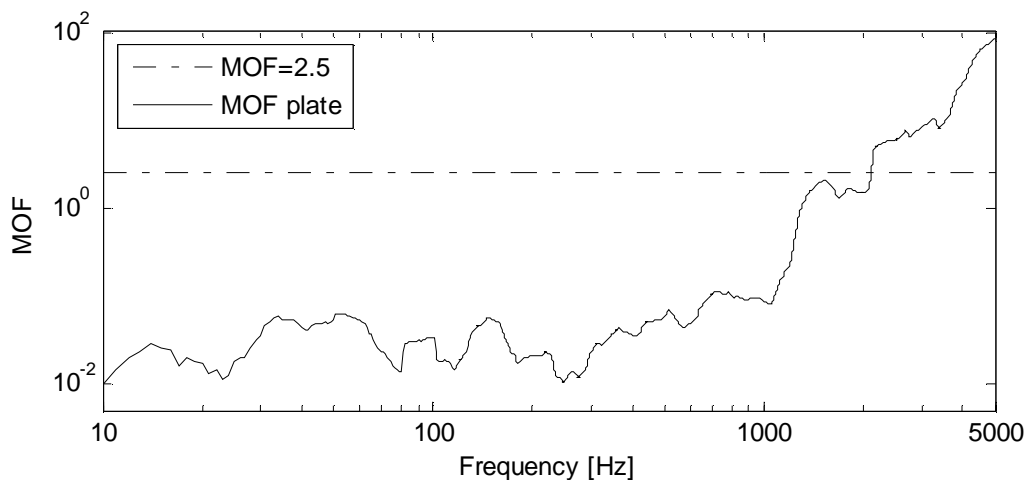
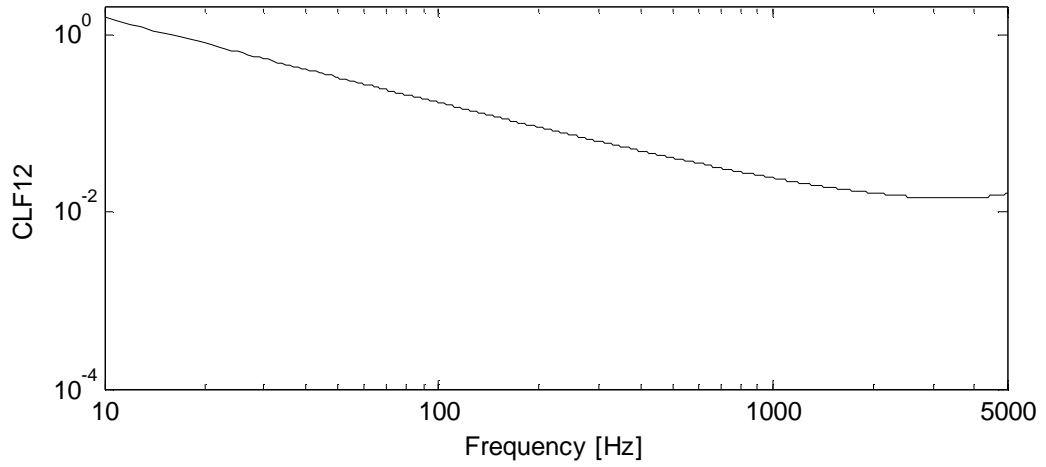


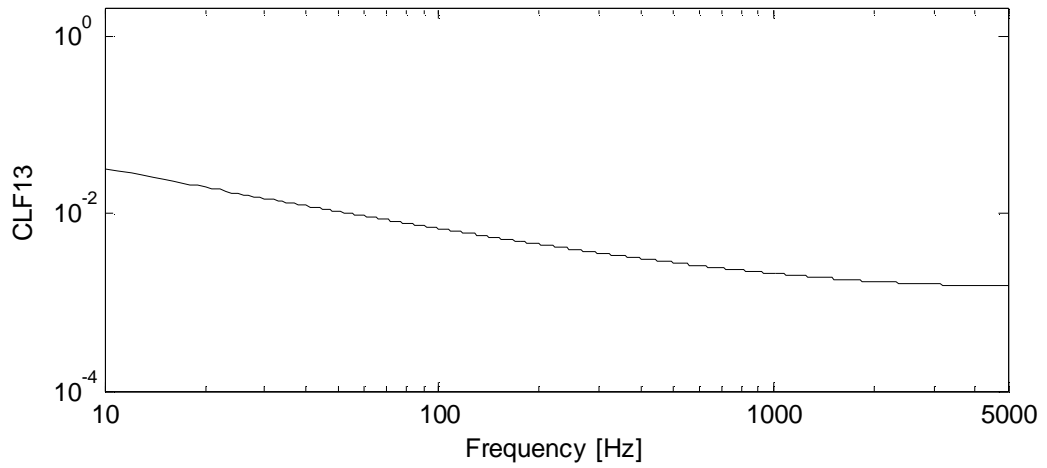
Figure 4.4 MOF of composite plate

4.1.3 Determination of Coupling Loss Factors (CLF)

In Figure 4.5, CLFs between subsystems are determined by using infinite system impedances with the procedure given in Section 2.2.1. For T type structure, it is seen that for fifth iteration, required balance is provided.

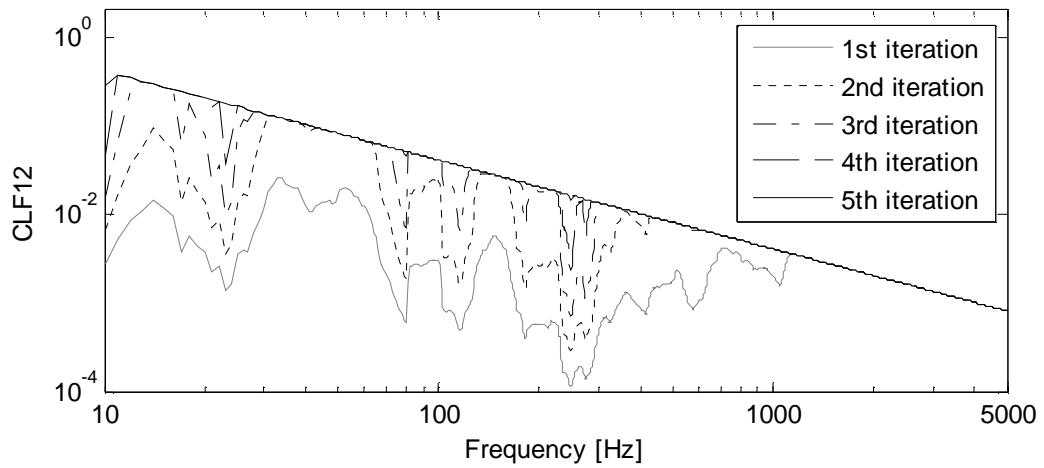


a)



b)

Figure 4.5 CLFs between subsystems a) I type, b) L type, c) T type



c)

Figure 4.5 CLFs between subsystems a) I type, b) L type, c) T type (continue)

CLF in very low frequencies for I-type connection is calculated as a value higher than 1 as shown in Figure 4.5a, this is not possible situation but it should be remembered that calculated CLFs by using infinite impedances are not accurate results in low frequency region. Analytical SEA results are given in Section 4.4 together with the other results for integrity.

4.2 Numerical Computation of Loss Factors

In numerical PIM, finite element method by ANSYS® is used. Each plate is discretised by using 25 of quadratic elements along the x-direction and 30 of quadratic elements for the y-direction. No boundary condition is applied to structure. In the process of power injection, each plate is forced from different points to simulate rain-on the roof excitation separately by random force excitation. Point mobilities of 200 different points (including driving point) are stored. Note that, it is assumed that spatially-averaged energy of each plate is well represented by mean energies of these points. After that the procedure given in Section 2.4 is followed to obtain CLF and DLFs and given in Figures 4.6-4.8, for I, L and T type structures, respectively. Beside that CLFs obtained from approximate analytical impedances are also presented in these figures for comparison. On the other hand, DLF of a single plate which is used in the computations of numerical PIM is also compared with *in*

situ DLFs of structures obtained by experimental PIM and presented in Figures 4.6-4.8.

By examining Figures 4.6-4.8, following main conclusions can be drawn;

- As shown in right diagonal of Figures 4.6-4.8, numerical DLFs of composite plates constructing the structures are coherent with DLF of a single composite plate as expected. Because, numerical analysis uses the experimental data of single plate. This shows that numerical (finite element) model and numerical procedure for power injection is successfully applied to the structures.
- Computed CLFs by numerical power injection, for each structure (I, L, and T type structures), shows no considerable discrepancies compared to approximate analytical results for higher frequencies. This is because the results at lower frequencies are not meaningful due to the fact that infinite system impedances are used in the computations.

4.3 Experimental Determination of Loss Factors

Experimental setup is built for each type of structures. Here, in Figure 4.9, only the setup for the T-type is shown. Following equipments are used to perform experiments:

1. Agilent 33210A Signal Generator
2. Bruel Kjaer Power Amplifier Type 2706
3. Bruel Kjaer Type 4809
4. PCB Impedance Head 352C33 Model
5. PCB Accelerometer 288D01
6. National Instruments 9234 4 Channel Signal Analyzer Card
7. National Instruments cDAQ 9174 chassis
8. Labview Signal Express 2012 Sound and Vibration toolkit
9. MatLAB software

All MatLAB codes to process signals are given in Appendix 1 including computations for classical SEA, numerical analysis with ANSYS and experimental analysis.

Structures are hanged by flexible ropes to supply free boundary conditions. In the process of power injection, each plate is forced from different points to simulate rain-on the roof excitation separately by a random excitation via Bruel Kjaer exciter Type 4809.

Point mobilities of 20 different points (including driving point) are stored for experimental PIM. Note that, it is assumed that spatially-averaged energy of each plate is well represented by mean energies of these points. After that the procedure given in Section 2.4 is followed to obtain CLF and DLFs and given in Figures 4.6-4.8, for I, L and T type structures, respectively.

For experimental PIM, these main conclusions can be drawn by examining Figures 4.6-4.8;

- DLFs of experimental power injection diverge from the numerical results. This can be because of the existence of the coupling to other plate(s).
- Computed CLFs by numerical and experimental power injection, for each structure (I, L, and T type structures), shows no considerable discrepancies compared to each other throughout the entire frequency range and, compared to approximate analytical results for higher frequencies.

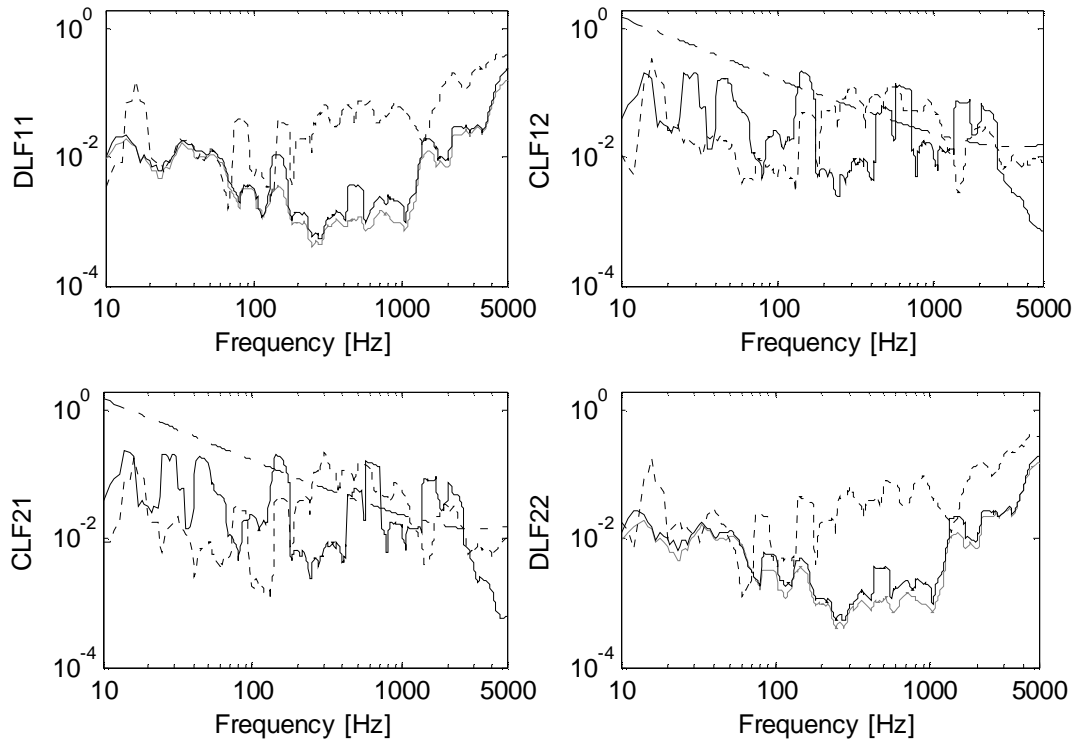


Figure 4.6 Loss factors of I-connected composite structure (dash-dot line: analytical, solid line: numerical PIM, dot line: experimental PIM, gray solid line: DLF of a single plate)

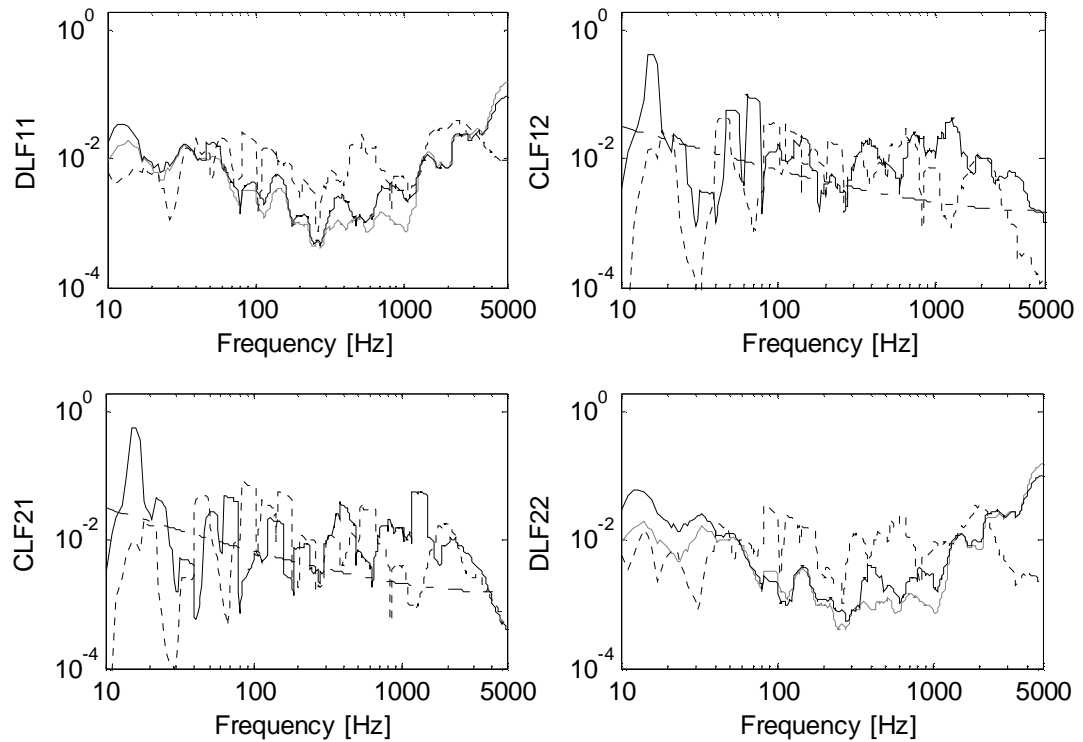


Figure 4.7 Loss factors of L-connected composite structure (dash-dot line: analytical, solid line: numerical PIM, dot line: experimental PIM, gray solid line: DLF of a single plate)

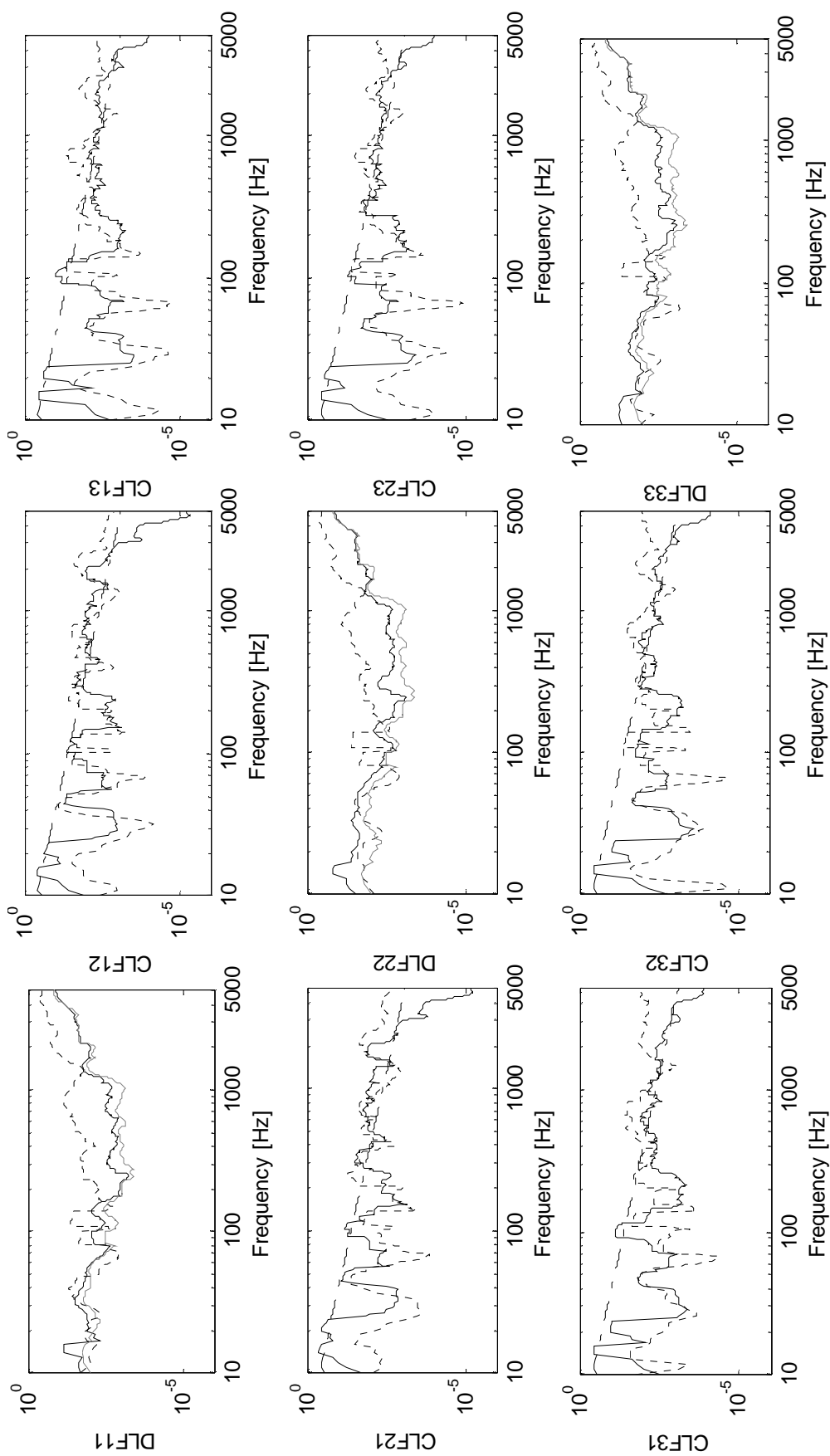


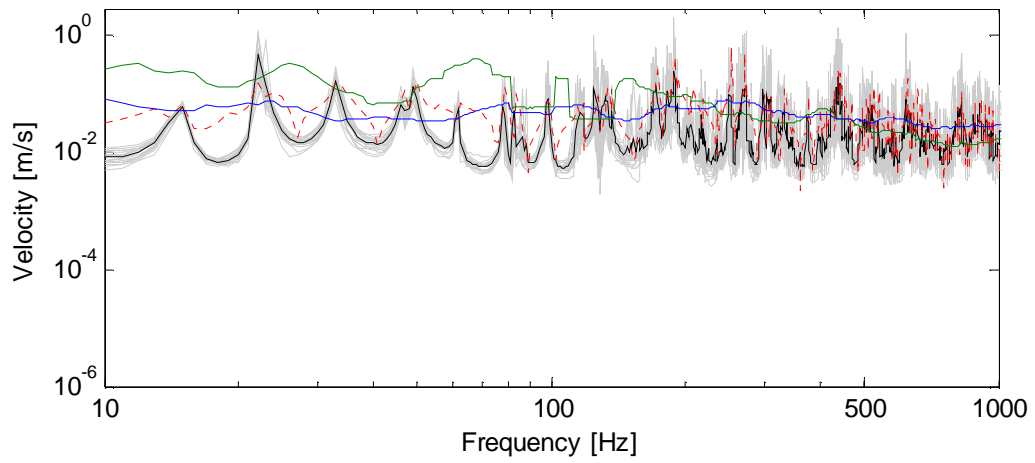
Figure 4.8 Loss factors of T-connected composite structure (dash-dot line: analytical, solid line: numerical PIM, dot line: experimental PIM, gray solid line: DLF of a single plate)



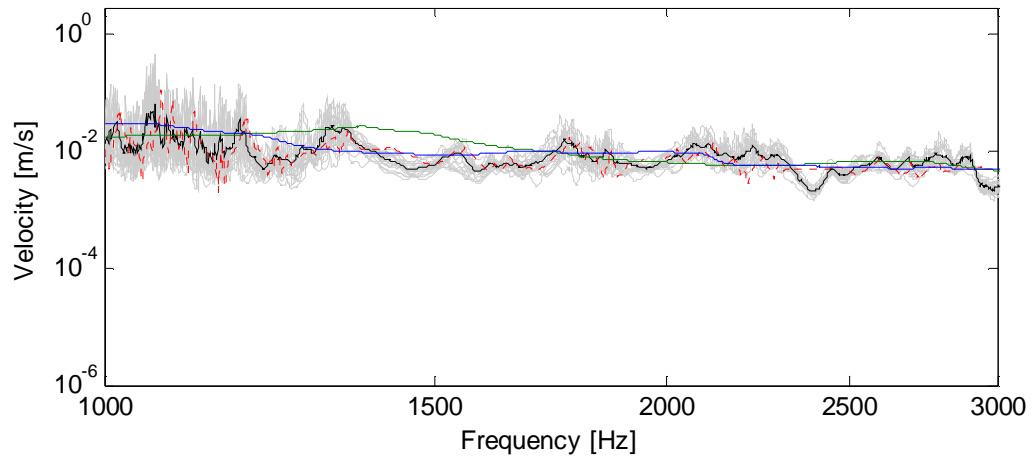
Figure 4.9 Experimental setup

4.4 Uncertainty Analysis via FEM-Monte Carlo Simulation

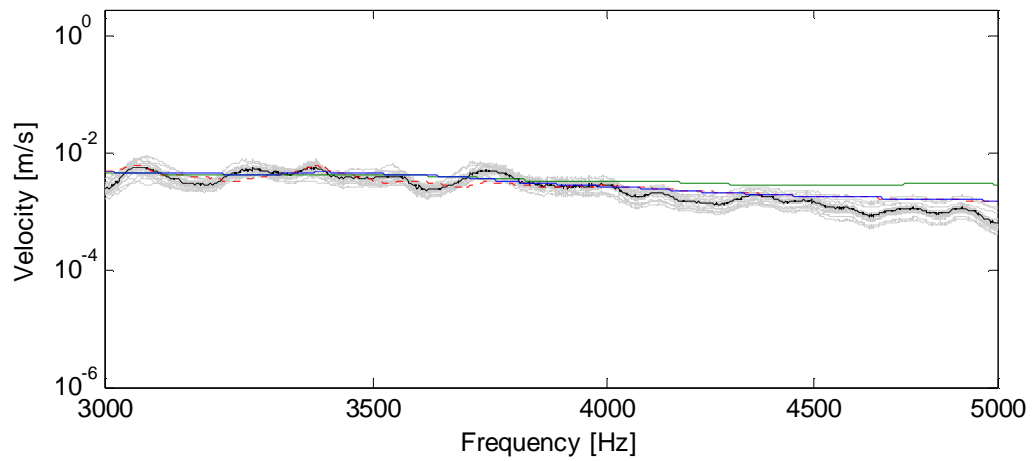
The effect of structural uncertainty on vibration response is demonstrated via FEM-Monte Carlo simulation. The uncertainty is simulated via the variation of plate mass with regard to normal (Gaussian) distribution. For this purpose, statistical distribution of the plate mass is selected as $h(m, \sigma) = h(1.169, 0.025 \times 1.169)$ mm. Note that, response of FEM-Monte Carlo simulation and SEA are examined for only excitation of subsystem 1. Subsystem 1 is excited by 1 N for FEM-Monte Carlo simulation and velocity response is taken into consideration. The results are compared with those of 1) analytical (infinite system impedances) SEA, 2) numerical SEA (numerical PIM) and 3) experimental SEA (experimental PIM). In the process of statistical energy analysis response, power input is calculated as mentioned in Section 2.2.2. By using power matrix and SEA matrix, energies of the subsystems are calculated to determine vibration velocity and presented with uncertainty results in Figures 4.10-4.12.



a)

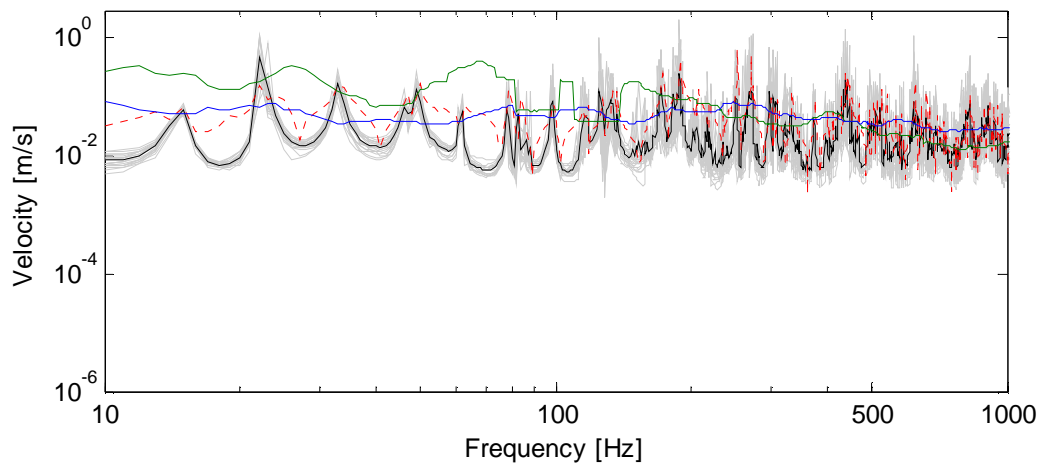


b)

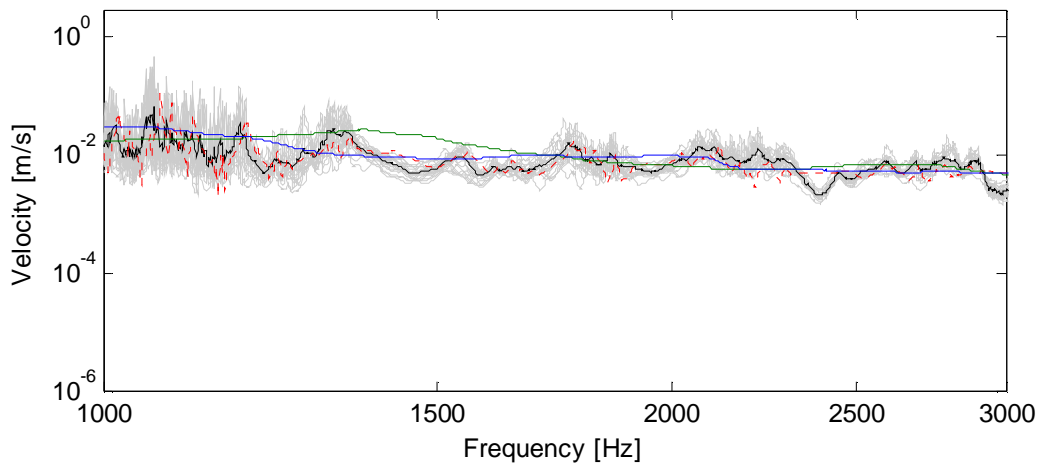


c)

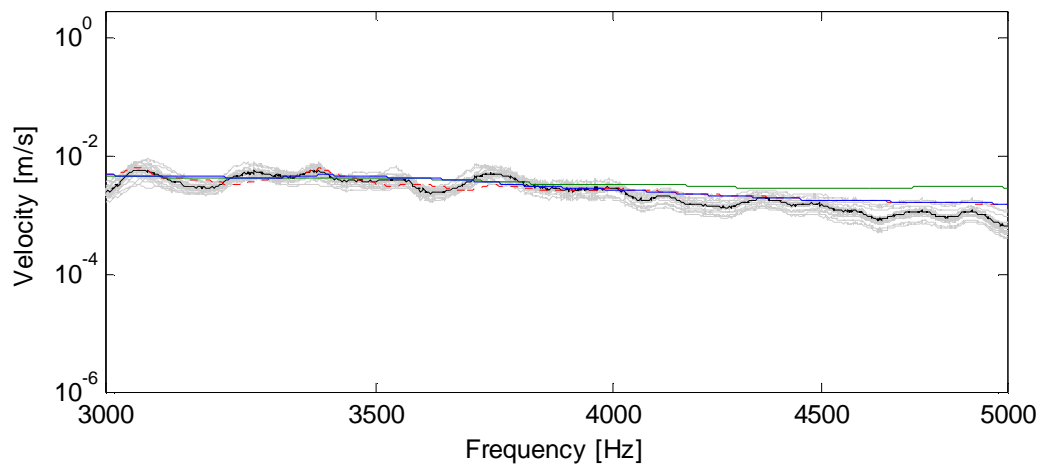
Figure 4.10 Velocity of subsystem 1, a) 10-1000 Hz, b) 1000-3000 Hz, c) 3000-5000 Hz (grey: uncertain results, black dot: mean of uncertain results, blue: classical SEA, red: numerical SEA, green: experimental SEA)



a)

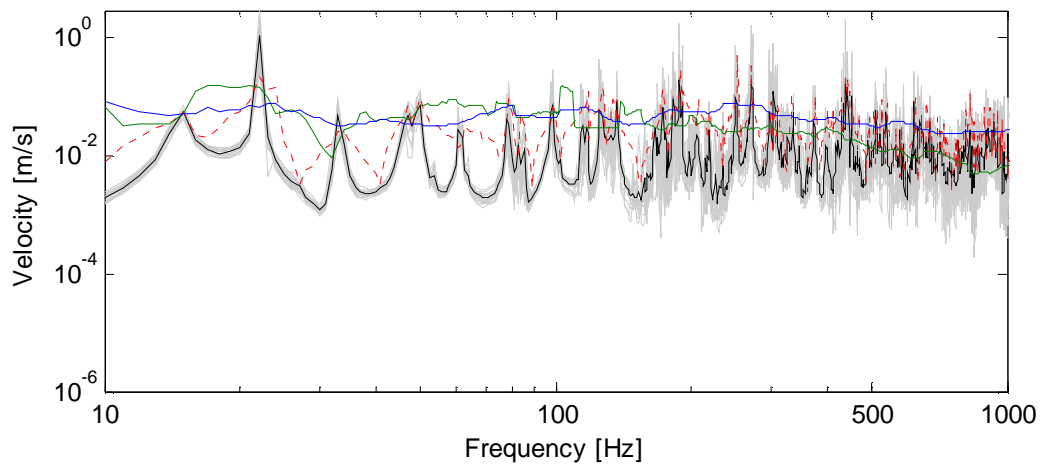


b)

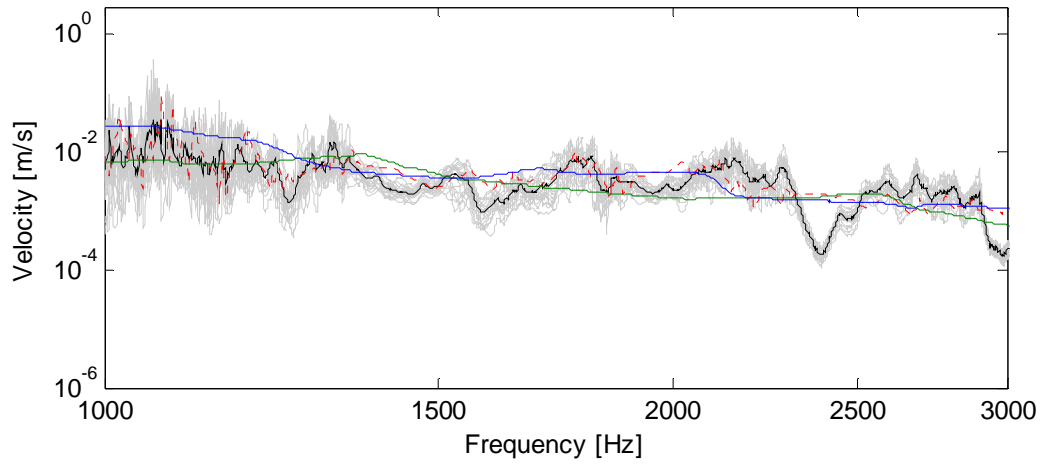


c)

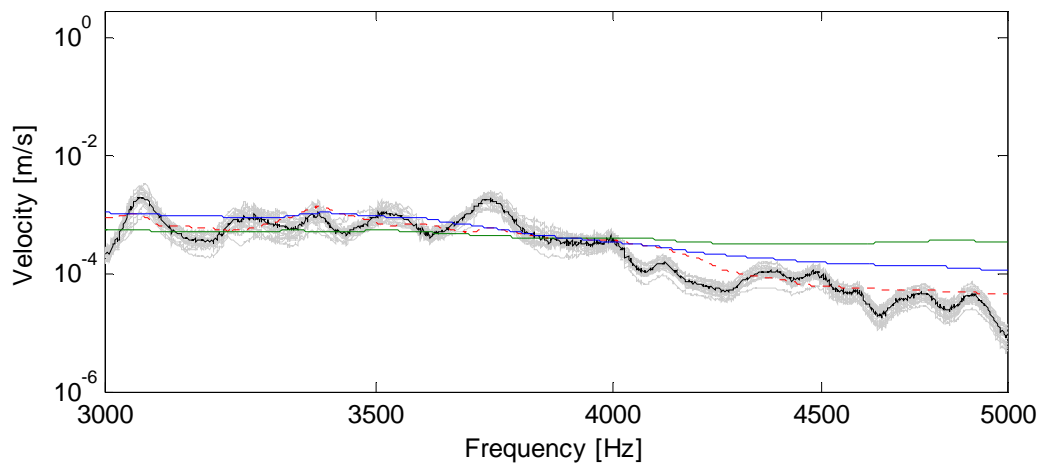
Figure 4.11 Velocity of subsystem 2, a) 10-1000 Hz, b) 1000-3000 Hz, c) 3000-5000 Hz (grey: uncertain results, black dot: mean of uncertain results, blue: classical SEA, red: numerical SEA, green: experimental SEA)



a)



b)



c)

Figure 4.12 Velocity of subsystem 3, a) 10-1000 Hz, b) 1000-3000 Hz, c) 3000-5000 Hz (grey: uncertain results, black dot: mean of uncertain results, blue: classical SEA, red: numerical SEA, green: experimental SEA)

Figure 4.10-4.12 show spatial-averaged vibration velocity amplitudes of 200 points in the plate, in three parts; a) 10-1000 Hz, b) 1000-3000 Hz, c) 3000-5000 Hz. In these figures, as FEM-Monte Carlo simulation results, spatial averaged mean results and their mean values of 20 samples are given. Wider difference in maximum and minimum dynamic response in a frequency band means that the response is more sensitive to the plate variation and keep in mind that the 2100 Hz is the high frequency threshold. In this regard, considering Figure 4.10-4.12, following outcomes can be drawn;

- As mentioned in Section 3.3.2, main drawback of Monte Carlo simulation is that it has high computation time and memory usage. Analyses are performed with the same software and computer. The analysis took about 14338 sec = 238.96 min = 3.98 hours for just 1 sample. Performing more sensitive uncertainty analyses will take much more time that it will make analyses insufficient. These results show us that FEM-Monte Carlo simulation is not a sufficient way to consider uncertainty analysis.
- As mentioned in Section 3.3.2, velocity response in mechanical excitation is more sensitive in low frequencies than in high frequencies.
- As shown in Figure 4.10-4.12, numerical SEA response can estimate the mean of uncertainty with a great accuracy also in lower frequencies (300 Hz and above).
- Response can also be predicted by using experimental SEA. But range for estimating response using experimental SEA is less than numerical SEA (1000-4000 Hz) if FEM-Monte Carlo results are assumed as reference results. Beside that it should be noted that FEM-Monte Carlo results are not reliable for very high frequencies.
- Classical SEA responses converge in high frequencies uncertainty results in high frequencies.
- The reason of inaccuracy of numerical SEA in low frequencies may be the fact that PIM is numerically inefficient in lower modes since there are not enough modes in the computation of average modal spacing.
- Finally, the study shows that SEA using PIM either numerical or experimental can reliably be used in structural systems having uncertainty.

CHAPTER FIVE

CONCLUSION

Since composite structures replaced with conventional materials in many areas in engineering, researchers have started to make investigations on their vibro-acoustic behavior. In automobile, vessel and aerospace engineering, together with preferring lightweight structures because of fuel expenses and other criteria, performing mid and high frequency analysis become much more important. Statistical energy analysis is one the most commonly used method in these areas.

In the thesis, mainly, statistical energy analysis (SEA) of composite structures consisting of laminated composite plates has been examined. Firstly, a coupled system composed of an acoustic volume-composite plate (AV-CP) is considered. For this system, SEA parameters are obtained by using analytical expressions and numerical determinations. For the numerical determination, power injection method (PIM) has been performed. It is observed that damping loss factors (DLF) is over-estimated according to the predetermined internal damping for each subsystem where coupling loss factors (CLF) converges to analytical results. The uncertainty of the system is then simulated via Monte Carlo (MC) simulation based on FEM. Thickness of the plate is selected as uncertainty parameter and vibro-acoustic responses are investigated for two different cases; 1) Plate excitation and 2) Acoustic volume excitation. It has been shown that FEM-MC responses converge to SEA using numerical/classical SEA parameters at high frequencies.

Secondly, I, L and T type composite structures composed of laminated composite plates are considered. Loss factors of these structures are determined via numerical and experimental power injection. It has been shown that numerical DLFs of structures converge to predetermined DLF which also shows correction of model. Beside that calculated CLFs have converged to each other and analytical results. Interestingly, moment and force power transmission occur between horizontal plates where there is no direct connection for T type structure. Next, mass of the plates is considered as uncertainty parameter and again FEA-MC has been carried out and

results have been compared with SEA. It has been also shown that SEA can take uncertainties into account. After these studies following main conclusions can be drawn;

- Numerical SEA can be successfully used in acoustic and composite plate interaction having structural uncertainty.
- Power injection method can be reliably used for numerically and experimentally for the computation of SEA parameters.
- FEM-MC is not an efficient way for considering uncertainty due to the CPU and memory limitations.
- Small variations in the thickness or the mass of composite plates affect the vibro-acoustic response much especially at higher frequencies.

Future works can be performed for the development of SEA to reduce its deviations in mid frequencies.

REFERENCES

- Ahmida, K.M., & Arruda, J.R.F. (2003). Estimation of the SEA coupling loss factors by means of spectral element modeling. *Journal of the Brazilian Society of Mechanical Sciences and Engineering*, 25(3), 259-263.
- Beranek, L.L. (1992). Waves and impedances. In L.L. Beranek & I.L. Ver (Eds.). *Noise and Vibration Control Engineering* (25-44). John Wiley & Sons Inc.
- Bies, D.A., & Hamid, S. (1980). In situ determination of coupling loss factors by the power injection method. *Journal of Sound and Vibration*, 70, 187–204.
- Bloss, B.C., & Rao, M.D. (2005). Estimation of frequency-averaged loss factors by the power injection and the impulse response decay methods. *Acoustical Society of America*, 117(1), 240-249.
- Brekke, A. (1981). Calculation methods for the transmission loss of single, double and triple partitions. *Applied Acoustics*, 14, 225-240.
- Cotoni, V., Shorter, P.J., & Langley, R.S. (2007). Numerical and experimental validation of a hybrid finite element-statistical energy analysis method. *Journal of the Acoustical Society of America*, 122(1), 259–270.
- Craggs, A. (1971). Transient response of a coupled plate-acoustic system using plate and acoustic finite elements. *Journal of Sound and Vibration*, 15(4), 509-528.
- Craik, R.J.M., & Smith, R.S. (2000). Sound transmission through double leaf lightweight partitions part I: Airborne sound. *Applied Acoustics*, 61, 223-245.
- Crocker, M.J., & Price, A.J. (1969). Sound transmission using statistical energy analysis. *Journal of Sound and Vibration*, 9(3), 469-486.

- DeRosa, S. & Franco, F. (2010). On the use of the asymptotic scaled modal analysis for time-harmonic structural analysis and for the prediction of coupling loss factors for similar systems. *Mechanical Systems and Signal Processing*, 24, 455–480.
- Evans, M., & Swartz, T. (2000). Approximating integrals via Monte-Carlo and deterministic methods. *Oxford University Press*, New York, United States.
- Fahy, F.J. (1994). Statistical energy analysis: a critical overview. *Philosophical Transactions of the Royal Society A: Mathematical, Physical & Engineering Sciences*, 346, 431-447.
- Fahy, F.J. & Ruivo, H.M. (1997). Determination of statistical energy analysis loss factors by means of an input power modulation technique. *Journal of Sound and Vibration*, 203(5), 763-779.
- Fredö, C.R. (1997). A SEA-like approach for the derivation of energy flow coefficients with a finite element model. *Journal of Sound and Vibration*, 199(4), 645-666.
- Hohenbichler, M., & Rackwitz, R. (1988). Improvement of second-order reliability estimates by importance sampling. *Journal of Engineering Mechanics*, 114, 2195–2199.
- Hodges, C.H., Nash P. & Woodhouse, J. (1987), Measurement of coupling loss factors by matrix fitting: An investigation of numerical procedures. *Applied Acoustics*, 22, 47-69.
- Ji, L., Mace, B.R., & Pinnington, R.J. (2006). A mode-based approach for the mid-frequency vibration analysis of coupled long and short wavelength structures. *Journal of Sound and Vibration*, 289, 148–170.

- Langhe, K.D., & Sas, P. (1996). Statistical analysis of the power injection method. *Acoustical Society of America*, 100(1), 294-303.
- Langley, R.S., & Cordioli, J.A. (2009). Hybrid deterministic-statistical analysis of vibro-acoustic systems with domain couplings on statistical components. *Journal of Sound and Vibration*, 321, 893-912.
- Langley, R.S., & Bremner, P. (1999). A hybrid method for the vibration analysis of complex structural-acoustic systems. *Acoustical Society of America*, 1657–1671.
- Lewis, E.E., & Böhm, F. (1984). Monte Carlo simulation of markov unreliability methods. *Nuclear Engineering and Design*, 77, 49-62.
- Lyon, R.H., & DeJong R.G. (1998). *Theory and application of statistical energy analysis* (2nd edition). RH Lyon Corp.
- Manik D.N. (1988). A new method for determining coupling loss factors for SEA, *Journal of Sound and Vibration*. 211(3), 521-526.
- Maxit, L., & Guyader, J-L. (2009a). Estimation of SEA coupling loss factors using a dual formulation and FEM modal information, part I: Theory. *Journal of Sound and Vibration*, 239(5), 907-930.
- Maxit, L. & Guyader, J-L. (2009b). Estimation of SEA coupling loss factors using a dual formulation and FEM modal information, part II. Numerical applications. *Journal of Sound and Vibration*, 239(5), 931-948.
- Nefske & Sung, (1992). Sound in small enclosures. In L.L. Beranek & I.L. Ver (Eds.). *Noise and Vibration Control Engineering* (145-174). John Wiley & Sons Inc.

- Price, A.J., & Crocker, M.J. (1970). Sound transmission through double panels using statistical energy analysis. *The Journal of the Acoustic Society of America*, 47(3), 683-693.
- Rabbiolo, G., Bernhard, R.J., & Milner, F.A. (2004). Definition of a high-frequency threshold for plates and acoustical spaces. *Journal of Sound and Vibration*, 277, 647–667.
- Rao, S.S., (1995). *Mechanical vibrations* (3rd ed.). Addison-Wesley Publishing Company.
- Renji, K., Nair, P.S., & Narayanan, S. (2001). Non-resonant response using statistical energy analysis. *Journal of Sound and Vibration*, 241(2), 253-270.
- Seçgin, A. (2013). Numerical determination of statistical energy analysis parameters of directly coupled composite plates using a modal-based approach. *Journal of Sound and Vibration*, 332, 361-377.
- Sgard, F., Nelisse, H., Atalla, N., Amedin, C.K. & Oddo, R. (2010). Prediction of the acoustical performance of enclosures using a hybrid statistical energy analysis: Image source model. *Acoustical Society of America*, 127(2), 784-795.
- Shorter, P.J., & Langley, R.S. (2005). Vibro-acoustic analysis of complex systems. *Journal of Sound and Vibration*, 288, 669–699.
- Steel, J.A., & Craik, R.J.M. (1994). Statistical energy analysis of structure-borne sound transmission by finite element methods. *Journal of Sound and Vibration*, 178(4), 553-561.
- Totaro, N., Dodard, C., & Guyader, J.L. (2009). SEA coupling loss factors of complex vibro-acoustic systems. *Journal of Vibration and Acoustics*, 131(4), 041009 - (1-8).

Vanmaele, C., Vandepitte, D., & Desmet, W. (2007). An efficient wave based prediction technique for plate bending vibrations. *Computer Methods in Applied Mechanics and Engineering*, 196(33-34), 3178–3189.

Vlahopoulos, N., & Zhao, X. (2001). An investigation of power flow in the mid-frequency range for systems of co-linear beams based on a hybrid finite element formulation. *Journal of Sound and Vibration*, 243(3), 445–473.

Whitney, J.M. (1987). *Structural analysis of laminated anisotropic plates*. Pennsylvania, Technomic Publishing Company Inc.

APPENDICES

A.1 Computer Programs

In this chapter, computer programs that are used in study are given. Note that “green” inscriptions are the explanation about the code.

A.1.1 Classical SEA for Composite Plate-Acoustic Volume Structure

Here, a Matlab code is created to determine the response of structure via statistical energy analysis. Note that, a similar code is utilized for composite structures (I, L and T type) where analytical impedances are shown in Table 2.3.

```
clc;clear;
% acoustic space with a flat plate
% Statistical Energy Analysis of SEA response
% subsystem 1:acoustic volume, subsystem 2:plate

f=1:1:5000; w=2*pi*f;           %Frequency
%---Properties of plate
Lp1=1;Lp2=1;                   %Dimension of plate
Ap=Lp1*Lp2;                    %Area of plate
hp=2.2*10^-3;                 %Thickness of plate
K=hp/sqrt(12);                %Radius of gyration of plate
E1=21.3e9;                    %Young Modulus of plate on direction-x
E2=21.1e9;                    %Young Modulus of plate on direction-y
rhop=1771.21;                 %Density of plate
mp=rhop*Ap*hp;               %Mass of plate
mu12=0.161;                  %Poisson ratio of plate on xy direction
mu21=E2*mu12/E1;            %Poisson ratio of plate on yx direction
cL1=sqrt(E1/(rhop*(1-mu12^2))); %Longitudinal wavespeed on direction x
cL2=sqrt(E2/(rhop*(1-mu21^2))); %Longitudinal wavespeed on direction y
```

```

cLp=sqrt(cL1*cL2); %Geometrical mean wave speed
ita22=2*0.01*ones(1,length(f)); %Damping loss factor of plate
Ls=2*(Lp1+Lp2); %Radiation length (perimeter of plate)

%---Properties of acoustic volume
Lx=1;Ly=1;Lz=1; %Dimensions of acoustic volume
Temp=20; %Temperature of air
cg2=20.046*sqrt(Temp+273.2);c0=cg2; %Speed of sound
V1=Lx*Ly*Lz; %Volume of acoustic volume
Ac=2*(Lx*Ly+Ly*Lz+Lx*Lz); %Total surface area of acoustic volume
Lc=4*(Lx+Ly+Lz); %Total length of all edges
rho0=1.2; %Density of fluid (air) at Temp
%Loop for damping of acoustic space for each frequency
for i=1:length(f);
ita11(i)=1e-4 %Damping loss factor of acoustic
volume
end
%Case=1:exciting acoustic volume, case=2:exciting plate
Case=1;
FF=1; %Excitation amplitude of plate

%Loop for determination wave speed, wave number, modal damping factor, AMS
and modal density for each frequency
for i=1:length(f);
cBp(i)=sqrt(w(i)*K*cLp); %Speed of wave
cgp(i)=2*cBp(i); %Group velocity of plate
kp(i)=w(i)/cBp(i); %Wave number of plate
k0(i)=w(i)/c0; %Wave number of acoustic space

delf1(i)=pi*c0/(k0(i)^2*V1); %Average modal spacing of acoustic
space
delf2(i)=2*K*cLp/Ap; %Average modal spacing of plate

```

```

    beta1(i)=f(i)*ita11(i)/delf1(i);           %Modal damping factor of acoustic
space
    beta2(i)=f(i)*ita22(i)/delf2(i);           %Modal damping factor of plate

%Modal damping factor correction for low frequencies
betacorr_1(i)=1/(1+(1/(2*pi*(beta1(i)+beta2(i))))^8)^(1/4);

nwp(i)=1/(2*pi*delf2(i));                     %Modal density of plate
nw1(i)=V1*w(i)^2/2/pi^2/c0^3+...
    Ac*w(i)/8/pi^2/c0^2+...
    Lc/16/pi/c0;                               %Modal density of acoustic volume
end

%Loop for impedances, transmission coefficients and coupling loss factors for each
frequency
for i=1:length(f);
    Z2(i)=1j*w(i)*rho0*hp;                     %Area impedance of plate
    Z1(i)=rho0*c0;                             %Area impedance of acoustic volume
    ReZ2(i)=abs(Z2(i));                       %Real part of area plate impedance

%Area transmission coefficient
to21a(i)=4*ReZ2(i)*real(Z1(i))/(abs(Z1(i)+Z2(i)))^2;

%Integral for area coupling over incident angle
I21a(i)=(Ap/(8*pi)*k0(i)^6/kp(i)^4)/sqrt((1-k0(i)^2/kp(i)^2)^2*(1+k0(i)^4
/(pi*kp(i)^4))^2+2/(pi*kp(i)*sqrt(Ap)));

%Area coupling loss factor from plate and acoustic volume
ita21a(i)=delf2(i)/pi/f(i)*betacorr_1(i)*I21a(i)/(2-to21a(i));

Z1l(i)=rho0*c0*k0(i)/2;                       %Line impedance of acoustic volume

```

```

Z2l(i)=2*rhop*cgp(i)*hp*kp(i)^2*(1+1j);%Line impedance of plate

%Line transmission coefficient
to21l(i)=4*real(Z2l(i))*real(Z1l(i))/(abs(Z1l(i)+Z2l(i))^2);

%Integral for line coupling over incident angle
I21l(i)=2/pi*(k0(i)*kp(i)^2*Ls)/(pi/2*k0(i)^2+kp(i)^2);

%Line coupling loss factor from plate and acoustic volume
ita21l(i)=delf2(i)/pi/f(i)*betacorr_1(i)*I21l(i)*to21l(i)/(2-to21l(i));

%Coupling Loss Factor from plate to acoustic volume
ita21(i)=ita21a(i)+ita21l(i);

%Reciprocity Relation determines CLF from acoustic volume to plate
ita12(i)=nwp(i)*ita21(i)/nw1(i);

%SEA Matrix
C=[ita11(i)+ita12(i) -ita21(i)
   -ita12(i) ita21(i)+ita22(i)];

%Response analysis via classical SEA
if Case==1;
% Acoustic Power
a=10e-3; %Radius of source
Pres=1; %Magnitude of sound pressure
Vr=Pres/rho0/c0; %Surface velocity of monopole source
Qs=4*pi*a^2*Vr; %Source strength
P1=rho0*c0*k0(i)^2/8/pi/(1+k0(i)^2*a^2)*Qs^2; %Acoustic excitation
P2=0; %Mechanic excitation
elseif Case==2;
P2=abs(FF^2)*real(1/(8*rhop*hp*K*cLp));%Mechanic power

```

```

P1=0; %Acoustic power
end
P(:,i)=1/w(i)*[P1;P2]; %Power vector
E(:,i)=inv(C)*P(:,i); %Determination of energies of
subsystems

Pres1(i)=sqrt(E(1,i)*rho0*cg2^2/V1); %Pressure of acoustic volume
vel2(i)=sqrt(E(2,i)/mp); %Velocity of plate
end

%Determination of Modal Overlap Factor for each subsystem
for i=1:length(f)
MOF1(i)=pi*beta1(i)/2; %MOF of acoustic volume
MOF2(i)=pi*beta2(i)/2; %MOF of plate
end
MOF3=2.5*ones(1,length(f)); %Threshold for composite plate
MOF4=3*ones(1,length(f)); %Threshold for acoustic volume
save('acoustic_excitation.mat') %Saving classical SEA results

figure(1) %Opens figure 1
%Plotting CLFs with color of blue(b), black(k) and green(g)
plot1=semilogy(f,ita21,'k',f,ita21l,'b',f,ita21a,'g',f,ita12,'r');
set(plot1(1),'DisplayName','CLF21total');
set(plot1(2),'DisplayName','CLF21line');
set(plot1(3),'DisplayName','CLF21area');
set(plot1(4),'DisplayName','CLF12total');
%Creating xlabel
xlabel('Frequency [Hz]');
%Creating ylabel
ylabel('Coupling Loss Factor');
%Showing legend
legend1=legend('show');

```

```

%Locating legend right down
set(legend1,'Location','SouthEast');
%Saving figure 1 in .fig and .eps format
saveas(figure(1),'CLF_plate_to_acoustic','fig');saveas(figure(1),'CLF_plate_to_acous
tic','eps');

```

```

figure(2)
%Plotting sound pressure of acoustic volume with color of red(r)
plot2=semilogy(f,Pres1,'r');
set(plot2(1),'DisplayName','pressure of cavity');
% Create xlabel
xlabel('frequency [Hz]');
% Create ylabel
ylabel('response of cavity [Pa]');
title('response of subsystem 1 under excitation of subsystem 1')
legend show
saveas(figure(2),'SEA_z1o1','fig');saveas(figure(2),'SEA_z1o1','eps');

```

```

figure(3)
%Plotting velocity of plate with color of blue(b)
plot3=semilogy(f,vel2,'b');
set(plot3(1),'DisplayName','velocity of plate');
% Create xlabel
xlabel('frequency [Hz]');
% Create ylabel
ylabel('response of plate [m/s]');
title('response of subsystem 2 under excitation of subsystem 1')
legend show
saveas(figure(3),'SEA_z1o2','fig');saveas(figure(3),'SEA_z1o2','eps');

```

```

figure(4)
%Plotting MOF of acoustic volume with color of blue(b) and MOF=3

```



```

plot1=semilogy(f,MOF1,'b',f,MOF4,'r');
set(plot1(1),'LineStyle',':','DisplayName','MOF of cavity');
% Create xlabel
xlabel('frequency [Hz]');
% Create ylabel
ylabel('Modal Overlap Factor');
legend1 = legend('show');
set(legend1,'Location','SouthEast');
saveas(figure(4),'MOF_cavity','fig');saveas(figure(4),'MOF_cavity','eps');

```

```

figure(5)
%Plotting MOF of plate with color of blue(b) and MOF=2.5
plot1=semilogy(f,MOF2,'b',f,MOF3,'r');
set(plot1(1),'LineStyle',':','DisplayName','MOF of plate');
% Create xlabel
xlabel('frequency [Hz]');
% Create ylabel
ylabel('Modal Overlap Factor');
legend1 = legend('show');
set(legend1,'Location','SouthEast');
saveas(figure(5),'MOF_plate','fig');saveas(figure(5),'MOF_plate','eps');

```

```

figure(6)
%Plotting AMS of acoustic volume with color of blue(b)
plot1=semilogy(f,delf1,'b');
set(plot1(1),'LineStyle',':','DisplayName','AMS of cavity');
% Create xlabel
xlabel('frequency [Hz]');
% Create ylabel
ylabel('Average Modal Spacing');
legend1 = legend('show');
saveas(figure(6),'AMS_cavity','fig');saveas(figure(6),'AMS_cavity','eps');

```

```

figure(7)
%Plotting AMS of plate with color of blue(b)
plot1=semilogy(f,delf2,'b');
set(plot1(1),'LineStyle',':','DisplayName','AMS of plate');
% Create xlabel
xlabel('frequency [Hz]');
% Create ylabel
ylabel('Average Modal Spacing');
legend1 = legend('show');
saveas(figure(7),'AMS_plate','fig');saveas(figure(7),'AMS_plate','eps');

```

A.1.2 Numerical SEA for Composite Plate-Acoustic Volume Structure

A.1.2.1 Determination of Average Modal Spacings of Subsystems

Here, a Matlab code is created to determine the average modal spacings of subsystems by using numerical natural frequencies.

```

clc;clear
fn=load('cavity_30.txt');           %Loading numerical natural frequencies
fcenter=1:1:5000;                   %Center frequency of 1/3 octave band
flow=fcenter/(2^(1/6));              %Low frequency of 1/3 octave band
fhigh=2^(1/3)*flow;                 %High frequency of 1/3 octave band

%Placing the natural frequencies to each 1/3 octave band center frequencies via for
loop
for i=1:length(fn);
    for k=1:length(fcenter);
        if fn(i)>flow(k)&& fn(i)<fhigh(k);
            x(i,k)=fn(i);           %Assigning natural frequencies to
matrix x
        end
    end
end

```

```

end
b=size(x); %Determines the size of matrix x

%Eliminating "0" values on top lines in matrix x
for k=1:b(2);
    m=1;
    for i=1:b(1);
        if x(i,k)~=0;
            x1(m,k)=x(i,k); %Result matrix x1
            m=m+1;
        end
    end
end

SIZE=size(x1); %Determines the size of matrix x1

%Determining modal spacings between natural frequency
for k=1:SIZE(2);
    for i=1:SIZE(1)-1;
        if x1(i+1,k)-x1(i,k)>0;
            df1(i,k)=x1(i+1,k)-x1(i,k); %Modal spacings for ith center
            frequency
        end
    end
end

%Determining the mode number for each frequency band which is (Pdelta in Eq. 3.5)
for k=1:SIZE(2);
    m=1;
    for i=1:SIZE(1);
        if x1(i,k)~=0;
            pdelta(k)=m;
        end
    end
end

```

```

    m=m+1;
end
end
end
%Determining average modal spacings by using Eq. 3.5
for k=1:SIZE(2);
delf(k)=1/(pdelta(k)-1)*sum(df1(:,k));
end
end
save('delf30_cavity.mat','delf')

```

Note that, the same procedure can be applied to composite plate. These results are compared with analytical results which are calculated as mentioned in Section A1.1.

A.1.2.2 Determination of Loss Factors of Subsystems via Numerical PIM

Here, a Matlab code is created to processing the data which are evaluated from Ansys and applied power injection method to determine loss factors. Creating ansys file will be presented in Section A1.3.1 with uncertainty results. Note that the same computer program is utilized to composite structures (I, L and T type).

```

clc;clear
load('P11.mat'),           %Loading mean sound pressure of
acoustic volume under excitation of acoustic volume
load('P12.mat'),           %Loading mean sound pressure of
acoustic volume under excitation of composite plate
load('V21.mat'),           %Loading mean velocity of composite
plate under excitation of acoustic volume
load('V22.mat'),           %Loading mean velocity of composite
plate under excitation of composite plate
load('ReY2.mat')           %Loading real part of driving point
velocity of composite plate under excitation of composite plate

```

```

f=1:1:5000; %Frequency range
w=2*pi*f;
%---Properties of plate
Lp1=1;Lp2=1; %Length of plate
Ap=Lp1*Lp2; %Area of plate
hp=2.2*10^-3; %Thickness of plate
rhop=1771.21; %Density of plate
mp=rhop*Ap*hp; %Mass of plate
%Energy of subsystem 2 under excitation of subsystem 1
E21=mp*V21m.^2;
%Energy of subsystem 2 under excitation of subsystem 2
E22=mp*V22m.^2;

% Mechanical Power
F=1; %Amplitude of excitation of subsystem
1
P2in=F^2*ReY2; %Power input as mentioned in Section
2.2.2

%---Properties of cavity (air)
Temp=20; %Temperature of air
cg2=20.0457*sqrt(Temp+273.2); c0=cg2; %Group velocity of air
rho0=1.225; %Density of air at temperature Temp
k=w/c0; %Wave number of acoustic volume

%Determination of acoustic power
a=1e-2; %Radius of source
Pres=1; %Pressure amplitude of excitation
Vr=Pres/rho0/c0; %Surface velocity of sound source
Qs=4*pi*a^2*Vr; %Source strength
%Energy of subsystem 1 under excitation of subsystem 1
E11=P11m.^2*V1/(rho0*(c0^2));

```

```

%Energy of subsystem 1 under excitation of subsystem 2
E12=P12m.^2*V1/(rho0*(c0^2));

%Power input as mentioned in Section 2.2.2
for i=1:length(f);
P1in(i)=rho0*c0*k(i)^2/8/pi/(1+k(i)^2*a^2)*Qs^2;
end

for i=1:length(f);
P=1/w(i)*[P1in(i),0;0,P2in(i)];           %Power matrix as mention in Section
2.3
E=[E11(i),E12(i);E21(i),E22(i)];         %Energy matrix as mention in Section
2.3
nu=P*inv(E);                             %Loss factor matrix application of Eq.
2.25

%Loss factors are determined by using Eq. 2.26
nu11(i)=nu(1,1)+nu(2,1);
nu12(i)=-nu(2,1);
nu21(i)=-nu(1,2);
nu22(i)=nu(1,2)+nu(2,2);
end

nu11=abs(nu11);nu12=abs(nu12);nu21=abs(nu21);nu22=abs(nu22);

%Determining of 1/3 octave band average of loss factors
nu11_ort=oktav_bandi_ort(nu11,f);
nu12_ort=oktav_bandi_ort(nu12,f);
nu21_ort=oktav_bandi_ort(nu21,f);
nu22_ort=oktav_bandi_ort(nu22,f);

```

```

%Plotting loss factors
figure(1),subplot(2,2,1),loglog(f,nu11_ort,'b'),axis([100 5000 1e-6 1])
figure(1),subplot(2,2,2),loglog(f,nu12_ort,'b'),axis([100 5000 1e-6 1])
figure(1),subplot(2,2,3),loglog(f,nu21_ort,'b',f,nu21r_ort,'b'),axis([100 5000 1e-6 1])
figure(1),subplot(2,2,4),loglog(f,nu22_ort,'b'),axis([100 5000 1e-6 1])
%Saving loss factors
save('PIM_results_new.mat','nu11_ort','nu12_ort','nu22_ort','f')

```

A.1.2.3 Determination of High Frequency Threshold for Subsystems

In this section, modal overlap factor using numerical results is calculated for each subsystem as following:

```

clc;clear
%Loading numerical power injection results and average modal spacings
load ('PIM_results_new.mat')
load ('delf100_plate.mat')
delf_plate=delf;
clear 'delf'
load ('delf100_cavity.mat')
delf_cavity=delf;
clear ('delf','nu12_ort','nu21r_ort')
%Determining modal overlap factor by using Eq. 2.22
MOF_plate_s=pi/2*f.*nu22_ort./delf_plate;
MOF_cavity_s=pi/2*f.*nu11_ort./delf_cavity;
%Plotting modal overlap factor and threshold for subsystems
figure(1),semilogy(f,2.5*ones(1,length(f)), 'k',f,MOF_plate_s,'b'),xlabel('Frequency [Hz]'), ylabel('MOF')
figure(2),semilogy(f,3*ones(1,length(f)), 'k',f,MOF_cavity_s,'b'),xlabel('Frequency [Hz]'), ylabel('MOF')

```

Note that these results are compared with analytical results which are calculated in Section A1.1. SEA response is determined by using numerical SEA parameters. For this purpose, the same program that is used to evaluate classical SEA response can be used.

A.1.3 Uncertainty Analysis

A.1.3.1 Creating Model and Exporting Responses to Notepad for Uncertainty Analysis

To perform analysis in Ansys APDL, a MatLAB code is prepared that creates .txt file for Ansys APDL. Note that, by running this program it is not needed to open Ansys separately. The code that is given above belongs to acoustic excitation where plate excitation code is very familiar.

```
%Changing directory
cd D:\TUBITAK_WORKSTATION\5.IS_PAKETI\monte_carlo\
clc; clear all
E1=21.3e9; % Young Modulus of plate on direction-x
E2=21.1e9; % Young Modulus of plate on direction-y
Ez=E1;
pr12=0.161; %Poisson ratio on xy direction
pr21=(E2/E1)*pr12; %Poisson ratio on yx direction
G=3.003e9; %Shear modulus
%Properties of layers
th1=0; % Theta1
th2=90; % Theta2
nl=8; %Number of layer

Ro_s=1771.2121; %Density of solid (plate)
Ro_a=1.2; %Density of air

Lx=1; %Width
```



```

Ly=1; %Length
Lz=-1; %Depth

es=30; %Number of elements
pressu=1; %Pressure Amplitude
nnode=(es^3)+3*(es^2)+3*es+1; %Number of nodes
sonic=343; %Speed of sound
beta=0; %Absorption coefficient
dratio_p=0.01; % Plate's damping ratio where
 $\eta=2*\text{dratio\_p}$ 

%Response measuring points for plate and acoustic volume
nnum_plate=50;
nnum_cavity=200;

%Harmonic analysis settings
%Beginning frequency for harmonic analysis
nbf=0;
%Ending frequency for harmonic analysis
nef=5000;
for ann=1:20; %Number of analysis
%THICKNESS OF PLATE
i=randi(50,1,1); %Creates 50 random numbers
ii=i*2.2e-5; %variation in thickness of plate
ht=16.5e-4+ii; %thickness of plate
%Creating a waitbar
hw = waitbar(0,'Analysis is progressing, Please wait...');

%Measuring points from plate with respect to analysis number
node_plate(:,ann)=randi([7747,10151],nnum_plate,1);
%Measuring points from acoustic volume with respect to analysis number
node_cavity(:,ann)=randi([10200,nnode],nnum_cavity,1);

```

```

%Function file that creates finite element model of structure
plate_cavity_comp_acoustic(ann,E1,E2,pr12,pr21,nl,th1,th2,G,ht,Ro_s,Ro_a,Lx,Ly,
Lz,nbf,nef,es,pressu,sonic,beta,dratio_p,nnum_plate,nnum_cavity,node_plate,node_c
avity);

%University computer path, opens Ansys and runs .txt file
eval(['!C:\Program Files\ANSYS Inc\v150\ansys\bin\winx64\ANSYS150.exe " -b -i
','D:\TUBITAK_WORKSTATION\5.IS_PAKETI\monte_carlo\cavitymodel.txt', ' -o
D:\TUBITAK_WORKSTATION\5.IS_PAKETI\monte_carlo\pressure\resultsout.txt
-np 16']);

%Creates messages on Matlab command window
d1=[int2str(ann),'. analysis is completed...']; disp(d1)
waitbar(ann,hw);
%Clearing temporary analysis files
delete D:\TUBITAK_WORKSTATION\5.IS_PAKETI\monte_carlo\file.*
%Closing waitbar
close(hw);
end;
%Saving measuring points for data processing
save('noderesult.mat','node_plate','node_cavity');

```

Following codes are included in function file:

```

%Function file uses materials properties, frequency range, element size,
measurement points of each subsystems
function
plate_cavity_comp_acoustic(ann,E1,E2,pr12,pr21,nl,th1,th2,G,ht,Ro_s,Ro_a,Lx,Ly,
Lz, nbf,nef,es,pressu,sonic,beta,dratio_p,nnum_plate,nnum_cavity,ii,jj);
fid=fopen('D:\TUBITAK_WORKSTATION\5.IS_PAKETI\monte_carlo\cavitymode
l.txt','wt');

```

```

%Publishing constants to .txt file
fprintf(fid,'FINISH\n');
fprintf(fid,'/CLEAR,NOSTART\n');
fprintf(fid,'/UNITS,mks\n');
fprintf(fid,'/NERR,1e6,1e6\n');
fprintf(fid,'/CONFIG,nres,1e6\n');
fprintf(fid,'*AFUN,deg\n');

fprintf(fid,'lx=%f\n',Lx);
fprintf(fid,'ly=%f\n',Ly);
fprintf(fid,'lz=%f\n',Lz);
fprintf(fid,'ht=%f\n',ht);
fprintf(fid,'es=%f\n',es);
fprintf(fid,'Ro_s=%f\n',Ro_s);
fprintf(fid,'Ro_a=%f\n',Ro_a);
fprintf(fid,'pressu=%f\n',pressu);
fprintf(fid,'sonic=%f\n',sonic);
fprintf(fid,'beta=%f\n',beta);
fprintf(fid,'dratio_p=%f\n',dratio_p);
fprintf(fid,'nl=%f\n',nl);
fprintf(fid,'tl=ht/nl\n');
fprintf(fid,'EX=%f\n',E1);
fprintf(fid,'EY=%f\n',E2);
fprintf(fid,'EZ=%f\n',E1);
fprintf(fid,'PRXY=%f\n',pr12);
fprintf(fid,'PRYZ=%f\n',pr21);
fprintf(fid,'PRXZ=%f\n',pr21);
fprintf(fid,'GXY=%f\n',G);
fprintf(fid,'GYZ=%f\n',G);
fprintf(fid,'GXZ=%f\n',G);

```

```

%Publishing model
%Creating elements type
fprintf(fid,'%prep7\n');
fprintf(fid,'ET,1,SHELL181\n');
fprintf(fid,'KEYOPT,1,1,0\n');
fprintf(fid,'KEYOPT,1,8,2\n');
fprintf(fid,'KEYOPT,1,9,0\n');

fprintf(fid,'ET,2,30\n');
fprintf(fid,'ET,3,30,,1\n');
fprintf(fid,'SECTYPE,1,shell,,cpart1\n');

% Angles of layers
for i=1:nl/2
    if mod(i,2)==1
        thl(i)=th1;
    else
        thl(i)=th2;
    end;
end;
thl=[thl,flipr(thl)];

% Writing the angles of layer to .txt
for i=1:nl
    s1 = int2str(i);
    s2=['th',s1,'=%f\n'];
    fprintf(fid,s2,thl(i));
    s3=['SECDATA,tl,1,', 'th',s1,',3\n'];
    fprintf(fid,s3);
end;

```

```
fprintf(fid,'SECDATA,ht,1,,3\n');  
fprintf(fid,'SECOFFSET,MID\n');  
fprintf(fid,'SECCONTROL,,,,,,,,\n');
```

% Assigning material properties

```
fprintf(fid,'MPTEMP,,,,,,,, \n');  
fprintf(fid,'MPTEMP,1,0\n');  
fprintf(fid,'MP,EX,1,EX\n');  
fprintf(fid,'MP,EY,1,EY\n');  
fprintf(fid,'MP,EZ,1,EZ\n');  
fprintf(fid,'MP,PRXY,1,PRXY\n');  
fprintf(fid,'MP,PRYZ,1,PRYZ\n');  
fprintf(fid,'MP,PRXZ,1,PRXZ\n');  
fprintf(fid,'MP,GXY,1,GXY\n');  
fprintf(fid,'MP,GYZ,1,GYZ\n');  
fprintf(fid,'MP,GXZ,1,GXZ\n');  
fprintf(fid,'MP,DENS,1,Ro_s\n');  
fprintf(fid,'MP,DMPR,1,dratio_p\n');  
fprintf(fid,'MP,DENS,2,Ro_a\n');  
fprintf(fid,'MP,SONC,2,sonic\n');  
fprintf(fid,'MP,MU,2,beta\n');  
fprintf(fid,'MP,DENS,3,Ro_a\n');  
fprintf(fid,'MP,SONC,3,sonic\n');  
fprintf(fid,'MP,MU,3,beta\n');
```

% Creating keypoints for geometry of structure

```
fprintf(fid,'K,1,0,0,0\n');  
fprintf(fid,'K,2,lx,0,0\n');  
fprintf(fid,'K,3,lx,ly,0\n');  
fprintf(fid,'K,4,0,ly,0\n');  
fprintf(fid,'K,5,0,0,lz\n');  
fprintf(fid,'K,6,lx,0,lz\n');
```

```
fprintf(fid,'K,7,lx,ly,lz\n');  
fprintf(fid,'K,8,0,ly,lz\n');
```

```
fprintf(fid,'L,1,2,es\n');  
fprintf(fid,'L,2,3,es\n');  
fprintf(fid,'L,3,4,es\n');  
fprintf(fid,'L,4,1,es\n');  
fprintf(fid,'L,1,5,es\n');  
fprintf(fid,'L,2,6,es\n');  
fprintf(fid,'L,3,7,es\n');  
fprintf(fid,'L,4,8,es\n');  
fprintf(fid,'L,5,6,es\n');  
fprintf(fid,'L,6,7,es\n');  
fprintf(fid,'L,7,8,es\n');  
fprintf(fid,'L,8,5,es\n');  
fprintf(fid,'V,1,5,8,4,2,6,7,3\n');
```

% Assigning element type 2 into volume

```
fprintf(fid,'VATT,2,2,2,,ALL\n');  
fprintf(fid,'ASEL,S,AREA,,4\n');  
fprintf(fid,'AATT,1,,1,,1\n');  
fprintf(fid,'VMESH,ALL\n');  
fprintf(fid,'NSEL,S,LOC,Y,ly\n');  
fprintf(fid,'ESLN\n');  
fprintf(fid,'CM,C_INT_FE,ELEM\n');  
fprintf(fid,'AMESH,ALL\n');  
fprintf(fid,'ALLS\n');
```

```
fprintf(fid,'NSEL,A,LOC,Y,ly\n');  
fprintf(fid,'ESLN\n');  
fprintf(fid,'ESEL,INVE\n');  
fprintf(fid,'TYPE,3\n');
```

```

fprintf(fid,'MAT,2\n');
fprintf(fid,'EMODIF,ALL\n');
fprintf(fid,'ALLS\n');
fprintf(fid,'NUMMRG,ALL\n');
fprintf(fid,'NSEL,NONE\n');

%Selecting area 4
fprintf(fid,'ASEL,S,AREA,,4\n');
fprintf(fid,'NSLA,S,1\n');
%Giving boundary conditions to plate
fprintf(fid,'NSLA,U,O\n');
fprintf(fid,'D,ALL,UX,,,,UY,UZ,ROTX,ROTY,ROTZ\n');
fprintf(fid,'ALLS\n');
%Applying fluid structure interaction
fprintf(fid,'NSEL,S,LOC,Y,ly\n');
fprintf(fid,'CMSEL,S,C_INT_FE\n');
fprintf(fid,'SF,ALL,FSI\n');
fprintf(fid,'ALLS\n');
fprintf(fid,'FINISH\n');

%Create harmonic analysis codes

fprintf(fid,'nbf=%f\n',nbf);
fprintf(fid,'nef=%f\n',nef);
%Point of excitation
fprintf(fid,'nf=node(lx/2,ly/2,lz/2)\n');

fprintf(fid,'*get,wall1,active,,time,wall\n');
fprintf(fid,'/SOLU\n');
fprintf(fid,'ANTYPE,HARMIC,NEW\n');
fprintf(fid,'hropt,full\n');
fprintf(fid,'hrout,on\n')

```

```

fprintf(fid,'LUMPM,0\n');
fprintf(fid,'FLST,5,1,1,ORDE,1\n');
fprintf(fid,'FITEM,5,nf\n');
fprintf(fid,'CM,prs,NODE\n');
fprintf(fid,'NSEL,R, , ,nf\n');
fprintf(fid,'CM,prs1,NODE\n');
fprintf(fid,'CMSEL,S,prs\n');
fprintf(fid,'CMDELE,prs\n');
fprintf(fid,'/GO\n');
% Amplitude sound pressure excitation
fprintf(fid,'D,prs1,PRES,pressu\n');
fprintf(fid,'CMDELE,prs1\n');
fprintf(fid,'HARFRQ,nbf,nef,\n');
fprintf(fid,'NSUBST,nef-nbf\n');
fprintf(fid,'KBC,1\n');
fprintf(fid,'SOLVE\n');
fprintf(fid,'FINISH\n');

fprintf(fid,'/POST26\n');
fprintf(fid,'numvar,200\n');

% Exporting data from the excitation point
fprintf(fid,'NSOL,2,nf,pres.,pres1,\n');
fprintf(fid,'PLCPLX,0\n');
fprintf(fid,'*CREATE,scratch,gui\n');
fprintf(fid,'*DEL,_P26_EXPORT\n');
fprintf(fid,'*DIM,_P26_EXPORT,TABLE,nef-nbf,2\n');
fprintf(fid,'VGET,_P26_EXPORT(1,0),1\n');
fprintf(fid,'VGET,_P26_EXPORT(1,1),2,,0\n');
fprintf(fid,'VGET,_P26_EXPORT(1,2),2,,1 \n');

```



```

%Creating .txt file to results
s0=char(39); %(') Character ASCII code
s1='/OUTPUT,';

s7=int2str(ann);
s2=[s0,'res_pres_nr1_a',s7,s0,','];s3=[s0,'txt',s0];
s4=',';
%Directory for publishing results
s5=[s0,'D:\TUBITAK_WORKSTATION\5.IS_PAKETI\monte_carlo\pressure',s0];
s6=[s1,s2,s3,s4,s5];

fprintf(fid,'%s\n',s6);
fprintf(fid,'*VWRITE,_P26_EXPORT(1,0),_P26_EXPORT(1,1),_P26_EXPORT(1,
2)\n');
fprintf(fid,'%s\n','%14.5G %14.5G %14.5G');
fprintf(fid,'/OUTPUT,TERM\n');
fprintf(fid,'*END\n');
fprintf(fid,'/INPUT,scratch,gui\n');

%Exporting plate results into .txt files
s0=char(39);
s00=',';
for j=1:nnum_plate;

    s1='NSOL,';
    s2=int2str(ii(j,ann)+1);
    s4=',u,y,';
    s5='uy_n_';
    s6=int2str(ii(j,ann));
    s7='\n';
    s10='2';
    s8=[s1,s10,s00,s6,s4,s5,s6,s00,s7];

```

```

fprintf(fid,s8);
fprintf(fid,'PLCPLX,0\n');
fprintf(fid,'*CREATE,scratch,gui\n');
fprintf(fid,'*DEL,_P26_EXPORT\n');

fprintf(fid,'*DIM,_P26_EXPORT,TABLE,nef-nbf,2\n');
fprintf(fid,'VGET,_P26_EXPORT(1,0),1\n');

fprintf(fid,'VGET,_P26_EXPORT(1,1),2,,0\n');
fprintf(fid,'VGET,_P26_EXPORT(1,2),2,,1\n');

s1='/OUTPUT,';
s8='a';
s7=int2str(ann);
s22=[s0,'res_uy_',s8,s7,'_n_',s6,s0,'];
s3=[s0,'txt',s0];
s4=',';

s5=[s0,'D:\TUBITAK_WORKSTATION\5.IS_PAKETI\monte_carlo\pressure\',s0];
s66=[s1,s22,s3,s4,s5];
fprintf(fid,'%s\n',s66);

fprintf(fid,'*VWRITE,_P26_EXPORT(1,0),_P26_EXPORT(1,1),_P26_EXPORT(1,
2)\n');
fprintf(fid,'%s\n','%14.5G %14.5G %14.5G');
fprintf(fid,'/OUTPUT,TERM\n');
fprintf(fid,'*END\n');
fprintf(fid,'/INPUT,scratch,gui\n');
fprintf(fid,'VARDEL,2\n');
end;

```

```

%Exporting acoustic volume results into .txt files
s0=char(39);
s00='';
for j=1:num_cavity
    s1='NSOL,';
    s2=int2str(jj(j,ann)+1);
    s4=',pres,,';
    s5='pres_n_';
    s6=int2str(jj(j,ann));
    s7='\n';
    s10='2';
    s8=[s1,s10,s00,s6,s4,s5,s6,s00,s7];
    fprintf(fid,s8);
    fprintf(fid,'PLCPLX,0\n');
    fprintf(fid,'*CREATE,scratch,gui\n');
    fprintf(fid,'*DEL,_P26_EXPORT\n');

    fprintf(fid,'*DIM,_P26_EXPORT,TABLE,nef-nbf,2\n');
    fprintf(fid,'VGET,_P26_EXPORT(1,0),1\n');

    fprintf(fid,'VGET,_P26_EXPORT(1,1),2,,0\n');
    fprintf(fid,'VGET,_P26_EXPORT(1,2),2,,1 \n');

    s1='/OUTPUT,';
    s8='a';
    s7=int2str(ann);
    s22=[s0,'res_pres_',s8,s7,'_n_',s6,s0,'];
    s3=[s0,'txt',s0];
    s4='';

    s5=[s0,'D:\TUBITAK_WORKSTATION\5.IS_PAKETI\monte_carlo\pressure\',s0];
    s66=[s1,s22,s3,s4,s5];

```

```

fprintf(fid,'%s\n',s66);

fprintf(fid,'*VWRITE,_P26_EXPORT(1,0),_P26_EXPORT(1,1),_P26_EXPORT(1,
2)\n');
fprintf(fid,'%s\n','%14.5G %14.5G %14.5G');
fprintf(fid,'/OUTPUT,TERM\n');
fprintf(fid,'*END\n');
fprintf(fid,'/INPUT,scratch,gui\n');
fprintf(fid,'VARDEL,2\n');
end;

%Exporting solution time for each analysis
fprintf(fid,'*get,wall2,active,,time,wall\n');
fprintf(fid,'solving_time = (wall2 - wall1)*3600\n');
s1='*CREATE,';
s2=[s0,'solution_time_',s7,s0,','];
s6=[s1,s2,s3,s4,s5];
fprintf(fid,'%s\n',s6);
fprintf(fid,'*END\n');
fprintf(fid,'*CREATE,ansuitmp\n');

s1='*CFOPEN,';
s6=[s1,s2,s3,s4,s5];
fprintf(fid,'%s\n',s6);
fprintf(fid,'*VWRITE,solving_time\n');
fprintf(fid,'(F10.1)\n');
fprintf(fid,'*CFCLOSE\n');
fprintf(fid,'*END\n');
fprintf(fid,'/INPUT,ansuitmp\n');
%Closing ansys macro file
fclose(fid);

```

A.1.3.2 Data Processing

Two different programs are created to process data those are evaluated from finite element analysis with Monte Carlo simulation. But here, program that is used to determine mean response of plate is given which is very familiar with mean response of acoustic volume.

```
clc;clear;
%Loading response nodes for each subsystem
load 'noderesult.mat';
%Determining number of analysis, number of response nodes
Noan=size(node_plate);
%Reading .txt files via loops
for m=1:Noan(2);
jj=node_plate(:,m);           %Analysis number
for i=1:length(jj);
%Directory of files
s1='C:\Users\samsungpc\Desktop\Bosluk_plaka\4temmuz_z1\FEM\';
%Creating name of .txt files
s2='res_uy_a';
s3=int2str(jj(i));
s4='_n_';
s5=int2str(m);                %Node number of jjth analysis
s6=[s1,s2,s5,s4,s3,'.txt'];
hu=load(s6);
freq=hu(:,1);                %Loading frequency range
%Loading displacements from .txt files
reU(:,i,m)=hu(:,2);
ImU(:,i,m)=hu(:,3);
magU(:,i,m)=abs(reU(:,i,m)+1j*ImU(:,i,m));
end
end
%Determining velocity response from displacements
```

```

for k=1:Noan(2);
for i=1:length(freq);
    V(i,:,k)=1j*2*pi*freq(i)*magU(i,:,k);
    magV(i,:,k)=abs(V(i,:,k));
end
end
save('FEM_z1o2.mat','magV','freq')
%Spatial averaging of each analysis
for m=1:Noan(2);
for i=1:length(freq);
ort1(i,m)=mean(magV(i,:,m));
end
%Plotting spatial-averaged results
figure(10),semilogy(freq,ort1(:,m),'color',[0.8 0.8 0.8]);hold on,
end
z1o2=ort1; save('belz1o2.mat','z1o2','freq')
%Determining mean response of all analyses
for i=1:length(freq);
ort(i)=mean(ort1(i,:));
end
%Plotting mean results
figure(10),semilogy(freq,ort,'k');

```

A.2 Mechanical Properties of Composite Plates

A.2.1 Determination of Rigidities

In this chapter, determination of bending rigidities is evaluated by using laminate theory. Assume that Young modulus (E_y) of the composite plate on each direction, Poisson ratio (μ_{xy}) and shear modulus (G_{12}) are known. By using this information, stiffness matrix can be expressed as:

$$[k] = \begin{bmatrix} k_{11} & k_{12} & 0 \\ k_{21} & k_{22} & 0 \\ 0 & 0 & k_{33} \end{bmatrix}, \quad (\text{A.1a})$$

where,

$$k_{11} = \frac{E_{y1}}{1 - \mu_{12}\mu_{21}}, \quad (\text{A.1b})$$

$$k_{12} = k_{21} = \frac{\mu_{21}E_{y1}}{1 - \mu_{12}\mu_{21}}, \quad (\text{A.1c})$$

$$k_{22} = \frac{E_{y2}}{1 - \mu_{12}\mu_{21}}, \quad (\text{A.1d})$$

$$k_{33} = G_{12}. \quad (\text{A.1e})$$

Here, E_{y1} is Young modulus in the principal axis and E_{y2} is Young modulus in the vertical axis of principal axis. Q matrix can be evaluated for each layer by using stiffness matrix as:

$$[Q]_i = \begin{bmatrix} Q_{11i} & Q_{12i} & Q_{13i} \\ Q_{21i} & Q_{22i} & Q_{23i} \\ Q_{31i} & Q_{32i} & Q_{33i} \end{bmatrix}, \quad (\text{A.2a})$$

and

$$Q_{11i} = k_{11} \cos^4(\theta_i) + k_{22} \sin^4(\theta_i) + 2(k_{12} + 2k_{33}) \cos^2(\theta_i) \sin^2(\theta_i), \quad (\text{A.2b})$$

$$Q_{12i} = Q_{21i} = (k_{11} + k_{22} - 4k_{33}) \cos^2(\theta_i) \sin^2(\theta_i) + k_{12} (\cos^4(\theta_i) + \sin^4(\theta_i)), \quad (\text{A.2c})$$

$$Q_{13i} = Q_{31i} = \cos(\theta_i)\sin(\theta_i)(k_{11}\cos^2(\theta_i) - k_{22}\sin^2(\theta_i)) + (\cos(\theta_i)\sin^3(\theta_i) - \cos^3(\theta_i)\sin(\theta_i))(k_{12} + 2k_{33}), \quad (\text{A.2d})$$

$$Q_{22i} = k_{11}\sin^4(\theta_i) + k_{22}\cos^4(\theta_i) + 2(k_{12} + 2k_{33})\cos^2(\theta_i)\sin^2(\theta_i), \quad (\text{A.2e})$$

$$Q_{23i} = Q_{32i} = \cos(\theta_i)\sin(\theta_i)(k_{11}\sin^2(\theta_i) - k_{22}\cos^2(\theta_i)) + (\cos^3(\theta_i)\sin(\theta_i) - \cos(\theta_i)\sin^3(\theta_i))(k_{12} + 2k_{33}), \quad (\text{A.2f})$$

$$Q_{33i} = Q_{32i} = \cos^2(\theta_i)\sin^2(\theta_i)(k_{11} + k_{22} - 2k_{12}) + (\cos^2(\theta_i) - \sin^2(\theta_i))^2 k_{33}, \quad (\text{A.2g})$$

where θ_i is angle of layer i . To determine rigidities of composite plates, one can determine distance of layer from the mid-plane of plate as:

$$h_l(i+1) = \frac{h}{2} + \sum_{i=0}^N i \frac{h}{N}. \quad (\text{A.3})$$

Here, $h_l(i+1)$ shows distance of layer i , h shows thickness of plate and N shows number of layer.

Finally, A , B and D matrix of laminated composite plate can be determined as:

$$A_{jt} = \sum_{i=1}^N Q_{jti} (h_l(i+1) - h_l(i)), \quad (\text{A.4})$$

$$B_{jt} = \sum_{i=1}^N Q_{jti} \frac{(h_l(i+1))^2 - (h_l(i))^2}{2}, \quad (\text{A.5})$$

$$D_{jt} = \sum_{i=1}^N Q_{jti} \frac{(h_l(i+1))^3 - (h_l(i))^3}{3}. \quad (\text{A.6})$$

Note that, j and t can be equal to 1, 2 and 6. $B=0$ for symmetrical composite plates and $D_{16} = D_{26} = 0$ for specially orthotropic plate which means composite plate has only 0 and 90 degree orientation angle.

A.2.2 Determination of Mechanical Properties

Appropriate testing methods are developed by ASTM (American Society for Testing Materials) for composite materials which can not be tested as done for traditional metallic materials.

A.2.2.1 Determination of Tensile Properties

Tensile test is the fundamental test which specifies appropriate properties for design in mechanics and used to evaluate Young's modulus, Poisson ratio, tensile strength and maximum deformation. This test is applied to structure whose geometry is shown in Figure A.1, via ASTM D3039 test method. Dimensions of test sample are tabulated in Table A.1.

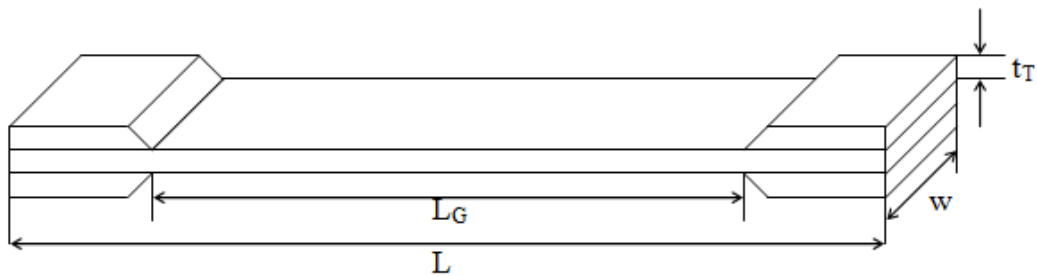


Figure A.1 Geometry of test sample according to ASTM D3039

Table A.1 Dimensions of sample according to the ASTM D3039

L (mm)	L_G (mm)	t_T (mm)	w
250	138	1.5	15

Tensile tests are performed via Shimadzu AG-100 Tensile tester which has 100 kN force capability. Tensile tester is shown in Figure A.2. Velocity of tensile test is selected as 1 mm/min. While force is acting on test sample, extension of sample is

measured via video extensometer. Young modulus is calculated by Trapezium program entering cross-section of sample.



Figure A.2 Shimadzu tensile tester

Poisson ratio is determined by using two strain gauges which are connected on direction of fiber (ϵ_1), and vertical to the fiber (ϵ_2) on the process of tensile test, respectively. Extension and contraction is measured while force acting on test sample is increasing and Poisson ratio is determined as:

$$\nu_{12} = -\frac{\epsilon_2}{\epsilon_1}. \quad (\text{A.7})$$

A.2.2.2 Determination of Shear Properties

Test samples are prepared according to ASTM D7078/D7078M V-Notched Rail Shear Method to determine shear modulus. Dimensions of sample are shown in Figure A.3.

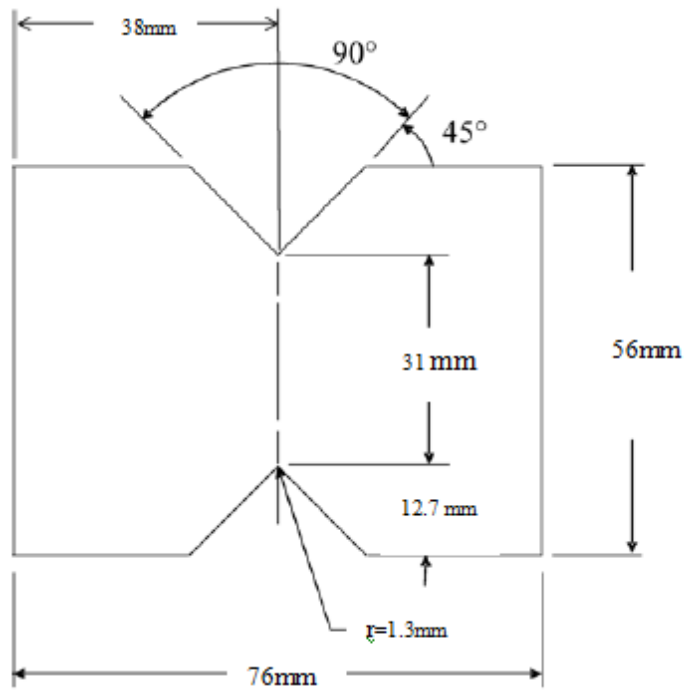


Figure A.3 Test sample for determination of shear modulus

Eq. (A.8) can be used to calculate shear modulus:

$$G = \frac{\tau_{12}}{\gamma_{12}} \quad (\text{A.8})$$

Here, a strain gauge is connected to sample with a 45° to determine shear strain. Shear strain can be determined from the measured strain as:

$$\gamma_{12} = 2\varepsilon \quad (\text{A.9})$$